NICOLAUS COPERNICUS
UNIVERSITY
IN TORUŃ

Nicolaus Copernicus University in Toruń
Faculty of Physics, Astronomy and Informatics

Regulation of Ferroptosis through 15LOX-1/PEBP1 Complex – Computational Modeling at Molecular Level

Thiliban Manivarma

Dissertation for a doctoral degree

Thesis supervised by
dr hab. Karolina Mikulska-Rumińska, prof. NCU – supervisor
and prof. dr hab. Wiesław Nowak – auxiliary supervisor

Department of Biophysics
Institute of Physics, Nicolaus Copernicus University in Torun

Toruń 2025

Table of contents

Acknowledgments

First and foremost, I would like to express my sincere gratitude to my supervisors, Dr. hab. Karolina Mikulska-Rumińska, Prof. UMK, and Prof. Dr. hab. Wiesław Nowak, for selecting me and believing in me during the challenging pandemic situation of 2020. I am deeply grateful for their trust and support. I would especially like to thank my primary supervisor, Dr. hab. Karolina Mikulska-Rumińska, Prof. UMK, for her constant guidance, regular meetings, insightful discussions, and unwavering financial support. Under her mentorship, I learned invaluable lessons in critical thinking, problem-solving, and the development of both technical and soft skills. Without her, completing my Ph.D. would have been much more difficult. I will greatly miss our engaging discussions on ferroptosis.

I would also like to extend my heartfelt thanks to Prof. Nowak for the enriching and insightful weekly discussions with colleagues, which I will cherish. The input and interactions with my supervisors have profoundly shaped my Ph.D. journey and positively impacted my personal and professional growth.

I am profoundly thankful to my co-authors, Prof. Ivet Bahar (Stony Brook University), Prof. Valerian E. Kagan (University of Pittsburgh), Prof. Hülya Bayır (Columbia University), and Dr. James Krieger (Centro Nacional de Biotecnología, Madrid), for their invaluable contributions, insights, and steadfast support throughout the research process.

I am immensely thankful to my entire family, my mother/Amma (Poongothai), my father/Appa (Manivarma), my brother/Anna (Anbu), my sister-in-law/Anni (Kaviya), Kanali, Neeran, my grandmother/Ayya (Chellamal), my grandfather/Thatha (Natarajan), my uncle/Mama (Srinivasan), and all my extended family members. I dedicate this work in particular to my late uncle/Mama (Venkatesan), whose presence I deeply feel and who I know is watching over me.

I would also like to express my gratitude to the National Science Centre, Poland (SONATA grant 2019/35/D/ST4/02203), the Emerging Field “Nanoscale Biophysics” – Excellence Initiative – Research University, Academia Scientiarum Thoruniensis doctoral school and staffs (mgr Agnieszka Górska-Pukownik), and *Inicjatywa Doskonałości – Uczelnia Badawcza (IDUB)* for providing financial support, travel grants, and conference funding and facilities of *Interdyscyplinarne Centrum Nowoczesnych Technologii* (ICNT-UMK), which greatly facilitated my research activities and daily allowances.

NATIONAL SCIENCE CENTRE
POLAND

List of abbreviations

AA – Arachidonic Acid

ACD – Accidental Cell Death

ERK – Extracellular Signal-Regulated Kinase

GPX4 – Glutathione Peroxidase 4

HpETE-PE – Hydroperoxy-Eicosatetraenoic Acid-Phosphatidylethanolamine

HPETEs – Hydroperoxyeicosatetraenoic Acids

LOX – Lipoxygenase

MD – Molecular Dynamics

MEK – Mitogen-Activated Protein Kinase Kinase

PE – Phosphatidylethanolamine

PEBP1 – Phosphatidylethanolamine-Binding Protein 1

PLs – Phospholipids

PPIs – Protein-Protein Interactions

PUFAs – Polyunsaturated Fatty Acids

RCD – Regulated Cell Death

RIP3 – Receptor-Interacting Protein Kinase 3

ROS – Reactive Oxygen Species

SAPE – Stearoyl/Arachidonoyl-Phosphatidylethanolamine

15LOX-1 – 15-lipoxygenase isoform 1

Abstract in English

Ferroptosis emerged in 2012 as a form of programmed cell death, different from known cell death pathways. It is triggered by iron-mediated lipid oxidation. Cells undergoing ferroptosis demonstrate significant mitochondrial alterations, including cellular shrinkage, increased membrane density, and reduced mitochondrial complexity.

The process is intricately controlled by iron metabolism dynamics and thiol regulation, creating a complex biochemical environment that drives extensive membrane lipid peroxidation. Ferroptosis has been associated with the pathogenesis of chronic degenerative diseases and injuries of the brain, and other organs.

This dissertation explores the molecular mechanism of ferroptosis regulation triggered by the protein-protein complex, 15-lipoxygenase-1 (15LOX-1), and phosphatidylethanolamine (PE)-binding protein 1 (PEBP1) in the presence of the substrate stearoyl/arachidonoyl-PE (SAPE) and a biological membrane model. The findings are detailed across three articles A, B, C.

In *Article A*, we employed computational structural modeling techniques, such as molecular docking, to study the complex formation between 15LOX-1 and PEBP1. We conducted molecular dynamics (MD) simulations to investigate conformational changes within the 15LOX-1/PEBP1 complex induced by a membrane. The study reveals that the association of the 15LOX-1/PEBP1 complex with cellular membrane facilitates access to the catalytic site for specific substrates, particularly SAPE. This substrate binding stabilizes the complex and enhances its catalytic activity. Additionally, the performed mutagenesis studies, both computational and experimental, observed the 15LOX-1/PEBP1 complex dissociation upon P112E mutation in PEBP1.

In *Article B*, we described the development of a new tool WatFinder – a part of ProDy framework to identify and visualize protein-water contacts. The tool detects and visualizes critical protein-water interactions, including water bridges and clusters. WatFinder processes ensembles of biomolecular structures, and snapshots from MD trajectories and provides statistical insights into the duration and frequency of water interactions. Accurate evaluation of protein-water interactions is vital for understanding biophysical processes. In *Article C* we investigate oxygen channels localized in 15LOX-1. It was shown that the membrane and substrate SAPE binding enhances oxygen access to the 15LOX-1/PEBP1 catalytic site. Conserved residues in the LOX

family indicate an evolutionary adaptation for oxygen transport through two tunnels, identified through MD, that connect surface regions to the catalytic center, aiding oxygen transport. Using the WatFinder tool, water and oxygen clusters within the 15LOX-1/PEBP1 complex were analyzed. We postulate that water clusters may facilitate oxygen transport. An analysis of 140 PDB structures from the lipoxygenase family highlights the importance of water clusters, which likely stabilize O_2 transport. Oxygen cluster analysis revealed two oxygen binding sites in the active site of 15LOX-1: one that supports single oxidation and another that may facilitate double oxidation. This study also incorporates lipidomics experiments. The results from computational biophysics approaches at the molecular/all-atoms level.

In summary, the results from structural modeling and computational biophysics approaches applied in this dissertation, and complemented by experimental studies conducted by US collaborators, reveal potential molecular mechanisms of ferroptosis regulation linked to the 15LOX-1/PEBP1 complex. These mechanisms include, among others, the structural details of the complex formation, the influence of the membrane environment, substrate acquisition processes, and the effect of substrate binding on O_2 association.

Abstract in Polish

Ferroptoza to odkryta w 2012 roku specyficzna forma zaprogramowanej śmierci komórkowej, różniąca się od innych znanych szlaków. Mechanizm ten jest inicjowany przez utlenianie lipidów za pośrednictwem żelaza, powodując poważne zmiany komórkowe. Proces ferroptozy jest ściśle kontrolowany przez metabolizm żelaza i regulację tioli, tworząc złożone środowisko biochemiczne, które napędza peroksydację lipidów błonowych. Ferroptoza jest powiązana z patogenezą przewlekłych chorób zwyrodnieniowych, urazów mózgu i innych narządów.

Rozprawa poświęcona jest badaniu molekularnego mechanizmu ferroptozy wywoływanej przez kompleks białkowy, 15-lipooksygenazy-1 (15LOX-1) z białkiem wiążącym fosfatydyloetanoloaminę (PE) 1 (PEBP1) w obecności substratu SAPE (pochodnej fosfatydyloetanoloaminy) i modelu błony biologicznej. Uzyskane wyniki zostały szczegółowo opisane w trzech artykułach A, B i C.

W *Artykule A* wykorzystaliśmy techniki biofizyczne obliczeniowego modelowania strukturalnego, m.in. dokowanie molekularne, do zbadania kompleksu składającego się z 15LOX-1 i PEBP1. Ponadto przeprowadziliśmy symulacje dynamiki molekularnej (MD) w celu zbadania zmian konformacyjnych w kompleksie 15LOX-1/PEBP1 indukowanych przez błonę. Badanie wykazało, że związanie kompleksu 15LOX-1/PEBP1 z błoną komórkową zapewnia dostęp do miejsca katalitycznego dla SAPE. Wiązanie substratu stabilizuje kompleks i zwiększa jego aktywność katalityczną. Badania mutagenezy, zarówno obliczeniowe, jak i eksperymentalne, wykazały dysocjację kompleksu 15LOX-1/PEBP1 po mutacji P112E w PEBP1.

W *Artykule B* przedstawiliśmy nowe narzędzie zintegrowane z programem ProDy służące do identyfikacji i wizualizacji oddziaływań białko-woda. WatFinder wykrywa oddziaływania białko-woda, w tym mostki wodne i klastry przetwarzając zespoły struktur biomolekularnych i trajektorie MD. Narzędzie zapewnia wiedzę statystyczną na temat czasu trwania i częstotliwości oddziaływań wody.

Artykuł C dotyczy kanałów transportowych dla tlenu zlokalizowanych w 15LOX-1 i kluczowych dla jego aktywności katalitycznej. Wykazano, że błonowe i substratowe wiązanie SAPE zwiększa dostęp tlenu do miejsca katalitycznego 15LOX-1/PEBP1. Zakonserwowane reszty w rodzinie LOX wskazują na ewolucyjną adaptację do transportu tlenu przez dwa tunele zidentyfikowane poprzez symulacje MD. Za pomocą narzędzia WatFinder zidentyfikowano

i przeanalizowano klastry wody i tlenu w kompleksie 15LOX-1/PEBP1. Przypuszczamy, że klastry wody mogą ułatwiać transport tlenu i przyczyniać się do aktywności katalitycznej tego kompleksu. Analiza 140 struktur PDB z rodziny lipooksygenaz podkreśla znaczenie klastrów wodnych. Ich analiza ujawniła dwa miejsca wiązania O_2 w miejscu aktywnym 15LOX-1: jedno, które wspiera pojedyncze utlenianie i drugie, które może sprzyjać podwójnemu utlenianiu. Wyniki modelowania strukturalnego i dynamiki metodami biofizyki obliczeniowej zastosowane w niniejszej rozprawie, uzupełnione badaniami eksperymentalnymi przeprowadzonymi przez współpracowników z USA, ujawniają potencjalne mechanizmy molekularne regulacji ferroptozy związane z kompleksem 15LOX-1/PEBP1. Mechanizmy te obejmują tworzenie kompleksu, wpływ środowiska błonowego, proces pozyskiwania substratu oraz wpływ wiązania substratu na asocjację z O_2.

1. Introduction

Modern biophysics addresses many processes related to human physiology and medicine. The present thesis is tightly linked to the molecular mechanisms leading to controlled cell death. Therefore, to provide proper context, the biological and biochemical foundations are presented in the first chapter.

1.1 Regulated cell death mechanisms

In 1842, Karl Vogt observed the metamorphosis of tadpoles and noted the disappearance of the tadpole notochord during development, marking one of the earliest recognitions of cell death in human observation [1]. Vogt's realization that the disappearance of specific cells held physiological significance for development high-lighted the phenomenon of cell death for the first time. However, technological limitations hindered the elucidation of the ultrastructural characteristics of cell death [2].

Cell death is a vital biological process that occurs in response to either normal physiological factors or pathological stress. It is typically divided into two main categories: Accidental Cell Death (ACD) and Regulated Cell Death (RCD) [3]. ACD happens as an uncontrolled reaction to severe and unexpected cellular damage that overwhelms the cell's regulatory systems. On the other hand, RCD relies on well-organized signaling pathways and precisely defined effector mechanisms. Among the various forms of RCD, apoptosis mainly driven by caspases has been widely studied and plays a crucial role in processes such as embryonic development [4], immune system maturation [5], and tumorigenesis [6].

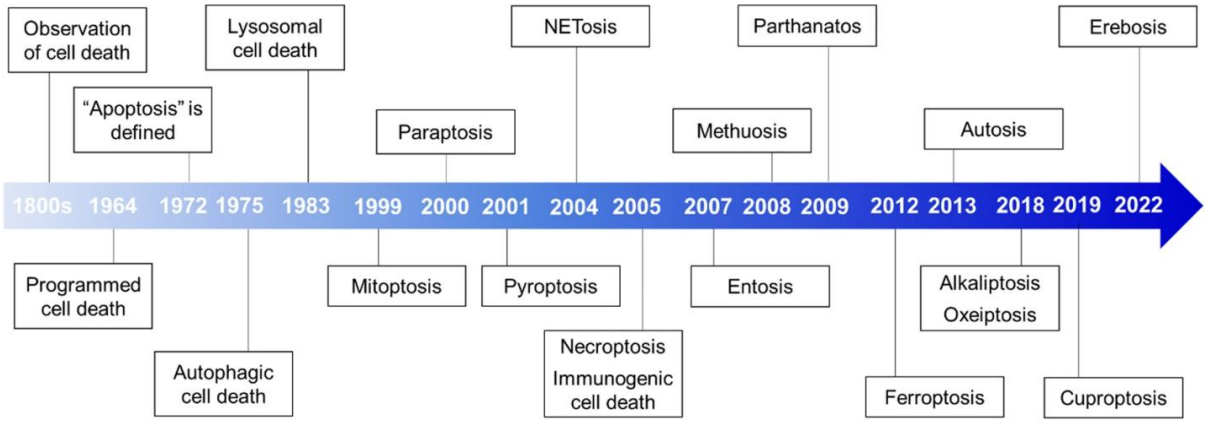

Figure 1. Timeline of discoveries in regulated cell death pathways [7].

Recent research has revealed various non-apoptotic forms of RCD (Fig. 1), each distinguished by specific morphological, biochemical, and genetic characteristics [8, 9]. These mechanisms are crucial for maintaining organismal homeostasis in both normal and disease conditions. Recent research has highlighted the unique machinery and (patho)physiological roles of various forms of regulated cell death, including apoptosis, necroptosis, pyroptosis, and ferroptosis [3] and others, as represented in Fig. 1. Below is a brief overview of various RCDs, while the ferroptosis process, as the primary focus of this dissertation, is described in detail in the next chapter.

Apoptosis

Apoptosis is a systematically organized process of cell death, often described as RCD, which was first identified in 1964 [10]. In 1972, Kerr, Wyllie, and Currie introduced the concept of apoptosis and outlined its morphological features, such as cell shrinkage, membrane blebbing, nuclear fragmentation, and pronounced chromatin condensation [2], as illustrated in Fig. 2. It occurs through two main pathways: the intrinsic and extrinsic pathways, both leading to the activation of caspases that execute cell death [2].

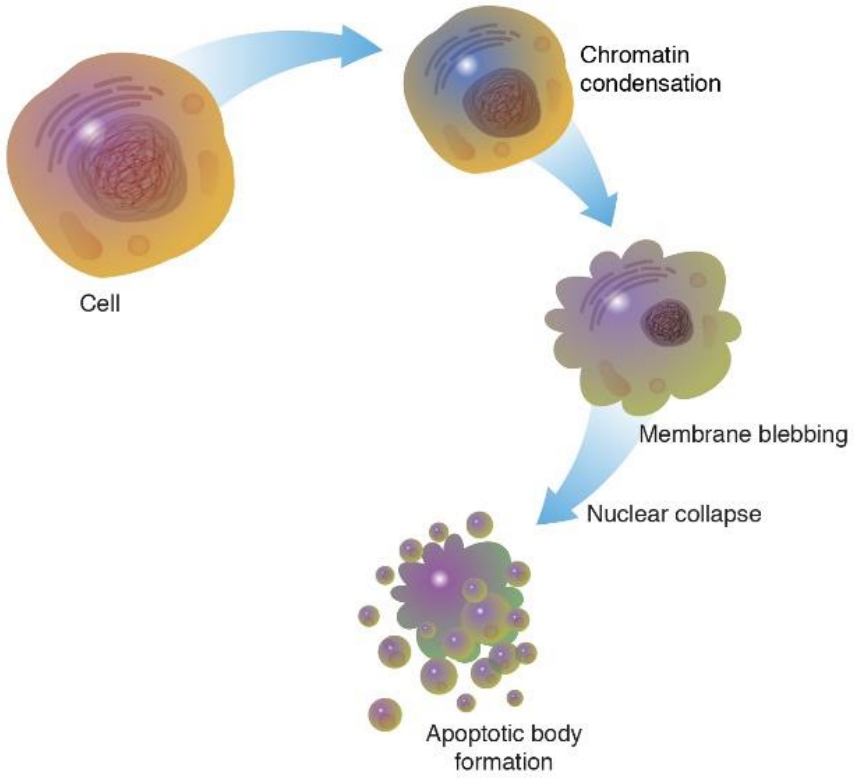

Figure 2. Schematic representation of a regulated cell death revealed by Vogt, further named apoptosis (Credits: National Human Genome Research Institute).

Apoptosis can be initiated via two primary signaling pathways. The intrinsic pathway entails the mitochondrial outer membrane permeabilization (MOMP), which is facilitated by pro-apoptotic regulators such as Bax and Bak [11]. This mechanism releases cytochrome c, which attaches to Apaf-1 to create the apoptosome, triggering the activation of caspase-9 and, in turn, executioner caspases such as caspase-3 and caspase-7, causing cellular disintegration [12, 13]. The extrinsic pathway is triggered by outside signals, involving ligands like tumor necrosis factor (TNF) that bind to death receptors, leading to the formation of the death-inducing signaling complex (DISC) with adaptor proteins and procaspase-8 [14, 15]. Both pathways of apoptosis are controlled by inhibitors of apoptosis proteins (IAPs) [16].

Necroptosis

Necroptosis is a type of regulated necrosis initiated by death receptors [17]. Cells that experience necroptosis display features such as cell swelling, a decrease in plasma membrane permeability, and eventual membrane rupture [18]. An essential feature of necroptosis is the disruption of the plasma membrane, leading to the liberation of Damage-Associated Molecular Patterns (DAMPs), such as mitochondrial DNA and the high-mobility group box 1 (HMGB1) protein [19]. These DAMPs can trigger a robust immune reaction and enhance inflammation [20].

Pyroptosis

Pyroptosis is a type of RCD that depends on the activation of caspases, caspase 1 in particular [21, 22] which activate members of the gasdermin family of proteins [23] causing cell lysis. Pyroptosis is initiated by proinflammatory signals and linked to inflammation such as interleukin (IL)-1β and IL-18 [24]. This form of cell death is mainly observed in inflammatory cells like macrophages and can be initiated by infections from bacteria or pathogens [25]. Additionally, pyroptosis is a crucial element of innate immunity and it triggers and enhances inflammation while eliminating the replication environment for intracellular pathogens [26].

Entotic cell death

Entotic cell death, which depends on a non-apoptotic pathway that does not require the apoptotic executioner to be activated [27], happens when one cell is engulfed or destroyed by another [28] and the dying cells don't display characteristic signs like nuclear condensation and fragmentation [29].

Lysosome-dependent cell death

Lysosome-dependent cell death (LCD) is a controlled type of cell death that happens when the membranes of lysosomes break down or by lysosomal membrane permeabilization [3]. This process naturally helps reshape tissue during mammary gland regression [30]. LCD is also linked to various diseases. Since cancer cells heavily rely on properly functioning lysosomes, scientists are exploring LCD as a potential target for cancer treatments [31].

Alkaliptosis

Alkaliptosis is a form of cell death triggered by excessive alkalinization of the cytoplasm, which disrupts ion homeostasis and can result in cellular dysfunction and ultimately cell death. This process is often part of the cellular stress response, occurring in reaction to metabolic disturbances that lead to an imbalance in pH levels [32]. As the cytoplasm becomes overly alkaline, the cell may struggle to maintain normal physiological functions, contributing to its demise.

Oxeiptosis

Oxeiptosis is RCD that occurs in response to oxidative stress. It involves signaling pathways activated by reactive oxygen species (ROS), leading to cell death that does not exhibit the typical characteristics of apoptosis [33]. Oxeiptosis plays a significant role in the body's response to oxidative damage, particularly in conditions where oxidative stress is common, such as chronic inflammatory diseases. This process helps to eliminate cells that may otherwise contribute to further tissue damage and inflammation.

1.2 Ferroptosis

Ferroptosis, an iron-dependent form of regulated cell death (RCD), distinct from apoptosis, necrosis, autophagy, and other RCD types, has garnered significant attention in recent years. Proposed by Brent R. Stockwell in 2012, ferroptosis is characterized by increased iron loading, leading to lipid peroxidation and distinct morphological changes in cells, such as mitochondrial shrinkage and altered membrane structure [34, 35]. This iron-dependent cell death process is regulated by multiple pathways involving glutamate and glutamine amino acid metabolism, lipid metabolism, and iron metabolism, making it a promising target for therapeutic interventions in

various diseases, including cancer, cardiovascular disorders, and liver damage [36]. The interplay between iron accumulation, lipid peroxidation, and antioxidant systems like glutathione peroxidase 4 (GPX4) highlights the complexity of ferroptosis and its implications in disease progression [37, 38]. Understanding the mechanisms of ferroptosis, its inhibitors and inducers, is crucial for developing targeted drugs that can effectively modulate this cell death pathway for the treatment of common human diseases.

Comparing ferroptosis with these traditional RCD programs provides valuable insights into its occurrence and characteristics, shedding light on its potential as a key player in cell proliferation, differentiation, and senescence [39].

Excessive lipid peroxides, particularly oxidized particularly oxidized polyunsaturated fatty acids (PUFA) and their derivatives, are central to ferroptosis. Other lipid oxidation products, such as 4-HNE, 8-OHdG, and malondialdehyde, are also proposed markers [40-42]. Also a few protein biomarkers, extracellular decorin (DCN) released by ferroptosis-prone pancreatic ductal adenocarcinoma (PDAC) cells and the accumulation of transferrin receptor (TFRC) on the plasma membrane have been identified as ferroptosis markers, although detection timing and variability in cellular responses may limit their effectiveness [43, 44]. Hyperoxidized peroxiredoxin 3 (PRDX3) has been identified as a ferroptosis-specific marker, especially in cells treated with ferroptosis inducers like erastin and RSL3. It has shown utility in distinguishing ferroptosis from other forms of cell death (apoptosis and necroptosis) and has been used in studying liver diseases in mice [45]. Glutathione (GSH) and GPX4, key regulators of ferroptosis, are commonly used as biomarkers.

Formation of lipid peroxides leads to ferroptosis

The plasma membrane serves as a primary barrier guarding cells against the extracellular environment, making it central to homeostatic maintenance. The rupture of the plasma membrane unequivocally leads to cell death, marking the cataclysmic endpoint for cellular life. Notably, this membrane rupture is the hallmark of necrotic cell death, except in apoptosis, where plasma membrane integrity is preserved [46]. Ferroptosis damages and integrity of the membrane, mechanistically, it has been considered excessive (phospho)lipid peroxidation in cellular membranes caused by disruption of the antioxidant defense system, disrupting membrane integrity and ultimately leading to cell death with plasma membrane rupture [34].

Ferroptosis is a regulated form of cell death characterized by the accumulation of lipid peroxides, which can arise from both enzymatic and non-enzymatic processes. Enzymatically, lipoxygenases (LOXs) play a pivotal role by catalyzing the incorporation of oxygen into polyunsaturated fatty acids (PUFAs) at precise position, leading to the formation of particular type of lipid peroxides critical for ferroptotic signaling [47, 48]. There are also other enzymes that are contributing to that process. For example, Acyl-CoA synthetase long-chain family 4 (ACSL4) converts PUFAs into acyl-CoA, facilitating their incorporation into phospholipids, which can then be oxidized to generate reactive lipid species [49]. Lysophosphatidylcholine acyltransferase 3 (LPCAT3) further contributes to this process by esterifying acyl-CoA to phospholipids, thus promoting the synthesis of oxidized phospholipids implicated in ferroptosis [50]. In contrast, non-enzymatic processes, such as lipid autoxidation and the Fenton reaction, also significantly contribute to ferroptosis. Lipid autoxidation is initiated by reactive oxygen species (ROS), resulting in a chain reaction that oxidizes PUFAs in cellular membrane [51], while the Fenton reaction generates hydroxyl radicals through the reaction of iron with hydrogen peroxide, leading to further lipid peroxidation [52]. However, those are oxidized at random positions when more bis-allylic carbons are available. Together, these enzymatic and non-enzymatic pathways underscore the complexity of ferroptosis and highlight potential therapeutic targets for modulating this process in various diseases.

Inhibition mechanisms of ferroptosis

Initially, my Ph.D. research aimed to identify potential inhibitors for 15LOX-1. However, since similar work has already been conducted by researchers worldwide [53], we decided to discontinue this focus. Instead, I would like to explore and write about the host inhibition mechanisms of ferroptosis.

Several mechanisms have been identified that inhibit this process, offering potential therapeutic strategies for diseases like cancer. Ferroptosis suppressor protein 1 (FSP1) plays a pivotal role in preventing ferroptosis through multiple mechanisms. One of the primary pathways involves the FSP1-coenzyme Q10 (CoQ10)-NAD(P)H axis, where FSP1 catalyzes the reduction of CoQ10, which acts as an antioxidant to prevent lipid peroxidation [54]. Another important pathway is the tetrahydrobiopterin (BH4) pathway, which involves GTP cyclohydrolase 1 (GCH1). This pathway contributes to ferroptosis resistance by producing BH4, a radical-trapping antioxidant that helps mitigate lipid peroxidation. By modulating the levels of PUFAs in cellular membranes, BH4 plays

a critical role in maintaining membrane stability during oxidative stress conditions [55]. GPX4 is essential for protecting cells against ferroptosis by reducing lipid peroxides in a glutathione-dependent manner. Inhibition of GPX4 leads to the accumulation of toxic lipid peroxides, triggering ferroptotic cell death. Thus, maintaining GPX4 activity is vital for cellular resistance to ferroptosis [56]. Additionally, metabolic products such as indole-3-pyruvate (I3P), generated by the enzyme interleukin-4-induced-1 (IL4I1) from tryptophan, exhibit anti-ferroptotic properties through radical scavenging and activation of protective gene expression pathways [57]. Phospholipase iPLA$_2$β helps prevent ferroptosis by breaking down specific oxidized lipids, especially 15-HpETE-PE, which is produced either by 15LOX in complex with PEBP1 or by 15LOXs alone [58, 59]. Dihydroorotate dehydrogenase (DHODH) inhibits ferroptosis in tumor cells by reducing P53 activity, a key tumor suppressor that promotes ferroptosis under oxidative stress. This suppression lowers ALOX15 expression, gene involved in lipid peroxidation, thereby decreasing lipid peroxide production [60]. A new thiol-independent defense mechanism in epithelial cells against Pseudomonas aeruginosa (PA) has been discovered, involving inducible nitric oxide synthase (iNOS) and nitric oxide (NO•). This process, demonstrates how NO• produced by macrophages inhibits ferroptosis in epithelial cells through intercellular communication [61]. Finally, the activation of AMP-activated protein kinase (AMPK) during glucose deprivation has been shown to inhibit PUFA biosynthesis, thereby limiting the substrates available for lipid peroxidation [62]. Recent findings revealed that ferroptosis can be inhibited through the development of highly selective inhibitors, known as FerroLOXINs (FerroLOXIN-1 and FerroLOXIN-2), which target the catalytic complex of 15LOX-2/PEBP1 [63].

1.3 Studied bio-molecular systems

Lipoxygenases (LOXs) are iron-containing enzymes that catalyze the oxygenation of PUFAs, playing a key role in lipid metabolism and biological processes such as inflammation. Phosphatidylethanolamine-binding protein 1 (PEBP1), also known as Raf kinase inhibitor protein (RKIP), is a multifunctional protein involved in regulating apoptosis, lipid metabolism, and signal transduction pathways [64]. Apart from proteins such as 15LOX-1 and PEBP1, we also examined the effects of substrates and a biological membrane composed of 1,2-Dioleoyl-sn-glycero-3-

phosphocholine (DOPC) (50%), 1,2-Dioleoyl-sn-glycero-3-phosphoethanolamine (DOPE) (30%), and the preferred substrate of 15LOX-1/PEBP1, 1-stearoyl-2-arachidonyl-phosphoethanolamine (SAPE) (20%). The structural representations of PUFA substrates are shown in Fig. 3.

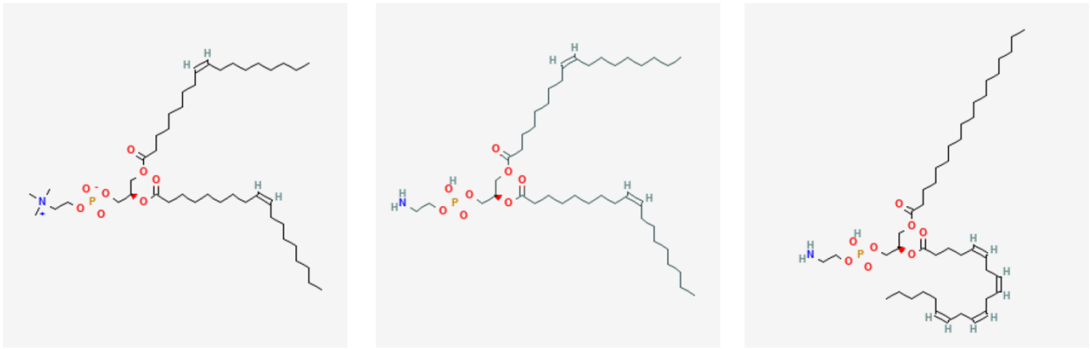

Figure 3. The structures of phospholipids that compose the membrane used in MD simulations. From left to right: DOPC with the molecular formula $C_{44}H_{84}NO_8P$, DOPE with the molecular formula $C_{41}H_{78}NO_8P$, and SAPE with the molecular formula $C_{46}H_{84}NO_8P$.

These LOXs and PEBP1 are central to understanding cellular mechanisms and are extensively studied in my thesis for their roles in the biophysical processes of ferroptosis and their interactions and dynamics with biological membranes and substrates. Previous investigations by my supervisor and collaborators into ferroptosis are detailed in the following publications [47, 59, 65-67].

15-lipoxygenase

LOXs are a family of non-heme iron-containing enzymes that catalyze the oxygenation of PUFAs to form lipid hydroperoxides and are found widely in nature and are abundant in plants and animals [68]. These enzymes play significant roles in various biological processes, including inflammation, cell differentiation, and programmed cell death, particularly ferroptosis [69]. PUFAs containing cis double bonds are the substrates of these enzymes. Linoleic and linolenic acids (18-carbon fatty acids) and arachidonic acid (AA; 20-carbon fatty acid) are the most common substrates for LOXs in plants and animals, respectively [70, 71]. The nomenclature of these enzymes is based on the specific position of the carbon on substrates that is oxygenated. For example, 9-LOX and 13-LOX are important LOXs in plants, whereas 5-LOX, 12-LOX, and 15-LOX are found in animals [72].

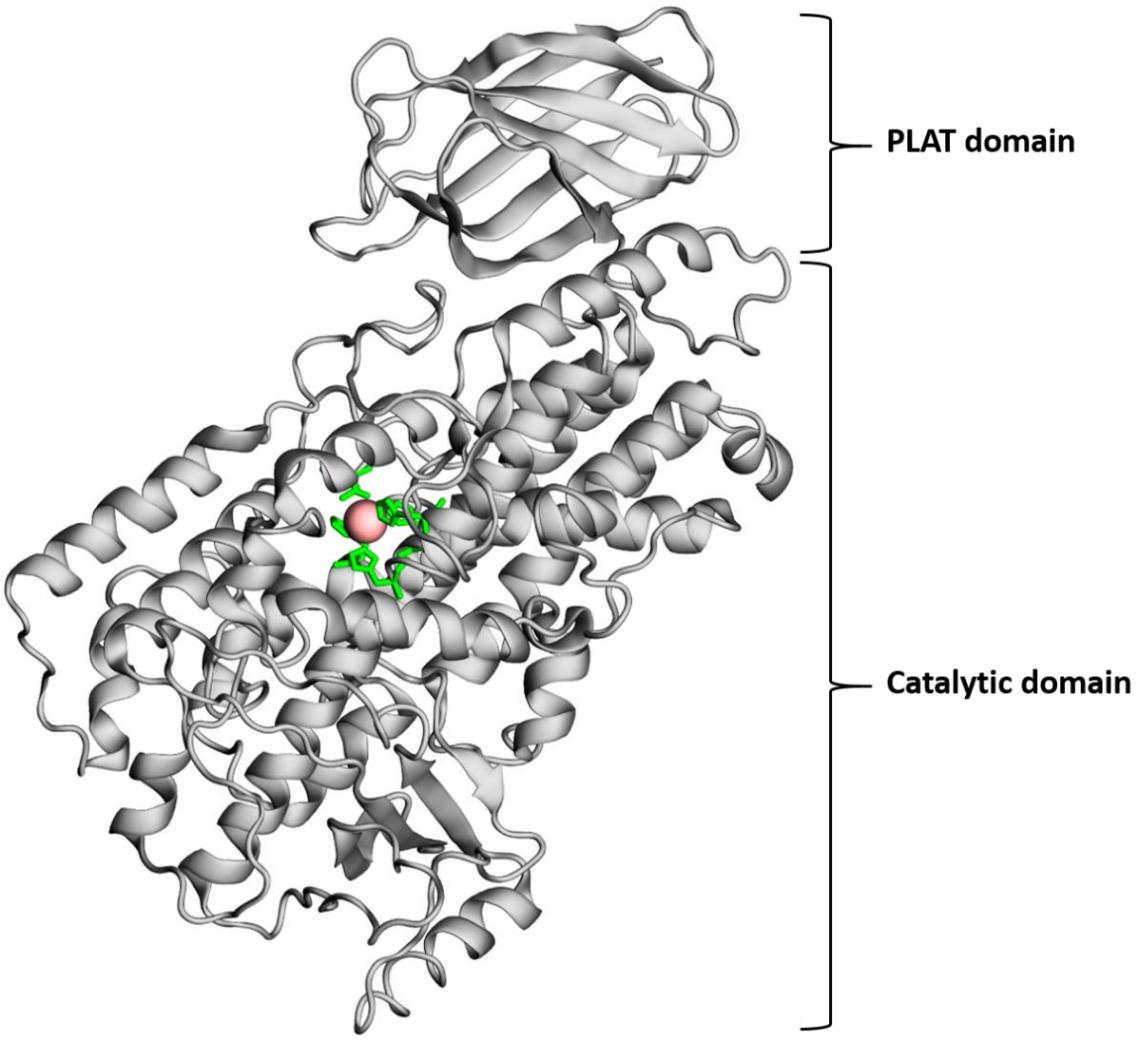

Figure 4. Crystal structure of human 15LOX-1. The iron atom is shown as a pink sphere, and catalytic residues, including H365, H540, H544, and I662, are depicted as green sticks.

The structure of human 15LOX-1, illustrated in Fig. 4, was built through homology modeling using the rabbit 15LOX-1 structure (PDB: 2P0M [73]) in the Swiss Model server [74]. The sequence similarity between human 15LOX-1 and rabbit LOX is greater than 81%. 15LOX-1 consists of 662 amino acids length with a total structural weight of 150.89 kDa. Its structure includes two main domains: a β-barrel domain, also known as the PLAT domain (G2-R114), and a catalytic domain (T115-I662).

Phosphatidylethanolamine-binding protein 1

Phosphatidylethanolamine-binding protein 1 (PEBP1) is a multifunctional protein that plays a key regulatory role in several cellular processes, including signal transduction, apoptosis, and lipid metabolism [75]. PEBP1 has an alternative name, Raf kinase inhibitor protein, or RKIP. PEBP1 suppresses cancer metastasis by targeting various stages, such as epithelial-to-mesenchymal transition (EMT), cell migration, and invasion [76, 77]. PEBP1 is primarily recognized for its specific binding to phosphatidylethanolamine and its capacity to inhibit the Raf1-MAPK pathway [78]. Several studies have also suggested its potential as a biomarker for Alzheimer's disease (AD) [79, 80]. PEBP1 is found most abundantly in the brain, especially in the hippocampus region, though it's also present in organs like the liver and kidneys [81].

PEBP1 interacts with many different protein partners in cells. It blocks the activity of Raf-1, which prevents signals from being sent through MEK and ERK proteins – this control is essential for proper cell growth and development [82]. PEBP1 also stops several other important cellular processes: it blocks the NF-κB signaling pathway by interacting with IKK, prevents cell death through necroptosis by binding to and inhibiting RIP3 [82, 83], and reduces starvation-triggered autophagy by interacting with LC3 [84].

Furthermore, the transcription factor BTB and CNC homology 1 (BACH1) is negatively regulated by RKIP or PEBP1 and promotes breast cancer metastasis [85]. PEBP1 has gained significant attention for its role in modulating ferroptosis through its interaction with 15-lipoxygenases (15LOXs). PEBP1 is a small, conserved protein known for its ability to bind phosphatidylethanolamine (PE), a major phospholipid component of cell membranes [47].

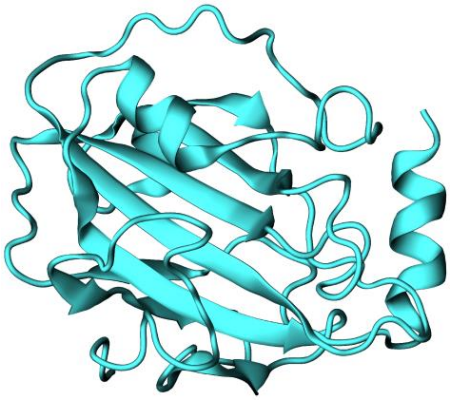

Figure 5. Crystal structure of human PEBP1. One chain is displayed (PDB: 1BEH).

PEBP1 shown in Fig. 5 consist of 187 amino acids length and the total structure weight of 42.17 kDa. To find the interaction between 15LOX-1 and PEBP1, we used four monomers in our protein-protein docking approach (PDB: 1BEH chain A, 1BEH chain B, 1BD9 chain A, 1BD9 chain B).

15LOX-1/PEBP1 complex

PEBP1 forms complexes with both isoforms, 15LOX-1 and 15LOX-2 that promotes phospholipid peroxidation, a key event leading to ferroptotic cell death [47]. The two isoforms, 15LOX-1 and 15LOX-2, differ significantly in tissue distribution, substrate specificity, and roles in various biological processes. 15LOX-1 is mainly expressed in leukocytes, such as eosinophils and macrophages, and in epithelial tissues like the gastrointestinal tract and lungs, while 15LOX-2 is found predominantly in epithelial tissues like the prostate, skin, and cornea, with limited expression in lung and retina tissues, and is notably absent in peripheral blood leukocytes [86-88]. In terms of enzymatic specificity, 15LOX-1 has dual positional specificity, converting arachidonic acid to both 15-HETE and 12-HETE (15-HpETE-PE and 12-HpETE-PE for SAPE), allowing it to produce a broader range of lipid mediators [89]. In contrast, 15LOX-2 exhibits singular positional specificity, primarily generating 15-HETE [90] (15-HpETE-PE for SAPE). 15LOX-1 is involved in the nonimmunogenic clearance of apoptotic cells (ACs) through a process called efferocytosis, which is essential for preserving tissue homeostasis and avoiding chronic inflammation. In macrophages, 15LOX-1 oxidizes PUFAs, such as arachidonic acid, generating lipid mediators that promote the identification and removal of ACs by phagocytic cells [91]. 15LOX-2, on the other hand, is involved in SPM synthesis as well as in maintaining cholesterol homeostasis [92]. Despite these functional differences, they share a significant degree of structural similarity, with about <30% sequence identity [93, 94]. PEBP1 binds to 15LOX-1, altering its substrate specificity from free PUFAs to PUFA-containing phosphatidylethanolamines (PEs). This binding is crucial for the oxidative activity of 15LOX-1, enabling it to catalyze the oxidation of PUFA-PEs, which are particularly vulnerable to peroxidation due to their unsaturated bonds. The representation of the 15LOX-1/PEBP1 complex is shown in Fig. 6a.

The production of pro-ferroptotic lipid peroxides is catalyzed by a complex created from 15LOX and PEBP1 [47]. This interaction is crucial as PEBP1 modifies the substrate specificity of 15LOX-1, allowing it to oxidize PE-bound PUFAs rather than free fatty acids. The interaction with PEBP1 not only stabilizes the enzyme but also increases its catalytic effectiveness on

phosphatidylethanolamine substrates that contain arachidonic acid (C20:4, AA), or adrenic acid (C22:4, AdA) [62] or SAPE [65, 93]. The enzyme converts Fe^{2+} to Fe^{3+}, creating a ferric iron-hydroxy complex that abstracts a hydrogen at carbon atom C13 and inserting an oxygen molecule at C15 resulting in the 15-HpETE-PE product and occasionally abstract a hydrogen at the C10 atom to generate an alternative product, 12-HpETE-PE [95]. The accumulation of lipid hydroperoxides such as 15-HpETE-PE and 12-HpETE-PE is associated with ferroptosis. The stages of lipid peroxidation that contribute to ferroptosis are depicted in Fig. 6b.

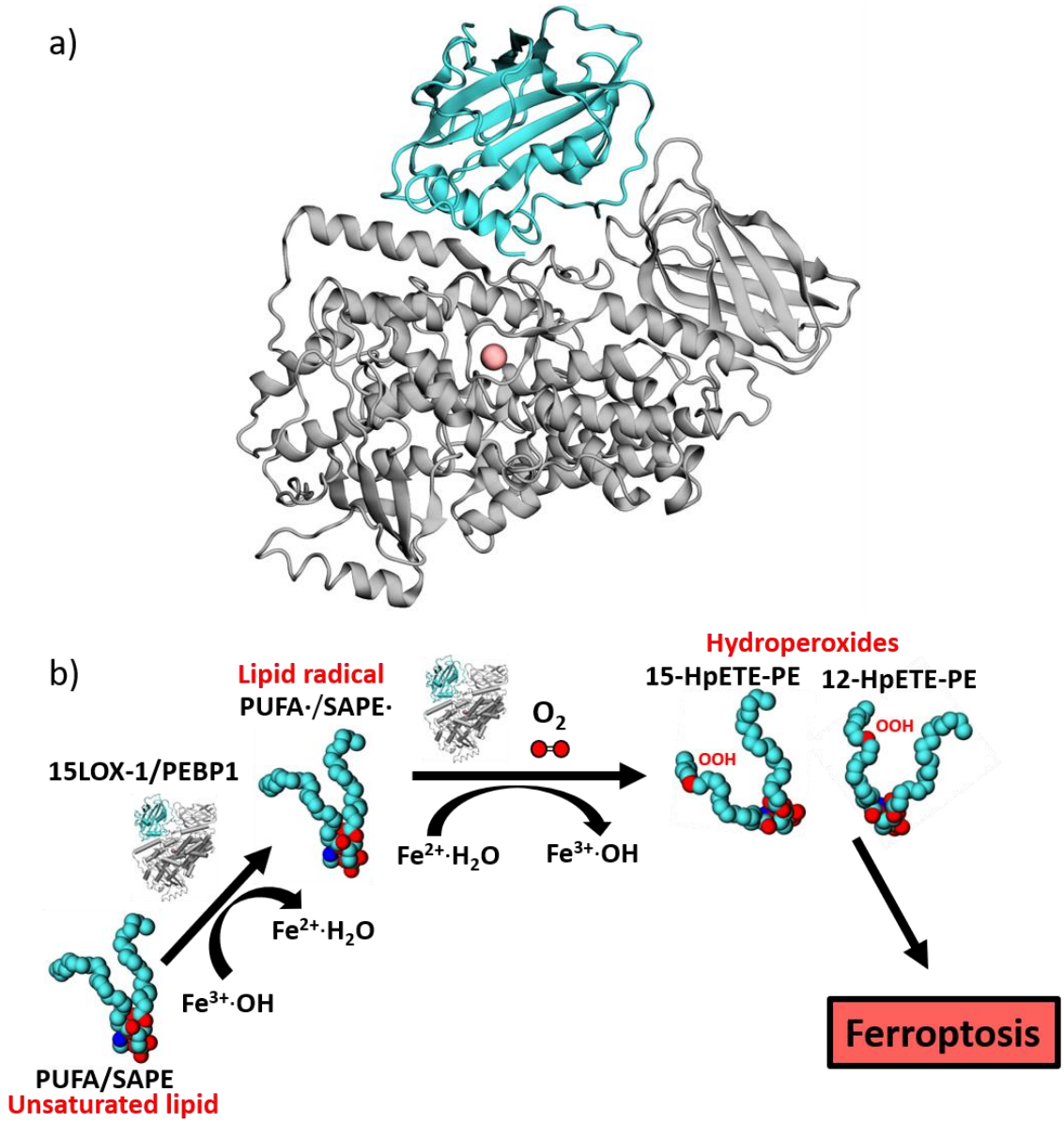

Figure 6. Lipid peroxidation mechanism of ferroptosis mediated by 15LOX-1/PEBP1 complex. (a) The structural representation of the human 15LOX-1/PEBP1 complex, with 15LOX-1 shown in gray and

PEBP1 highlighted in cyan. The pink sphere denotes the iron cofactor within the catalytic site of 15LOX-1. (b) The sequential steps of lipid peroxidation leading to ferroptosis. Unsaturated lipids (left) undergo hydrogen abstraction by 15LOX-1, generating lipid radicals, and finally, lipid hydroperoxides, such as 15-HpETE-PE and 12-HpETE-PE (right), which trigger ferroptotic cell death. For visual clarity, hydrogen atoms were omitted in the molecular representations.

1.4 Computational biophysics methods

Molecular docking

Molecular docking is one of the most widely used computational methods in structure-based drug design and has been extensively employed since the early 1980s [96]. It is the preferred tool when the three-dimensional (3D) structure of the target protein is available. The growing popularity of molecular docking has been driven by advancements in computational power, the increasing availability of small molecule and protein structures, and easier access to these resources. The primary aim of molecular docking is to understand and predict molecular recognition, both in terms of structure (identifying potential binding modes) and energetics (predicting binding affinity) [97]. Initially, molecular docking focused on interactions between small molecules (ligands) and target macromolecules (proteins). However, over the past decade, interest has expanded to include protein-protein docking, nucleic acid (DNA and RNA)-ligand docking, and nucleic acid-protein-ligand docking [98]. Molecular docking has found applications across various fields in physical and chemical sciences, such as understanding ligand-protein interactions, structure elucidation, virtual screening for drug discovery [99], drug repurposing [100], studying signal transduction.

Protein-protein docking is a rapidly growing area of research due to its potential in predicting protein-protein interactions (PPIs) and identifying key residues at the protein-protein interface [101]. While it shares the basic principles with protein-small molecule docking, protein-protein docking presents unique challenges, particularly in exploring the vast conformational space. Even for relatively rigid proteins, it is difficult to account for the rotational and conformational space of possible orientations that two proteins might adopt during interaction. This complexity leads to a significant computational cost due to the large number of degrees of freedom involved [102]. Because protein-protein interfaces tend to be large, flat, and lack distinct pockets, the search algorithms used for protein-protein docking must differ from those used in protein-ligand docking

[103]. The dynamic nature of proteins adds another layer of complexity, as they continuously transition between various conformers with different energy states. Capturing this inherent flexibility during docking remains a significant challenge [104].

HDOCK is a web server for modeling protein-protein and protein-DNA/RNA complex structures based on a hybrid docking algorithm that combines template-based modeling and ab initio free docking [105]. We used HDOCK for protein-protein docking to find the 15LOX-1/PEBP1 complex and Smina program for protein-substrate docking to find the spatial structure of 15LOX-1/PEBP1/SAPE complex. Smina is a fork for AutoDock Vina [106] that provides enhanced support for minimization and scoring [107].

Molecular dynamics simulations

Molecular dynamics (MD) is a computer-based technique that predicts how atoms and molecules move over time by calculating their motion using Newton's physics laws [108]. MD simulations have resulted in significant progress across various scientific fields, including chemistry, materials science, and biophysics [109]. This computational approach has shown significant importance in the thorough characterization of biomolecular systems such as proteins, nucleic acids, lipid membranes at atomic resolution across timescales from nanoseconds to microseconds [110].

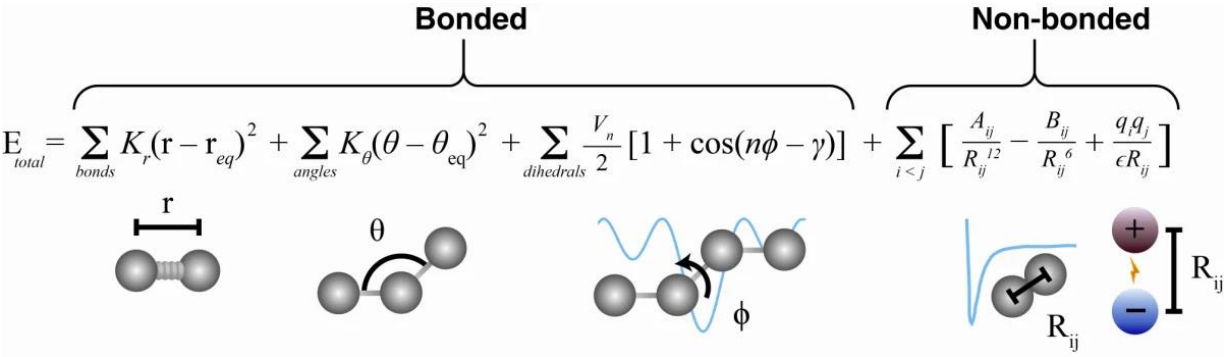

Figure 7. Molecular mechanics potential energy function. Illustrating the contributions from bonded interactions (bonds, angles, and dihedrals) and non-bonded interactions [111, 112] (van der Waals and electrostatics). These components form the basis for energy calculations in molecular dynamics simulations [113]. Bonded terms are bond stretching (r: bond length, r_{eq}: equilibrium bond length, k_b: bond force constant), angle bending (θ: bond angle, θ_{eq}: equilibrium bond angle, k_θ: angle force constant), and dihedral torsion (ϕ: dihedral angle, V_n: barrier height, n: periodicity, γ: phase angle). Non-bonded terms include Van der Waals interactions (A_{ij},B_{ij}: constants, R_{ij}: distance between atoms i and j) and electrostatic interactions (q_i, q_j: atomic charges, ϵ: dielectric constant, R_{ij}: distance between charges).

A force field function is made up of two main elements: bonded and non-bonded, which are illustrated in Fig. 7 [114] depicts the overall potential energy (E_{total}) of a molecular system. Force fields are fundamental tools for understanding the potential energy within particle systems. They are constructed using parameters obtained from experimental data and quantum mechanical analyses of both biological molecules and small molecules [115]. Various force fields, including AMBER [113], CHARMM [116], GROMOS [117], and OPLS-AA [118], are commonly employed for biomolecular simulations.

To replicate experimental conditions, MD simulations must consider various physical parameters, such as temperature and pressure. Protein simulations are often performed in a canonical (NVT) or isothermal-isobaric (NPT) ensemble, particularly during the equilibration phase. The protein is placed in a simulation box and solvated with an explicit solvent. Common water models used for this purpose include TIP3P, TIP4P, TIP5P, SPC, and SPC/E. These models, based on quantum mechanics and validated by experiments [119], simulate complex hydration dynamics such as solvent dipole orientation, electrostatic shielding, hydrogen bonding, and hydrophobic interactions. Due to the time limitations of MD simulations and the complex quantum nature of hydrogen bonds, explicit treatments of hydrogen bonds are often approximated. Techniques like the SHAKE algorithm [120] are employed to maintain solvent hydrogen positions by constraining bond lengths involving hydrogen atoms. Implicit solvent models are sometimes used to approximate the solute's potential of mean force, averaging over the solvent's degrees of freedom. To maintain charge neutrality in the system, ions are often added, replacing some solvent molecules. Periodic boundary conditions are frequently applied, replicating the system in all directions to avoid edge effects and ensure the conservation of mass and particle number. Long-range electrostatic interactions in these periodic systems are typically handled using the Ewald summation method [121].

Energy minimization aims to identify the system's global minimum energy configuration by optimizing the atomic geometry to a state where the net attractive forces on each atom are maximized [116]. Two common techniques for energy minimization are the steepest descent and conjugate gradient methods. The steepest descent method, a first-order iterative approach, uses the gradient of the potential energy surface to guide the system toward the nearest energy minimum [122]. Additionally, correcting the protonation states of titratable residues is crucial for accurate

simulations. This can be achieved through methods like Free Energy Perturbation (FEP) [123] in MD simulations or by using continuum electrostatics models such as Finite Difference Poisson-Boltzmann (FDPB) [124] or Protein Dipole-Langevin Dipole (PDLD) [125]. These methods help account for the electrostatic environment, ensuring the system's protonation states are correctly represented.

During the heating phase of MD simulations, atoms are initially assigned velocities corresponding to a temperature of close to 0 K, and the system's temperature is gradually increased by adjusting these velocities. Newton's equations of motion are integrated over time to evolve the system, with constraints on various regions being progressively removed as the system heats up and structural tensions relax. Thermalization typically occurs at constant volume using Langevin dynamics [126].

Following the heating phase, equilibration is conducted to balance the kinetic and potential energies, ensuring that the kinetic energy introduced during heating is evenly distributed among all degrees of freedom [87]. In simulations involving explicit solvents, the position of the protein is initially fixed while the solvent equilibrates around it. Once the solvent has reached equilibrium, constraints on the protein are lifted, allowing the entire system to evolve cohesively.

The final step, the production phase, involves running the simulation for the desired timescale, typically ranging from hundreds of picoseconds to microseconds or longer, without constraints on the protein. This phase generates a trajectory of the protein under specific equilibrium conditions like NVT, NPT, or NVE ensembles [127]. Recently, in MD simulations, machine learning has accelerated simulations by predicting molecular behaviors and optimizing energy landscapes, thereby reducing computational costs [128]. Additionally, ML can handle large datasets from MD simulations, extracting meaningful features and enhancing insight into molecular interactions, with convolutional neural networks (CNNs) being particularly effective for image-based data processing [129].

Full-atomic MD simulations were performed using NAMD [130] package and the CHARMM36m force field, and 2 fs time steps. The proteins were solvated with explicit water (TIP3P) at physiological salt concentrations. CHARMM force field parameters for bonded iron were obtained using Gaussian [131] (DFT B3LYP/6–31(d,p) method). We performed two sets of simulations for each system, with and without membrane. Prior to productive runs without membrane, the following

protocol was adopted: 0.2 ns of water equilibration, 10,000 steps of minimization, 0.35 ns of heating from 0 to 300 K, and 0.15 ns equilibration of the whole system. A cutoff of 12 Å for non-bonded interactions was applied. Langevin dynamics and the Langevin piston algorithm were used to maintain the temperature at 300 K [132] and the pressure at 1 atm [133]. Simulations with the membrane composed of 1,2-dioleoy-sn-glycero-3-phosphocholine (DOPC, 50%), 1,2-dioleoy-sn-glycero-3-phosphoethanolamine (DOPE, 30%), and 1-stearoyl-2-arachidonyl-phosphoethanolamine (SAPE, 20%) were prepared in CHARMM GUI server [134]. We used the PPM/OPM [135] server to predict the orientation of the protein complex in the membrane.

2. Publications constituting the dissertation

This dissertation investigates the biological mechanism of ferroptosis, a form of cell death triggered by a complex formed between the enzyme 15-lipoxygenase-1 (15LOX-1) and its binding partner phosphatidylethanolamine (PE)-binding protein 1 (PEBP1), in the presence of different components, such as the substrate SAPE, O_2 molecules, and a biological membrane. Computational biophysical approaches, including molecular dynamics simulations and molecular docking calculations, were employed to model and analyze the interactions between these components and their effect on the ferroptosis mechanism. The findings are presented in three articles, referred to as articles A, B, and C**.**

Article A examines the use of computational structural modeling techniques, such as molecular docking, to study the complex formation between human 15LOX-1 and PEBP1. Additionally, MD simulations were performed to observe the evolution of conformational changes within the 15LOX-1/PEBP1 complex. The study demonstrates that the association of the human 15LOX-1/PEBP1 complex with cellular membranes induces significant conformational adjustments, facilitating access to the catalytic site for specific substrates, particularly stearoyl/arachidonoyl-PE (SAPE). This binding stabilizes the complex and enhances its catalytic activity, supporting lipid peroxidation reactions that generate hydroperoxy derivatives, such as 15-HpETE-PE or 12-HpETE-PE in a ratio of 5:1. Furthermore, the study examines experimentally observed mutations using MD simulations of H86A, H86E, P74L, and P112E on PEBP1 and their potential

effects on complex formation. Evaluations of the predicted 15LOX-1/PEBP1 interactions with PEBP1 mutants at residues participating in interfacial interactions with 15LOX-1, both in silico and through liquid chromatography-mass spectrometry (LC-MS) experiments provided by our collaborators, revealed the key role of residue P112. These findings, supported by experimental validation, present significant opportunities for developing novel therapeutics that specifically target 15LOX-1/PEBP1 complexes, providing valuable insights into ferroptotic processes and the detailed biophysical mechanisms of 15LOX-1/PEBP1 at the atomic scale.

Article B elaborates on WatFinder, a tool developed and integrated into the ProDy framework, an open source Python package used by the scientific community (> 2 mln downloads), to identify and visualize protein-water interactions, including water bridges and clusters, which are important for understanding protein dynamics and stability. It supports ensemble analysis to track interaction patterns and temporal changes in explicit water environments. WatFinder provides raw data, statistical outputs, and visualizations to evaluate recurrent protein-water interaction patterns and their probabilistic occurrence. It supports various input formats, such as PDB, mmCIF, and MD trajectory files (DCD format), enabling the analysis of individual structures, ensembles of NMR models, homologous structures, or molecular dynamics simulations. WatFinder aids in understanding biophysical processes by providing insights into hydration dynamics to support applications in drug design, enzyme catalysis, and membrane protein studies.

Article C investigates oxygen diffusion pathways in human 15LOX-1 under varying oxygen concentrations and in the presence of key components, including the substrate SAPE, binding partner PEBP1, and the membrane environment. The study demonstrates that membrane and substrate SAPE binding open the 15LOX-1/PEBP1 complex, enhancing O_2 acquisition at the catalytic site. Sequence and structural comparisons among different LOX family members revealed conserved residues and motifs for O_2 transport through two identified tunnels: *Entrance A* (I-[ND]-x-x-[AG]-R-x-x-L-[IV]) and *Entrance B* ([ST]-H-[LW]-[AL]-x-x-H-[LA]). Moreover, two O_2 binding sites were identified at the 15LOX-1 catalytic site: one supports single oxidation, while the other may facilitate double oxidation of the substrate. Additionally, lipidomics experiments provide insights into the formation of oxidized products by the 15LOX-1/PEBP1 complex, pointing to both single- and double-oxidized products. Moreover, frequently observed water clusters at the catalytic site found among 140 crystal structures of LOX family members

may potentially stabilize O_2 transport and/or aid product release. These findings advance our understanding of 15LOX activity and open new avenues for exploring targeted interventions to modulate ferroptosis, with potential implications for therapeutic strategies and biophysical processes in diseases involving lipid peroxidation.

3. Author Contribution statement

This thesis consists of three papers. In the first paper A, I was the first author. In the second paper B, I was a co-author. In the third paper C, I am the first author, and it is available as pre-print on SSRN.

Hereby, I declare that my contributions to the paper A are as follows:

> **Manivarma, T**., Kapralov, A. A., Samovich, S. N., Tyurina, Y. Y., Tyurin, V. A., VanDemark, A. P., Nowak, W., Bayir, H., Bahar, I., Kagan, V. E., & Mikulska-Ruminska, K. (2023). *Membrane regulation of 15LOX-1/PEBP1 complex prompts the generation of ferroptotic signals, oxygenated PEs*. Free Radic Biol Med, 208, 458-467.
>
> Impact factor: 7.1, MNiSW points: 140, Q1

As the first author, I conducted the molecular docking of the protein-protein interaction (15LOX-1 and PEBP1) using HDOCK, as well as the molecular docking of the protein-substrate complex (15LOX-1/PEBP1 and SAPE substrate) using Smina tool. Molecular dynamics simulations of 15LOX-1/PEBP1 with and without a membrane were performed using NAMD package, as described in sections 3, 3.1, and 3.2. The initial setups for the membrane-based simulations were prepared via the CHARMM-GUI server. Additionally, I prepared simulations with point mutations in PEBP1 (P112E, H86A, H86E, and P74L) as described in section 3.3. Simulations were performed on NVIDIA GeForce RTX 3090 clusters, and figures (most of the panels in Figures 1-3 and 5) were created using the VMD program, with plots generated using Python. I also wrote a Tcl script to compute the time evolution of the angle θ for the 15LOX-1/PEBP1 complex shown in Figure 2.

Hereby, I declare that my contributions to the paper B are as follows:

> Krieger, J. M., Doljanin, F., Bogetti, A. T., Zhang, F., **Manivarma, T**., Bahar, I., & Mikulska-Ruminska, K. (2024). *WatFinder: A ProDy tool for protein-water interactions*. Bioinformatics.
>
> Impact factor: 4.4, MNiSW points: 200, Q1

As a co-author, I was responsible for testing all functions and verifying various parameters to assess water clusters using different files, including PDBs, PDB ensembles, and trajectory files. Tests were performed on various biological systems, starting from single- to multiple-chain systems like chaperones, with parallel computations also being conducted to enhance efficiency and scalability.

Hereby, I declare that my contributions to the paper C (under review in *Redox Biology* journal, available on SSRN as pre-print) are as follows:

Link to the paper : https://papers.ssrn.com/sol3/papers.cfm?abstract_id=5060100

> **Manivarma T**, Nowak W, Tyurina YY, Tyurin VA, Bayir H, Kagan VE, Mikulska-Ruminska K. (2024). *The presence of substrate warrants oxygen access tunnels toward the catalytic site of lipoxygenases*. SSRN. *(under review in Redox Biol)*
>
> Impact factor: 10.7, MNiSW points: 140, Q1 (if accepted)

As the first author, I conducted simulations of 15LOX-1/PEBP1 under various oxygen concentrations (1 O_2, 2 O_2, and 15 O_2). These simulations were performed both with and without the substrate SAPE, as well as in the presence or absence of a membrane, totaling 20 μs of simulation time. Additionally, I carried out multiple sequence alignment, electrostatic potential surface analysis, and perturbation response scanning analysis. I also used the WatFinder tool to identify oxygen and water clusters in the MD simulations. I created figures (most of the panels in Figures 1–5) using VMD, with plots generated in Python. All simulations were conducted on an NVIDIA GeForce RTX 3090 GPU Clusters.

4. The aims of the PhD project

The aims of the doctoral thesis were to:

1. Examine the dynamics and interactions of the 15LOX-1/PEBP1 complex in the presence of a phospholipid membrane and the substrate SAPE at the atomic level.

2. Explore the structural changes in the 15LOX-1/PEBP1 complex induced by membrane association and substrate SAPE binding and how these interactions facilitate substrate access to the catalytic site and regulate enzymatic activity.

3. Evaluate the impact of PEBP1 mutations at interfacial residues on the formation of the 15LOX-1/PEBP1 complex and its peroxidation mechanism.

4. Investigate the contribution of PEBP1 to substrate specificity and product generation (15-HpETE-PE and 12-HpETE-PE) on the catalytic activity.

5. Explore how the membrane environment influences the structural rearrangement of 15LOX-1/PEBP1, facilitates substrate entry, directs oxygen transport, and regulates catalytic activity leading to ferroptotic lipid peroxidation.

6. Identify oxygen diffusion pathways and binding sites within the 15LOX-1 catalytic pocket, exploring the role of conserved residues, oxygen tunnels, and water clusters in regulating oxygen acquisition and peroxidation.

7. Investigate the molecular basis of pre-peroxidation stage of singly- and doubly-oxidized PUFA-PEs. A quantum-level study of the mechanism will be conducted in the near future.

The results of the investigation described above are presented in three original articles, *Article A,* *Article B,* and *Article C* presented below.

5. References

1. Clarke, P.G. and S. Clarke, *Nineteenth century research on naturally occurring cell death and related phenomena.* Anat Embryol (Berl), 1996. **193**(2): p. 81-99.

2. Kerr, J.F., A.H. Wyllie, and A.R. Currie, *Apoptosis: a basic biological phenomenon with wide-ranging implications in tissue kinetics. Br. J. Cancer*, 1972. **26**(4): p. 239-57.

3. Galluzzi, L., et al., *Molecular mechanisms of cell death: recommendations of the Nomenclature Committee on Cell Death 2018. Cell Death Differ*, 2018. **25**(3): p. 486-541.

4. Voss, A.K. and A. Strasser, *The essentials of developmental apoptosis.* F1000Res, 2020. **9**.

5. Lee, E., et al., *Regulated cell death pathways and their roles in homeostasis, infection, inflammation, and tumorigenesis. Exp. Mol. Med.*, 2023. **55**(8): p. 1632-1643.

6. Nguyen, T.T.M., G. Gillet, and N. Popgeorgiev, *Caspases in the Developing Central Nervous System: Apoptosis and Beyond.* Front. Cell Dev. Biol., 2021. **9**.

7. Park, W., et al., *Diversity and complexity of cell death: a historical review. Exp. Mol. Med.*, 2023. **55**(8): p. 1573-1594.

8. Tang, D., et al., *The molecular machinery of regulated cell death.* Cell Res, 2019. **29**(5): p. 347-364.

9. Yuan, J. and D. Ofengeim, *A guide to cell death pathways.* Nat Rev Mol Cell Biol, 2024. **25**(5): p. 379-395.

10. Lockshin, R.A. and C.M. Williams, *Programmed cell death—II. Endocrine potentiation of the breakdown of the intersegmental muscles of silkmoths.* J. Insect Physiol.. 1964. **10**(4): p. 643-649.

11. Jourdain, A. and J.-C. Martinou, *Mitochondrial outer-membrane permeabilization and remodelling in apoptosis. Int. J. Biochem. Cell Biol.*, 2009. **41**(10): p. 1884-1889.

12. Jan, R. and G.E. Chaudhry, *Understanding Apoptosis and Apoptotic Pathways Targeted Cancer Therapeutics.* Adv Pharm Bull, 2019. **9**(2): p. 205-218.

13. Brentnall, M., et al., *Caspase-9, caspase-3 and caspase-7 have distinct roles during intrinsic apoptosis.* Bmc Cell Biol, 2013. **14**: p. 32

14. Sessler, T., et al., *Structural determinants of DISC function: New insights into death receptor-mediated apoptosis signalling.* Pharmacol. Ther., 2013. **140**(2): p. 186-199.

15. Zaman, S., R. Wang, and V. Gandhi, *Targeting the apoptosis pathway in hematologic malignancies.* Leukemia Lymphoma, 2014. **55**(9): p. 1980-1992.

16. Erekat, N.S., *Apoptosis and its therapeutic implications in neurodegenerative diseases.* Clin Anat, 2022. **35**(1): p. 65-78.

17. Galluzzi, L., et al., *Molecular definitions of cell death subroutines: recommendations of the Nomenclature Committee on Cell Death 2012.* Cell Death Differ, 2012. **19**(1): p. 107-120.

18. Ofengeim, D. and J.Y. Yuan, *Regulation of RIP1 kinase signalling at the crossroads of inflammation and cell death.* Nat Rev Mol Cell Bio, 2013. **14**(11): p. 727-736.

19. Zhang, Q., et al., *Circulating mitochondrial DAMPs cause inflammatory responses to injury.* Nature, 2010. **464**(7285): p. 104-U115.

20. Afonso, M.B., et al., *Necroptosis is a key pathogenic event in human and experimental murine models of non-alcoholic steatohepatitis.* Clin Sci, 2015. **129**(8): p. 721-739.

21. Aachoui, Y., et al., *Inflammasome-mediated pyroptotic and apoptotic cell death, and defense against infection.* Curr Opin Microbiol, 2013. **16**(3): p. 319-326.

22. Bergsbaken, T., S.L. Fink, and B.T. Cookson, *Pyroptosis: host cell death and inflammation.* Nat Rev Microbiol, 2009. **7**(2): p. 99-109.

23. Kayagaki, N., et al., *Caspase-11 cleaves gasdermin D for non-canonical inflammasome signalling.* Nature, 2015. **526**(7575): p. 666-671.

24. Hao, W.D., et al., *Aluminum impairs cognitive function by activating DDX3X-NLRP3-mediated pyroptosis signaling pathway.* Food Chem Toxicol, 2021. **157**.

25. Jorgensen, I. and E.A. Miao, *Pyroptotic cell death defends against intracellular pathogens.* Immunol Rev, 2015. **265**(1): p. 130-142.

26. Hachim, M.Y., et al., *Pyroptosis: The missing puzzle among innate and adaptive immunity crosstalk.* J Leukocyte Biol, 2020. **108**(1): p. 323-338.

27. Lee, A.R. and C.Y. Park, *Orai1 is an Entotic CaChannel for Non-Apoptotic Cell Death, Entosis in Cancer Development.* Adv Sci, 2023. **10**(14).

28. Florey, O., et al., *Autophagy machinery mediates macroendocytic processing and entotic cell death by targeting single membranes.* Nat Cell Biol, 2011. **13**(11): p. 1335-U118.

29. Overholtzer, M., et al., *A nonapoptotic cell death process, entosis, that occurs by cell-in-cell invasion.* Cell, 2007. **131**(5): p. 966-79.

30. Arnandis, T., et al., *Calpains mediate epithelial-cell death during mammary gland involution: mitochondria and lysosomal destabilization.* Cell Death Differ, 2012. **19**(9): p. 1536-1548.

31. Dielschneider, R.F., et al., *Lysosomotropic agents selectively target chronic lymphocytic leukemia cells due to altered sphingolipid metabolism.* Leukemia, 2016. **30**(6): p. 1290-1300.

32. Chen, F.Q., et al., *Mechanisms of alkaliptosis.* Front. Cell Dev. Biol., 2023. **11**.

33. Scaturro, P. and A. Pichlmair, *Oxeiptosis: a discreet way to respond to radicals.* Curr. Opin. Immunol., 2019. **56**: p. 37-43.

34. Dixon, S.J., et al., *Ferroptosis: an iron-dependent form of nonapoptotic cell death.* Cell, 2012. **149**(5): p. 1060-72.

35. Li, S. and Y. Huang, *Ferroptosis: an iron-dependent cell death form linking metabolism, diseases, immune cell and targeted therapy.* Clin Transl Oncol, 2022. **24**(1): p. 1-12.

36. Jiang, Y., et al., *Ferroptosis: a new hunter of hepatocellular carcinoma.* Cell Death Discov, 2024. **10**(1): p. 136.

37. Stoyanovsky, D.A., et al., *Iron catalysis of lipid peroxidation in ferroptosis: Regulated enzymatic or random free radical reaction?* Free Radic Biol Med, 2019. **133**: p. 153-161.

38. Lee, J.-Y., et al., *Lipid Metabolism and Ferroptosis.* Biology, 2021. **10**(3): p. 184.

39. Mao, X., et al., *Ferroptosis, a new form of cell death: mechanisms, biology and role in gynecological malignant tumor.* Am J Cancer Res, 2023. **13**(7): p. 2751-2762.

40. Dai, E., et al., *Autophagy-dependent ferroptosis drives tumor-associated macrophage polarization via release and uptake of oncogenic KRAS protein.* Autophagy, 2020. **16**(11): p. 2069-2083.

41. Chen, X., et al., *Identification of HPCAL1 as a specific autophagy receptor involved in ferroptosis.* Autophagy, 2023. **19**(1): p. 54-74.

42. Liu, L., et al., *Deubiquitinase OTUD5 as a Novel Protector against 4-HNE-Triggered Ferroptosis in Myocardial Ischemia/Reperfusion Injury.* Adv. Sci., 2023. **10**(28): p. 2301852.

43. Liu, J., et al., *DCN released from ferroptotic cells ignites AGER-dependent immune responses.* Autophagy, 2022. **18**(9): p. 2036-2049.

44. Feng, H., et al., *Transferrin Receptor Is a Specific Ferroptosis Marker.* Cell Rep, 2020. **30**(10): p. 3411-3423.e7.

45. Cui, S., et al., *Identification of hyperoxidized PRDX3 as a ferroptosis marker reveals ferroptotic damage in chronic liver diseases.* Mol Cell, 2023. **83**(21): p. 3931-3939.e5.

46. Vitale, I., et al., *Apoptotic cell death in disease-Current understanding of the NCCD 2023.* Cell Death Differ, 2023. **30**(5): p. 1097-1154.

47. Wenzel, S.E., et al., *PEBP1 Wardens Ferroptosis by Enabling Lipoxygenase Generation of Lipid Death Signals.* Cell, 2017. **171**(3): p. 628-641 e26.

48. Pratt, D.A., *Targeting lipoxygenases to suppress ferroptotic cell death. Proc. Natl. Acad. Sci. U. S. A*, 2023. **120**(29).

49. Kuwata, H., et al., *Role of ACSL4 in the chemical-induced cell death in human proximal tubule epithelial HK-2 cells.* Biosci. Rep., 2022. **42**(2).

50. Shao, G.X., et al., *Research progress in the role and mechanism of LPCAT3 in metabolic related diseases and cancer.* J. Cancer, 2022. **13**(7): p. 2430-2439.

51. Shah, R., M.S. Shchepinov, and D.A. Pratt, *Resolving the Role of Lipoxygenases in the Initiation and Execution of Ferroptosis.* ACS Cent. Sci., 2018. **4**(3): p. 387-396.

52. Lei, P.X., T. Bai, and Y.L. Sun, *Mechanisms of Ferroptosis and Relations With Regulated Cell Death: A Review.* Front Physiol, 2019. **10**.

53. Liao, Y., P. Cao, and L. Luo, *Identification of Novel Arachidonic Acid 15-Lipoxygenase Inhibitors Based on the Bayesian Classifier Model and Computer-Aided High-Throughput Virtual Screening.* Pharmaceuticals (Basel), 2022. **15**(11).

54. Bersuker, K., et al., *The CoQ oxidoreductase FSP1 acts parallel to GPX4 to inhibit ferroptosis.* Nature, 2019. **575**(7784): p. 688-692.

55. Soula, M., et al., *Metabolic determinants of cancer cell sensitivity to canonical ferroptosis inducers.* Nat Chem Biol, 2020. **16**(12): p. 1351-1360.

56. Ma, T., et al., *GPX4-independent ferroptosis-a new strategy in disease's therapy.* Cell Death Discov, 2022. **8**(1): p. 434.

57. Zeitler, L., et al., *Anti-ferroptotic mechanism of IL4i1-mediated amino acid metabolism.* Elife, 2021. **10**: p. e64806.

58. Mao, C., et al., *Phospholipase iPLA2β acts as a guardian against ferroptosis.* Cancer Commun., 2021. **41**(11): p. 1082-1085.

59. Sun, W.Y., et al., *Phospholipase iPLA(2)β averts ferroptosis by eliminating a redox lipid death signal.* Nat. Chem. Biol., 2021. **17**(4): p. 465-476.

60. Li, D.C., et al., *Dihydroorotate dehydrogenase regulates ferroptosis in neurons after spinal cord injury via the P53-ALOX15 signaling pathway.* CNS Neurosci Ther, 2023. **29**(7): p. 1923-1939.

61. Dar, H.H., et al., *A new thiol-independent mechanism of epithelial host defense against : iNOS/NO' sabotage of theft-ferroptosis.* Redox Biol., 2021. **45**: p. 102045.

62. Kagan, V.E., et al., *Oxidized arachidonic and adrenic PEs navigate cells to ferroptosis.* Nat Chem Biol, 2017. **13**(1): p. 81-90.

63. Dar, H.H., et al., *Discovering selective antiferroptotic inhibitors of the 15LOX/PEBP1 complex noninterfering with biosynthesis of lipid mediators.* Proc Natl Acad Sci U S A, 2023. **120**(25): p. e2218896120.

64. Tavel, L., et al., *Ligand binding study of human PEBP1/RKIP: interaction with nucleotides and Raf-1 peptides evidenced by NMR and mass spectrometry.* PLoS One, 2012. **7**(4): p. e36187.

65. Mikulska-Ruminska, K., et al., *NO(●) Represses the Oxygenation of Arachidonoyl PE by 15LOX/PEBP1: Mechanism and Role in Ferroptosis.* Int J Mol Sci, 2021. **22**(10).

66. Anthonymuthu, T.S., et al., *Resolving the paradox of ferroptotic cell death: Ferrostatin-1 binds to 15LOX/PEBP1 complex, suppresses generation of peroxidized ETE-PE, and protects against ferroptosis.* Redox Biol., 2021. **38**: p. 101744.

67. Dar, H.H., et al., *Pseudomonas aeruginosa utilizes host polyunsaturated phosphatidylethanolamines to trigger theft-ferroptosis in bronchial epithelium.* J Clin Invest, 2018. **128**(10): p. 4639-4653.

68. Mosblech, A., I. Feussner, and I. Heilmann, *Oxylipins: structurally diverse metabolites from fatty acid oxidation.* Plant Physiol Biochem, 2009. **47**(6): p. 511-7.

69. Proneth, B. and M. Conrad, *Ferroptosis and necroinflammation, a yet poorly explored link.* Cell Death Differ, 2019. **26**(1): p. 14-24.

70. Newcomer, M.E. and A.R. Brash, *The structural basis for specificity in lipoxygenase catalysis.* Prot. Sci., 2015. **24**(3): p. 298-309.

71. Sloane, D.L., et al., *A primary determinant for lipoxygenase positional specificity.* Nature, 1991. **354**(6349): p. 149-52.

72. Brash, A.R., *Lipoxygenases: Occurrence, functions, catalysis, and acquisition of substrate.* J. Biol. Chem., 1999. **274**(34): p. 23679-23682.

73. Choi, J., et al., *Conformational flexibility in mammalian 15S-lipoxygenase: Reinterpretation of the crystallographic data.* Proteins, 2008. **70**(3): p. 1023-32.

74. Waterhouse, A., et al., *SWISS-MODEL: homology modelling of protein structures and complexes.* Nucleic Acids Res, 2018. **46**(W1): p. W296-W303.

75. Schoentgen, F. and S. Jonic, *PEBP1/RKIP behavior: a mirror of actin-membrane organization.* Cell. Mol. Life Sci., 2020. **77**(5): p. 859-874.

76. Park, S., et al., *RKIP downregulates B-Raf kinase activity in melanoma cancer cells.* Oncogene, 2005. **24**(21): p. 3535-3540.

77. Zou, Q.Y., et al., *RKIP suppresses the proliferation and metastasis of breast cancer cell lines through up-regulation of miR-185 targeting HMGA2.* Arch. Biochem. Biophys., 2016. **610**: p. 25-32.

78. Abd Alla, J. and U. Quitterer, *The RAF Kinase Inhibitor Protein (RKIP): Good as Tumour Suppressor, Bad for the Heart.* Cells, 2022. **11**(4): p. 654.

79. Maki, M., et al., *Decreased expression of hippocampal cholinergic neurostimulating peptide precursor protein mRNA in the hippocampus in Alzheimer disease.* J. Neuropathol. Exp. Neurol., 2002. **61**(2): p. 176-185.

80. Nilsson, J., et al., *Cerebrospinal fluid biomarker panel for synaptic dysfunction in Alzheimer's disease.* Alzheimers Dement. (Amst), 2021. **13**(1).

81. Zeng, L.C., A. Imamoto, and M.R. Rosner, *Raf kinase inhibitory protein (RKIP): A physiological regulator and future therapeutic target.* Expert Opin. Ther. Targets, 2008. **12**(10): p. 1275-1287.

82. Noh, H.S., et al., *PEBP1, a RAF kinase inhibitory protein, negatively regulates starvation-induced autophagy by direct interaction with LC3.* Autophagy, 2016. **12**(11): p. 2183-2196.

83. Yang, X.Y., et al., *PEBP1 suppresses HIV transcription and induces latency by inactivating MAPK/NF-κB signaling.* Embo Reports, 2020. **21**(11): p. e49305.

84. Wang, S.F., et al., *PEBP balances apoptosis and autophagy in whitefly upon arbovirus infection.* Nat Commun, 2022. **13**(1).

85. Lee, J., et al., *Network of mutually repressive metastasis regulators can promote cell heterogeneity and metastatic transitions.* Proc. Natl. Acad. Sci. U. S. A, 2014. **111**(3): p. E364-E373.

86. Shappell, S.B., et al., *15-lipoxygenase-2 (15-LOX-2) is expressed in benign prostatic epithelium and reduced in prostate adenocarcinoma.* Am. J. Pathol., 1999. **155**(1): p. 235-245.

87. Basconi, J.E. and M.R. Shirts, *Effects of Temperature Control Algorithms on Transport Properties and Kinetics in Molecular Dynamics Simulations.* J Chem Theory Comput, 2013. **9**(7): p. 2887-99.

88. Vaezi, M.A., et al., *15-Lipoxygenase and its metabolites in the pathogenesis of breast cancer: A double-edged sword.* Lipids Health Dis., 2021. **20**(1).

89. Henricks, P.A.J., et al., *9-and 13-hydroxy-linoleic acid posses chemotactic activity for bovine and human polymorphonuclear leukocytes.* Prostaglandins, 1991. **41**(1): p. 21-27.

90. Ivanov, I., H. Kuhn, and D. Heydeck, *Structural and functional biology of arachidonic acid 15-lipoxygenase-1 (ALOX15).* Gene, 2015. **573**(1): p. 1-32.

91. Snodgrass, R.G. and B. Brüene, *Regulation and Functions of 15-Lipoxygenases in Human Macrophages.* Front. Pharmacol., 2019. **10**.

92. Benatzy, Y., M.A. Palmer, and B. Brune, *Arachidonate 15-lipoxygenase type B: Regulation, function, and its role in pathophysiology.* Front Pharmacol, 2022. **13**: p. 1042420.

93. Dar, H.H., et al., *utilizes host polyunsaturated phosphatidylethanolamines to trigger theft-ferroptosis in bronchial epithelium.* J. Clin. Invest., 2018. **128**(10): p. 4639-4653.

94. Mikulska-Ruminska, K., et al., *Characterization of Differential Dynamics, Specificity, and Allostery of Lipoxygenase Family Members.* J. Chem. Inf. Model., 2019. **59**(5): p. 2496-2508.

95. Manivarma, T., et al., *Membrane regulation of 15LOX-1/PEBP1 complex prompts the generation of ferroptotic signals, oxygenated PEs.* Free Radic Biol Med, 2023. **208**: p. 458-467.

96. Kuntz, I.D., et al., *A geometric approach to macromolecule-ligand interactions.* J Mol Biol, 1982. **161**(2): p. 269-88.

97. Kitchen, D.B., et al., *Docking and scoring in virtual screening for drug discovery: methods and applications.* Nat Rev Drug Discov, 2004. **3**(11): p. 935-49.

98. Vakser, I.A., *Protein-protein docking: from interaction to interactome.* Biophys J, 2014. **107**(8): p. 1785-1793.

99. Shoichet, B.K., et al., *Lead discovery using molecular docking.* Curr Opin Chem Biol, 2002. **6**(4): p. 439-46.

100. Ashburn, T.T. and K.B. Thor, *Drug repositioning: identifying and developing new uses for existing drugs.* Nat Rev Drug Discov, 2004. **3**(8): p. 673-83.

101. Huang, S.Y., *Exploring the potential of global protein-protein docking: an overview and critical assessment of current programs for automatic ab initio docking.* Drug Discov Today, 2015. **20**(8): p. 969-77.

102. Lensink, M.F. and S.J. Wodak, *Docking, scoring, and affinity prediction in CAPRI.* Proteins, 2013. **81**(12): p. 2082-95.

103. Huang, S.Y., *Search strategies and evaluation in protein-protein docking: principles, advances and challenges.* Drug Discov Today, 2014. **19**(8): p. 1081-96.

104. Kurcinski, M. and A. Kolinski, *Hierarchical modeling of protein interactions.* J Mol Model, 2007. **13**(6-7): p. 691-8.

105. Yan, Y., et al., *HDOCK: a web server for protein-protein and protein-DNA/RNA docking based on a hybrid strategy.* Nucleic Acids Res, 2017. **45**(W1): p. W365-W373.

106. Trott, O. and A.J. Olson, *AutoDock Vina: improving the speed and accuracy of docking with a new scoring function, efficient optimization, and multithreading.* J Comput Chem, 2010. **31**(2): p. 455-61.

107. Koes, D.R., M.P. Baumgartner, and C.J. Camacho, *Lessons Learned in Empirical Scoring with smina from the CSAR 2011 Benchmarking Exercise.* J. Chem. Inf. Model., 2013. **53**(8): p. 1893-1904.

108. Karplus, M. and J.A. McCammon, *Molecular dynamics simulations of biomolecules.* Nat Struct Biol, 2002. **9**(9): p. 646-52.

109. Filipe, H.A.L. and L.M.S. Loura, *Molecular Dynamics Simulations: Advances and Applications.* Molecules, 2022. **27**(7).

110. Lazim, R., D. Suh, and S. Choi, *Advances in Molecular Dynamics Simulations and Enhanced Sampling Methods for the Study of Protein Systems.* Int J Mol Sci, 2020. **21**(17).

111. Lennard-Jones, J., *II. From the Equation of State of a Gas.* Proc. Roy. Soc. A., 1924. **106**(738): p. 463.

112. Mayo, S.L., B.D. Olafson, and W.A. Goddard, *DREIDING: a generic force field for molecular simulations.* J. Phys. Chem., 1990. **94**(26): p. 8897-8909.

113. Cornell, W.D., et al., *A Second Generation Force Field for the Simulation of Proteins, Nucleic Acids, and Organic Molecules.* J. Am. Chem. Soc., 1995. **117**(19): p. 5179-5197.

114. Durrant, J.D. and J.A. McCammon, *Molecular dynamics simulations and drug discovery.* BMC Biol., 2011. **9**(1): p. 71.

115. Patel, S. and C.L. Brooks, *Fluctuating charge force fields: Recent developments and applications from small molecules to macromolecular biological systems.* Mol Simulat, 2006. **32**(3-4): p. 231-249.

116. MacKerell, A.D., et al., *All-atom empirical potential for molecular modeling and dynamics studies of proteins.* J. Phys. Chem. B, 1998. **102**(18): p. 3586-616.

117. Oostenbrink, C., et al., *A biomolecular force field based on the free enthalpy of hydration and solvation: the GROMOS force-field parameter sets 53A5 and 53A6.* J Comput Chem, 2004. **25**(13): p. 1656-76.

118. Jorgensen, W.L., D.S. Maxwell, and J. Tirado-Rives, *Development and testing of the OPLS all-atom force field on conformational energetics and properties of organic liquids.* J. Am. Chem. Soc., 1996. **118**(45): p. 11225-11236.

119. Paci, E., *High pressure simulations of biomolecules.* Biochim Biophys Acta, 2002. **1595**(1-2): p. 185-200.

120. Ruymgaart, A.P. and R. Elber, *Revisiting Molecular Dynamics on a CPU/GPU system: Water Kernel and SHAKE Parallelization.* J Chem Theory Comput, 2012. **8**(11): p. 4624-4636.

121. Fennell, C.J. and J.D. Gezelter, *Is the Ewald summation still necessary? Pairwise alternatives to the accepted standard for long-range electrostatics.* J. Chem. Phys., 2006. **124**(23).

122. Troyer, J.M. and F.E. Cohen, *Protein conformational landscapes: energy minimization and clustering of a long molecular dynamics trajectory.* Proteins, 1995. **23**(1): p. 97-110.

123. Jorgensen, W.L. and L.L. Thomas, *Perspective on Free-Energy Perturbation Calculations for Chemical Equilibria.* J Chem Theory Comput, 2008. **4**(6): p. 869-876.

124. Nina, M., W. Im, and B. Roux, *Optimized atomic radii for protein continuum electrostatics solvation forces.* Biophys Chem, 1999. **78**(1-2): p. 89-96.

125. Xu, Y.W., C.X. Wang, and Y.Y. Shi, *Improvements on the protein–dipole Langevin–dipole model.* J. Comput. Chem., 1992. **13**(9): p. 1109-1113.

126. Vanden-Eijnden, E. and G. Ciccotti, *Second-order integrators for Langevin equations with holonomic constraints.* Chem. Phys. Lett., 2006. **429**(1): p. 310-316.

127. Tobias, D.J., G.J. Martyna, and M.L. Klein, *Molecular dynamics simulations of a protein in the canonical ensemble.* J. Phys. Chem., 1993. **97**(49): p. 12959-12966.

128. Mannan, S., et al., *Navigating energy landscapes for materials discovery: Integrating modeling, simulation, and machine learning.* MGE Advances, 2024. **2**(1): p. e25.

129. Peivaste, I., et al., *Rapid and accurate predictions of perfect and defective material properties in atomistic simulation using the power of 3D CNN-based trained artificial neural networks.* Sci. Rep., 2024. **14**(1): p. 36.

130. Phillips, J.C., et al., *Scalable molecular dynamics on CPU and GPU architectures with NAMD.* J Chem Phys, 2020. **153**(4): p. 044130.

131. Frisch, M., et al., *Gaussian 2003, Revision B. 05. Gaussian*. Inc., Pittsburgh, PA, 2003.

132. Pastor, R.W., *Techniques and Applications of Langevin Dynamics Simulations*, in *The Molecular Dynamics of Liquid Crystals*, G.R. Luckhurst and C.A. Veracini, Editors. 1994, Springer Netherlands: Dordrecht. p. 85-138.

133. Feller, S.E., et al., *Constant-Pressure Molecular-Dynamics Simulation - the Langevin Piston Method.* J. Chem. Phys., 1995. **103**(11): p. 4613-4621.

134. Jo, S., et al., *CHARMM-GUI Membrane Builder for Mixed Bilayers and Its Application to Yeast Membranes.* Biophys. J., 2009. **97**(1): p. 50-58.

135. Lomize, M.A., et al., *OPM database and PPM web server: resources for positioning of proteins in membranes.* Nucleic Acids Res., 2012. **40**(D1): p. D370-D376.

136. Chaplin, M.F., *Water: its importance to life.* Biochem Mol Biol Educ, 2001. **29**(2): p. 54-59.

137. Bhattacherjee, A. and S. Wategaonkar, *Water bridges anchored by a C-HO hydrogen bond: the role of weak interactions in molecular solvation.* Phys Chem Chem Phys, 2016. **18**(40): p. 27745-27749.

138. Tame, J.R.H., et al., *The role of water in sequence-independent ligand binding by an oligopeptide transporter protein.* Nat. Struct. Mol. Biol., 1996. **3**(12): p. 998-1001.

139. Chen, W., et al., *Uncovering water effects in protein-ligand recognition: importance in the second hydration shell and binding kinetics.* Phys. Chem. Chem. Phys., 2023. **25**(3): p. 2098-2109.

140. Pocker, Y., *Water in enzyme reactions: biophysical aspects of hydration-dehydration processes. Cell. Mol. Life Sci.*, 2000. **57**(7): p. 1008-1017.

141. Yuan, H., et al., *Exploration of the Existence Forms and Patterns of Dissolved Oxygen Molecules in Water.* Nanomicro Lett, 2024. **16**(1): p. 208.

142. Zhang, S., et al., *ProDy 2.0: increased scale and scope after 10 years of protein dynamics modelling with Python.* Bioinformatics, 2021. **37**(20): p. 3657-3659.

143. Krieger, J.M., et al., *WatFinder: A ProDy tool for protein-water interactions.* Bioinformatics, 2024: p. btae516.

144. Bordner, A.J. and R. Abagyan, *Statistical analysis and prediction of protein-protein interfaces.* Proteins: Struct., Funct., Bioinf., 2005. **60**(3): p. 353-366.

145. Ozdemir, E.S., A. Gursoy, and O. Keskin, *Analysis of single amino acid variations in singlet hot spots of protein-protein interfaces.* Bioinformatics, 2018. **34**(17): p. i795-i801.

146. Moreira, I.S., et al., *SpotOn: High Accuracy Identification of Protein-Protein Interface Hot-Spots.* Sci Rep, 2017. **7**(1): p. 8007.

147. Jones, S. and J.M. Thornton, *Principles of protein-protein interactions.* Proc. Natl. Acad. Sci. U. S. A., 1996. **93**(1): p. 13-20.

6. Papers

6.1 Article A

Membrane regulation of 15LOX-1/PEBP1 complex prompts the generation of ferroptotic signals, oxygenated PEs

Free Radical Biology and Medicine 208 (2023) 458–467

Contents lists available at ScienceDirect

Free Radical Biology and Medicine

journal homepage: www.elsevier.com/locate/freeradbiomed

Membrane regulation of 15LOX-1/PEBP1 complex prompts the generation of ferroptotic signals, oxygenated PEs

Thiliban Manivarma [a], Aleksandr A. Kapralov [b], Svetlana N. Samovich [b,d], Yulia Y. Tyurina [b], Vladimir A. Tyurin [b], Andrew P. VanDemark [c], Wieslaw Nowak [a], Hülya Bayır [b,d], Ivet Bahar [e,**], Valerian E. Kagan [b,f,g,h,***], Karolina Mikulska-Ruminska [a,*]

[a] Institute of Physics, Faculty of Physics, Astronomy and Informatics, Nicolaus Copernicus University in Torun, Torun, Poland
[b] Department of Environmental and Occupational Health and Center for Free Radical and Antioxidant Health University of Pittsburgh, Pittsburgh, PA, USA
[c] Department of Biological Sciences, University of Pittsburgh, Pittsburgh, PA, USA
[d] Department of Pediatrics, Division of Critical Care and Hospital Medicine, Redox Health Center, Vagelos College of Physicians and Surgeons, Columbia University Irving Medical Center, New York, NY, USA
[e] Laufer Center for Physical and Quantitative Biology and Department of Biochemistry and Cell Biology, Stony Brook University, New York, USA
[f] Department of Radiation Oncology, University of Pittsburgh, Pittsburgh, PA, USA
[g] Department of Chemistry, University of Pittsburgh, Pittsburgh, PA, USA
[h] Department of Pharmacology and Chemical Biology, University of Pittsburgh, Pittsburgh, PA, USA

ARTICLE INFO

Keywords:
Ferroptosis
15-Lipoxygenase
PEBP1
Lipid peroxidation
Membrane effect

ABSTRACT

Ferroptosis is a regulated form of cell death, the mechanism of which is still to be understood. 15-lipoxygenase (15LOX) complex with phosphatidylethanolamine (PE)-binding protein 1 (PEBP1) catalyzes the generation of pro-ferroptotic cell death signals, hydroperoxy-polyunsaturated PE. We focused on gaining new insights into the molecular basis of these pro-ferroptotic interactions using computational modeling and liquid chromatography-mass spectrometry experiments. Simulations of 15LOX-1/PEBP1 complex dynamics and interactions with lipids revealed that association with the membrane triggers a conformational change in the complex. This conformational change facilitates the access of stearoyl/arachidonoyl-PE (SAPE) substrates to the catalytic site. Furthermore, the binding of SAPE promotes tight interactions within the complex and induces further conformational changes that facilitate the oxidation reaction. The reaction yields two hydroperoxides as products, 15-HpETE-PE and 12-HpETE-PE, at a ratio of 5:1. A significant effect of PEBP1 is observed only on the predominant product. Moreover, combined experiments and simulations consistently demonstrate the significance of PEBP1 P112E mutation in generating ferroptotic cell death signals.

1. Introduction

Ferroptosis is an iron-dependent programmed cell death that occurs upon massive accumulation of lipid hydroperoxides [1] – a unique feature that distinguishes it from other cell death programs [2]. It is one of the most preserved and ancient forms of cell death characteristic of all domains of life, including evolutionarily remote species [3–5]. It is implicated in a broad range of diseases [3,6], including neurodegenerative diseases (e.g., Alzheimer's [7,8] and Parkinson's [9,10] where iron-dependent accumulation of lipid peroxides is enhanced), cerebello-cortical atrophy, sepsis, or bacterial and viral diseases [11,12], as well as multiple organ inflammation in COVID-19 [13–16], kidney failure, brain trauma, and asthma [17–19]. Targeted induction of ferroptosis has been proposed to have a potential in cancer therapy and in treating auto-immune diseases [20–22].

Three major factors trigger ferroptosis in cells: accumulation of redox-active iron, lipid peroxidation, and thiol dysregulation. Lipid peroxidation occurs through enzymatic or non-enzymatic mechanisms

* Corresponding author.
** Corresponding author.
*** Corresponding author. Department of Environmental and Occupational Health and Center for Free Radical and Antioxidant Health University of Pittsburgh, Pittsburgh, PA, 15260, United States.
E-mail addresses: bahar@laufercenter.org (I. Bahar), kagan@pitt.edu (V.E. Kagan), karolamik@fizyka.umk.pl (K. Mikulska-Ruminska).

https://doi.org/10.1016/j.freeradbiomed.2023.09.001
Received 22 July 2023; Received in revised form 24 August 2023; Accepted 1 September 2023
Available online 9 September 2023

[23,24] and depends on reactive oxygen species, iron, and polyunsaturated phospholipids (PLs) rich in bis-allylic carbons. Here we focus on the generation of pro-ferroptotic lipid peroxides catalyzed by a complex formed between 15-lipoxygenase (15LOX) (a non-heme Fe-enzyme) and phosphatidylethanolamine-binding protein 1 (PEBP1). In 15LOX, a Fe^{2+} to Fe^{3+} oxidation generates a ferric iron-(-Fe^{3+})-hydroxy species that triggers a stereoselective hydrogen abstraction from the polyunsaturated fatty acids (PUFAs) substrate, which is thus oxidized to a carbon-centered radical capable of reaction with unactivated molecular oxygen to yield a peroxyl radical as the primary oxygenated intermediate [25,26]. Iron is also essential for the proper positioning of the substrate enabling the oxygenation reaction to take place. While different types of PUFAs are involved in peroxidation, two fatty acyls – arachidonoyl (C20:4, AA) and adrenoyl (C22:4, AdA), esterified into PE are major substrates of the 15LOX/PEBP1 complex [19,27,28].

There are two isoforms of 15LOX, 15LOX-1 and 15LOX-2. These isoforms exhibit distinct expression in different tissues and generate partially diverse oxygenation products [25,29]. 15LOX-1 and -2 share high structural similarity with 36% sequence identity [4,5]. Either isoform binds to PEBP1 complexed with 15LOX, which enables PL peroxidation leading to ferroptotic cell death [19]. PEBP1 binding changes the substrate specificity of 15LOX to endow catalytic competence towards the esterified PUFA-PL, stearoyl/arachidonoyl-PE (SAPE), and generate hydroperoxy-PEs [19,30–33]. However, the atomic-level mechanism of PL peroxidation by 15LOX/PEBP1 remains to be elucidated.

The role of the PL membrane had been initially underestimated and considered only as a mere scaffold for facilitating the binding of membrane proteins. Numerous studies in the past years have shown that the lipids themselves regulate the localization and activity of many membrane-associated/peripheral proteins [34]. Among such proteins exhibiting membrane-mediated activities, we distinguish cytochromes [35–37] or phospholipases [10,38], which possess an ability to selectively associate with the PL bilayer, facilitating the extraction of PL substrates from the membrane to initiate the enzymatic reaction.

In the present study, we report the first computational study of the dynamics and interactions within the 15LOX-1/PEBP1 complex in the presence of a PL membrane that reveals the mechanism of SAPE substrate acquisition to the catalytic site of 15LOX, triggered by protein-membrane interactions. We confirmed the mechanistic model deduced from molecular dynamics (MD) simulations by mutagenesis studies using liquid chromatography-mass spectrometry (LC-MS) experiments, including the significance of PEBP1 P112E mutation in generating ferroptotic cell death signals. Moreover, we demonstrated the regulatory role of PEBP1 in the peroxidation of SAPE to the most predominant product, 15-HpETE-PE.

2. Methods

Molecular docking. In order to determine the structural model of the human 15LOX-1/PEBP1 complex, we applied a series of molecular docking simulations using the HDOCK server [39]. The initial structure of the human 15LOX-1 (Uniport ID: P16050) was obtained from the homology model of rabbit form (PDB ID: 2p0m [40]) using the Swiss-Model server [41]. The sequence identity between these sequences is >81%. To have an ensemble of PEBP1 structures, we used four monomers in our protein-protein docking approach (PDB ID: 1behA [42], 1behB, 1bd9A [42], 1bd9B). In total, we generated 100 hypothetical models for the 15LOX-1/PEBP1 complex which we narrowed down to four based on experimental findings [19], i.e. the effect mutations at P112 in PEBP1 and role of C-terminal helix of PEBP1 in the complex formation. These four computational models (called *Models 1–4*) were subjected to further investigation (see Supplementary Fig. S1A). Docking simulations were performed using the SMINA package [43] to identify the initial position of SAPE at the catalytic site of 15LOX-1 complexed with PEBP1, to be adopted in MD simulations of *Models 1* and *3*. We performed 5 runs for each system and selected SAPE conformations which had the highest binding affinity and placing the sn-2 chain C13 carbon atom of SAPE in a close proximity to the iron at the catalytic site as required for the peroxidation reaction.

Molecular Dynamics simulations. Full-atomic MD simulations were performed for *Models 1–4* using NAMD [44] package and the CHARMM [45] force field, and 2 fs time steps. The proteins were solvated with explicit water (TIP3P) at physiological salt concentrations. CHARMM force field parameters for bonded iron were obtained using Gaussian [46] (DFT B3LYP/6–31(d,p) method).

We performed two sets of simulations for each system, with and without membrane. Prior to productive runs without membrane, the following protocol was adopted: 0.2 ns of water equilibration, 10,000 steps of minimization, 0.35 ns of heating from 0 to 300 K, and 0.15 ns equilibration of the whole system. A cutoff of 12 Å for non-bonded interactions was applied. Langevin dynamics and the Langevin piston algorithm were used to maintain the temperature at 300 K and the pressure at 1 atm. For each system we performed >600 ns (3 MD runs, each >200 ns). We further eliminated *Model 4* which was highly unstable.

Simulations with the membrane composed of 1,2-dioleoy-sn-glycero-3-phosphocholine (DOPC, 50%), 1,2-dioleoy-sn-glycero-3-phosphoethanolamine (DOPE, 30%), and 1-stearoyl-2-arachidonyl-phosphoethanolamine (SAPE, 20%) were prepared in CHARMM GUI server [47]. We used the PPM/OPM [48] server to predict the orientation of the protein complex in the membrane. For each system, we performed 250 ns simulations (**Supplementary Table 2**). *Model 2* due to the increase in the distance between P112 and 15LOX-1 structure was eliminated from further consideration.

Next, for *Models 1* and *3*, we performed 200 ns long simulations of the 15LOX-1/PEBP1 complex with SAPE as a substrate bound to the catalytic site. For *Model 1,* we further performed 75 ns simulations with point mutations in PEBP1 (P112E, H86A, H86E, and P74L). We used our own scripts in ProDy [49] API and VMD [50] for analyses and visualization. The Adaptive Poisson–Boltzmann Solver (ABPS) [51] software was used to predict the electrostatics.

PEBP1 expression and purification: Full-length human PEBP1 and related mutants were cloned into a pET21-derived bacterial expression plasmid (EMD Millipore, Billerica, MA) modified to express PEBP1 with N-terminal His 10-and mRuby 2 tags [52]. All PEBP1 constructs were cloned into the modified pET21-mRuby2 vector by Gibson Assembly (New England Biolabs, Billerica, MA) using primers with homology at the upstream (sense) NdeI site (5′-GGTCTGAGGGGATACACTCA TATG-3′) and downstream (antisense) EcoRI site (5′-GCTTGTCGA CGGAGCTCGAATTC-3′) of the vector. Preparation of mutations, evaluation of clones, expression and purification of proteins were performed as described in [19]. Before performing experiments, PEBP1 was desalted into 5 mM Bis-Tris (pH 6.5), 25 mM NaCl as described previously.

15LOX-1 expression and purification: Plasmids for expressing the catalytic domain (residues 112–663) of porcine 15LO1 was generously provided to us by Max Funk. Purification was carried out as previously described [19,53].

Cross-linking: Recombinant human PEBP1 (2 μM) and porcine 15 LOX1 (2 μM) crosslinking was performed by incubation with 0.1% glutaraldehyde in 20 mM HEPES (pH 7.4) for 15 min. The reaction was stopped by addition of tris-HCl (pH 7.5) to final concentration 200 mM followed by ncubation for 15 min at room temperature. SDS PAGE of samples was performed in 7.5% running gel and proteins were stained by GelCode SilverSNAP kit (ThermoFisher Scientific). In some cases, proteins were electro-transferred to nitrocellulose membrane, blocked by 5% skim milk and PEBP was immunodetected using PEBP-specific antibodies (Santa Cruz, # SC-28837, 1:1000), HRP-conjugated goat anti-rabbit IgG H&L (Sigma, #A0545, 1:1000) as secondary antibodies and SuperSignal West Pico Substrate (ThermoFisher Scientific). The densities of protein bands were assessed by an open source image

processing program: Image J.

Far-western blotting: The interaction between PEBP and 15LOX *in vitro* was examined with far-western blotting. To assess the interaction of wild type and mutated PEBP1 with 15LO1, wt PEBP1 as well as mutants PEBP1 (4 μM) were separated on 10% Tris-glycine SDS-PAGE and electrically transferred to a nitrocellulose membrane. Proteins were renatured by incubation of the membrane in buffer (100 mM NaCl, 20 mM Tris (pH 7.6), 0.5 mM EDTA, 10% glycerol, 0.1% Tween-20, 2% skim milk powder and 1 mM DTT) containing decreasing concentration of guanidine HCl (6 M, 3 M, 1 M, 0.1 M, 0 M) and the membrane was blocked with 5% skim milk.

Then the membrane was incubated in 0.5 ml of protein-binding buffer (100 mM NaCl, 20 mM Tris (pH 7.6), 0.5 mM EDTA, 10% glycerol, 0.1% Tween-20, 2% skim milk powder and 1 mM DTT) containing 3 μM 15LOX-1 and DOPE/DOPC liposomes (1:1) (ratio DOPE to 15 LO1 25:1) at 4 °C overnight. Bound with membrane 15LOX-1 was immunodetected with 15LOX-specific antibodies (Life Span Biosciences Inc, #LS-111783, 1:2000) after 1.5 h incubation at room temperature. HRP-conjugated goat anti-rabbit IgG H&L (Sigma, #A0545,1:1000), was used as the secondary antibody, and bands were detected using SuperSignal West Femto Maximum Sensitivity Substrate (ThermoFisher Scientific)

Liposome preparation: Liposomes of DOPC/SAPE (1:1) were prepared using Avanti® Mini-Extruder. Briefly, 1,2-dioleoyl-PC (DOPC) and 1-stearoyl-2-arachidonyl-PE (SAPE) (Avanti Polar Lipids Inc.), lipids were dried with a stream of nitrogen gas and resuspended in 25 mM HEPES buffer, containing 100 μM diethylenetriaminepentaacetic acid (DTPA) pH 7.4 to achieve a final lipid concentration of 200 μM. The suspension was shaken vigorously and extruded through a polycarbonate membrane with 100 nm pores.

Lipoxygenase activity was assessed by the formation of primary products of SAPE oxidation, 15-HpETE and 12-HpETE. Briefly, DOPC/SAPE liposomes were incubated with human recombinant 15LOX1 (0.04 μM) in the presence or in the absence of PEBP1 or PEBP1 mutant P112E (0.04 μM) for 2.5 min at 37 °C. To prevent the conversion of lipid hydroperoxides to secondary products during incubation, the HEPES buffer was saturated with oxygen. At the end of incubation lipids were extracted using Folch procedure [54] and analyzed by LC-ESI-MS/MS.

LC-ESI-MS/MS analysis of phospholipids: LC-ESI-MS/MS analysis was performed on a Thermo Ultimate 3000 HPLC system coupled to a hybrid quadrupole-orbitrap mass spectrometer, (Q-Exactive, ThermoFisher Scientific) with an Xcalibur operating system. The instrument was operated in negative ion mode at a voltage differential of −4.0 kV and source temperature of 320 °C. Sheath gas and s-lens were set at 20 and 65, respectively. The resolution was set at 140,000 with a scan range of *m/z* 150–1800 and a user-defined mass tolerance of 5 ppm m/z values for the oxidized species are presented to 4 decimal places. MS/MS was performed in data dependent mode with HCD fixed at 24 and a resolution of 17,500. Non-oxidized and oxidized lipids were separated on a reverse phase Accucore C30 column (2.6 μm, 250 × 2.1 mm (ThermoFisher Scientific)) at a flow rate of 0.1 mL/min. Column temperature was set at 35 °C. The column was eluted using a gradient solvent system consisting of mobile phase A (acetonitrile/water, 50/50 v/v) and mobile phase B (2-propanol/acetonitrile/water, 85/10/5 v/v). Both mobile phases contained 5 mM ammonium formate and 0.1% formic acid. The gradient was performed as follows: 30%–70% B, 0–20 min; 70%–100% B, 20–55 min; 100% B, 55–70; 100%–30% B, 70–85 min; 30% B, 85–95 min for equilibration of the column. All gradients were linear.

3. Results

Docking and molecular dynamics simulations indicate that 15LOX-1/PEBP1 complex preferentially selects closed conformers in solution.

To establish a structural model for the human 15LOX-1/PEBP1 complex, we performed extensive molecular docking simulations and generated over 100 conformations. We used as input 15LOX-1 [40] and several crystallographic PEBP1 [42] structures (with pairwise root-mean-square deviations (RMSDs) of ~0.3 Å). Simulations revealed several hot spots on PEBP1, including A30, K47-R49, K80-Y81, D96-V102, D105, P112-K113, I137-H145, and the C-terminal helix D175-Y186 (Supplementary Fig. S1A). 15LOX-1 exhibited a preference for interfacial interactions at the F174-N192 (α2) and F583-L596 helices (Supplementary Table 1).

Based on our previous experiments [19] suggesting that PEBP1 residue P112 and C-terminal helix might be essential to association with 15LOX-1, we selected four models, *Models 1–4* (Supplementary Fig. S1B): (i) *Model 1*, proposed in our previous work [19] (also reproduced here); (ii) a 180°-rotated structure where P112 (*in red*) and C-terminal helix (*in orange*) face the 15LOX-1 β-barrel instead of its α2 helix (*Model 2,* Supplementary Fig. S1B); (ii-iv) two variants of *Model 1* with slightly different association sites on 15LOX-1 α2 helix (*Models 3* and *4*). Examination of the stability of these models by MD simulations of 200 ns in explicit water showed that *Models 1–3* were stable in solution and retained their closed form (tight interactions between PEBP1 and the α2 helix and β-barrel of 15LOX-1) as indicated by the RMSDs in atomic coordinates that remained around 3–4 Å; whereas *Model 4* exhibited three times higher RMSDs. Supplementary Fig. S2 provides a description of the simulation protocol, and Supplementary Fig. S3 displays the time evolution of RMSDs for the four systems, each conducted in triplicate, except for *Model* 4 that showed large departures from the original pose in two runs. *Model 4* was excluded from further studies due to its instability, and the conformational dynamics of *Models 1–3* were further investigated.

Membrane interactions trigger opening of the complex to expose a pore for phospholipid access to the catalytic site.

Several studies have shown that membrane association may elicit conformational changes in peripheral proteins, thus impacting their function [55–58]. We performed MD simulations for *Models 1–3*. Supplementary Table 2 describes the set of MD runs (a total of 7.7 μs) carried out for *Models 1–3* under different conditions (with/without membrane; with wildtype PEBP1 or its mutants, anchored to the membrane). The membrane was composed of DOPC (50%), DOPE (30%) and the most favorable 15LOX-1/PEBP1 substrate [1,12], SAPE (20%).

Simulations indicated that the interactions of the 15LOX-1/PEBP1 complex with the membrane promoted a conformational change that exposed the catalytic site of 15LOX-1 to the membrane, thus making the site more accessible to substrates (SAPEs) embedded in the membrane. Fig. 1 and Supplementary Fig. S4 illustrate the results for *Models 1* and *3*, respectively. This type of conformational change was not observed in the absence of membrane; whereas it was consistently reproduced in multiple runs in the presence of membrane. However, in *Model 2*, P112 was displaced by approximately 10 Å from the nearest 15LOX-1 residue. This conformational change disrupted the interactions involving P112, which have been reported to be crucial for complex formation [19]. As a result, we focused on *Models 1* and *3* for analyzing the opening mechanism. Specifically, we performed a comparative analysis of the atomic interactions at the initial and final stages of the simulations. The analysis revealed a reorganization of the interactions between 15LOX-1/PEBP1 and the membrane leading to an increase in the number of hydrogen bonds formed between the lipids and 15LOX-1 β-barrel residues N19, K37-R43, E48-E52, R68-H69 and K72-D74 and PEBP1 residues S60, D56, G61, D128, R129 and R161, compared to the initial stage of the simulation (Supplementary Fig. S5).

Next, we examined the cavities and interior surfaces of the complex in the open form, so as to identify a pore that connects the newly exposed surface and the catalytic site. Fig. 1B for *Model 1* and Supplementary Fig. S4B for *Model 3* display a *blue trace* across 15LOX-1, which also connects the exposed region to the catalytic site. We note that the entry of this predicted pore corresponds well to those previously observed for entry of AA into various LOXs, including rabbit 15LOX-1 (R403), 8(R)-LOX (R183, Y179), and soybean LOX1 (T259, L541) [59]. Alignment of these three structures within 15LOX-1 specifically highlights the significance of R402 and L178. The analysis of the

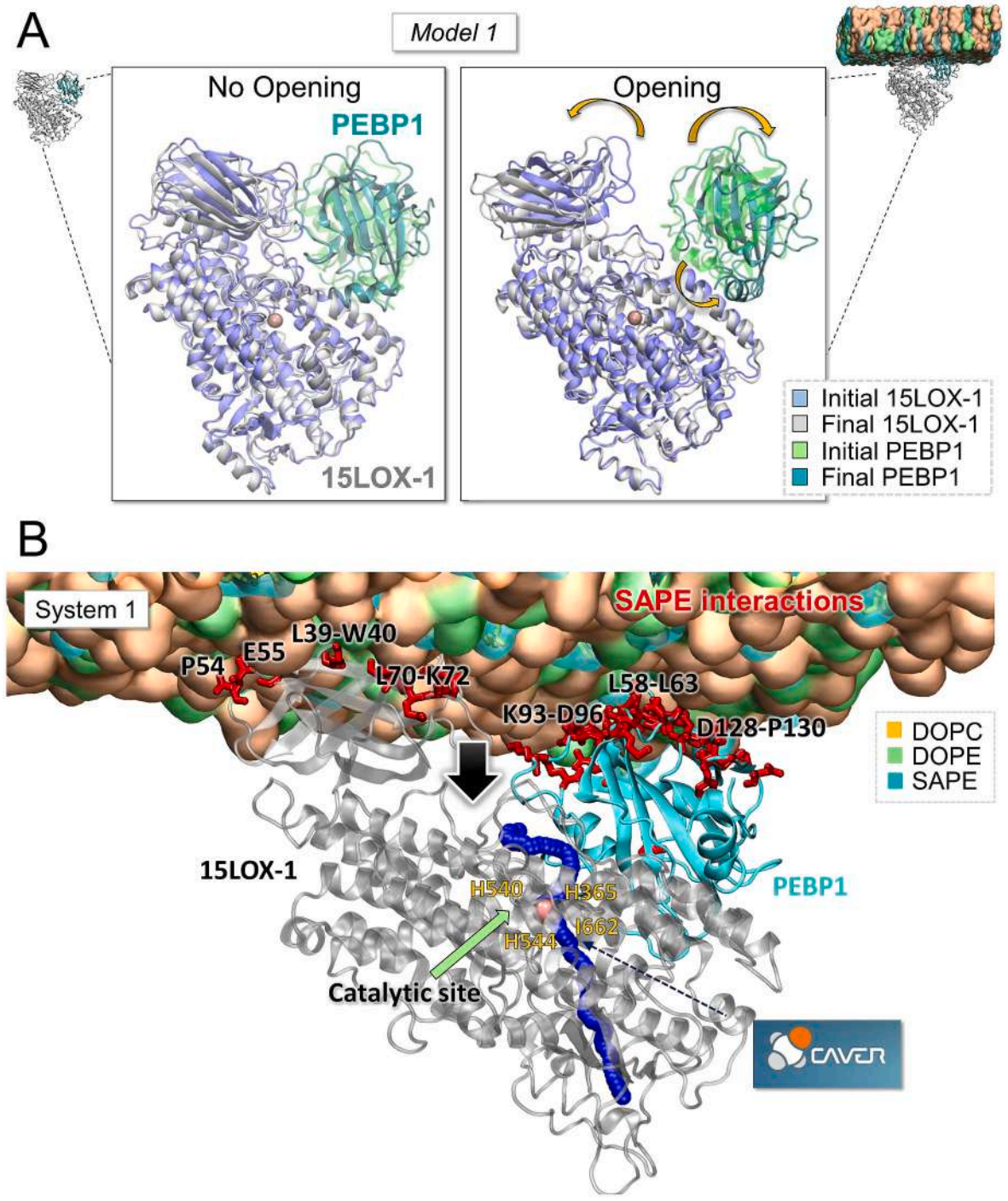

Fig. 1. MD simulations of 15LOX-1/PEBP1 complex for *Model 1*. (A) Initial and final conformations of *Model 1* in the absence (*left* panel) and presence (*right* panel) of the membrane. **(B)** Closeup view of the open conformation of 15LOX-1/PEBP1 associated with the membrane (DOPC in *orange*, DOPE in *green*, and SAPE in *blue*) captured after 250-ns MD simulation. Catalytic residues (H365, H540, H544 and I662) are labeled. The *pink sphere* represents the iron in the catalytic site of 15LOX-1. Residues displayed as *red sticks* make close contacts with SAPE molecules. *Blue trace* along the 15LOX-1 structure is a visualization of the tunnel predicted by CAVER (see Methods). *Black arrow* points to the entrance of the channel for the potential insertion of SAPE molecules into the catalytic site. Results for *Model 3* can be found in Supplementary Fig. S4.

interactions with the lipid molecules further indicates that membrane SAPEs were attracted by several residues, including L70-K72 (15LOX-1) and L58-K62 and R129 (PEBP1), as displayed in Supplementary Figs. S4 and S6, and Fig. 1B by *red sticks*. These residues are localized at both sides of the opening. The open space between PEBP1 and 15LOX-1 β-barrel, revealed here, is proposed to serve as an entry for SAPE molecules to reach the catalytic site of 15LOX-1 and generate the ferroptotic cell death signals, lipid hydroperoxides (15-HpETE-PE or 12-HpETE-PE).

3.1. Substrate binding locks the complex in a closed form

To directly assess the ability of the membrane-embedded SAPE to approach and insert near the catalytic site of 15LOX-1, we performed MD simulations to examine the docking of SAPE onto the complex, and the stabilization of the SAPE-bound complex (Supplementary Table 2).

The simulations revealed the propensity of SAPE to induce tight interactions and relatively more compact conformers upon binding to 15LOX-1/PEBP1. Fig. 2 shows the time evolution of the angle θ defined between the center of the mass of the 15LOX-1 β-barrel, its catalytic domain, and the PEBP1 mass center, as a measure of the degree of exposure of 15LOX-1 catalytic site in the complex. The angle increased by about 20° upon association of the complex with the membrane, in the absence of direct interactions with SAPE molecules (*red curve* in Fig. 2 for *Model 1*; see also the data from multiple runs in Supplementary Fig. S7). In contrast, in the case of membrane- and substrate-bound complex, θ decreased by about ~5° (*green curve*, Fig. 2).

The opening/closure of the catalytic site in 15LOX-1 was found to be strictly dependent on its occupancy. In the open form, the complex facilitated the diffusion of the substrate, while substrate binding led to the closure and stabilization of the catalytic pocket, enabling the oxidation reaction. SAPE-bound *Model 3* generally exhibited a lower binding affinity (−12.62 ± 0.15 kcal/mol) compared to *Model 1* (−14.99 ± 0.28 kcal/mol), and it displayed a potentially unreactive orientation with respect to the iron at the catalytic site (Supplementary Fig. S8).

3.2. Key residues stabilize the 15LOX-1/PEBP1 complex and enable its association with SAPE

Statistical analysis of interfacial interaction between 15LOX-1 and PEBP1 revealed several critical contacts (Supplementary Fig. S9). Residues engaged in stable interactions include D169-K170, E175-V176, A179-I187, R402, L157-L160, and D410-M411 on 15LOX-1, and K80-Y81, R141-H145, K148, with P112-K113 and C-terminal helix residues (Y181-E182, S185-G186) on PEBP1, consistent with those reported to be critical to complex formation [19].

In the presence of substrate, the interactions of 15LOX-1 D410 were replaced by those of R598-R599 due to the reconfiguration of the 15LOX-1/PEBP1 complex into a closed conformer. This reconfiguration, observed in *Model 1*, was stabilized after ~50 ns simulation (*green curve*, Fig. 2) and tightened upon binding a SAPE molecule. SAPE made stable contacts with several residues highly conserved among LOX family members (*red dots*, Fig. 3C), e.g., leucines (L596, L407, L361). The counterparts of these leucines in 15LOX-2 (L610, L420 and L374, respectively) have been identified to play a critical role in 15LOX-2/SAPE interactions [33]. Moreover, 15LOX-1 R402 and F166 (highlighted as *green dots*, Fig. 3C) occupy a central hinge region of LOX, shared between mammalian and bacterial forms, but not at the same sequential position [5]. The presence of arginine at this specific location has been documented in various studies on LOXs, including 12LOX (R403 [60]), 15LOXs (R402 [5]), PA-LOX (R422 [5]), or 8(R)-LOX (R182 [61]), not only as an entry to the catalytic site but also in relation to substrate interactions. Finally, we notice that PEBP1 residues S142, D144, and H145 are engaged in close interactions with SAPE (Fig. 3C). This region may be critical for PEBP1 dimerization [62] triggered by PKC-mediated phosphorylation of S153 and has been considered as an important mechanistic feature of PEBP1 substrate specificity [62,63]. Our model, shown in Fig. 3A (*inset*), indicates the accessibility of S153 (*pink sphere*) to a potential modification that may trigger complex dissociation.

Both 15LOX-1 and 15LOX-2 catalyze the oxidation of SAPE by abstracting a hydrogen at carbon atom C13 and inserting an oxygen atom at C15 resulting in the 15-HpETE-PE product. The isoform studied here is also able to occasionally abstract a hydrogen at the C10 atom (ratio 1:9 for arachidonic acid as substrate [25,64]) to generate an alternative product, 12-HpETE-PE. To determine whether one or both products could be produced according to our computational model, we checked the distance between the hydrogen donors (C13 and C10) and the iron at the catalytic site (Fig. 3A and B). The results showed that the iron generally maintains a shorter distance from C13 (mean distance: ~7.2 Å, *yellow histogram*) compared to C10 (~9 Å, *magenta histogram*). We detected only a few cases where C10 was at a close distance of ~7.2 Å (*pink arrow*). The lower probability of C10 to be close to the iron at the catalytic site, compared to C13, is in agreement with the experimentally observed (Fig. 4A, D) lower production of 12-HpETE-PE (ratio 1:5 for 15LOX-1/PEBP1 complex), compared to 15HpETE-PE. Moreover, the production of 12-HpETE-PE, in contrast to 15-HpETE-PE, was not affected by the presence of PEBP1.

3.3. Experiments demonstrate the critical role of P112 among the interfacial residues of PEBP1

Next, we used two different protocols to experimentally assess PEBP1

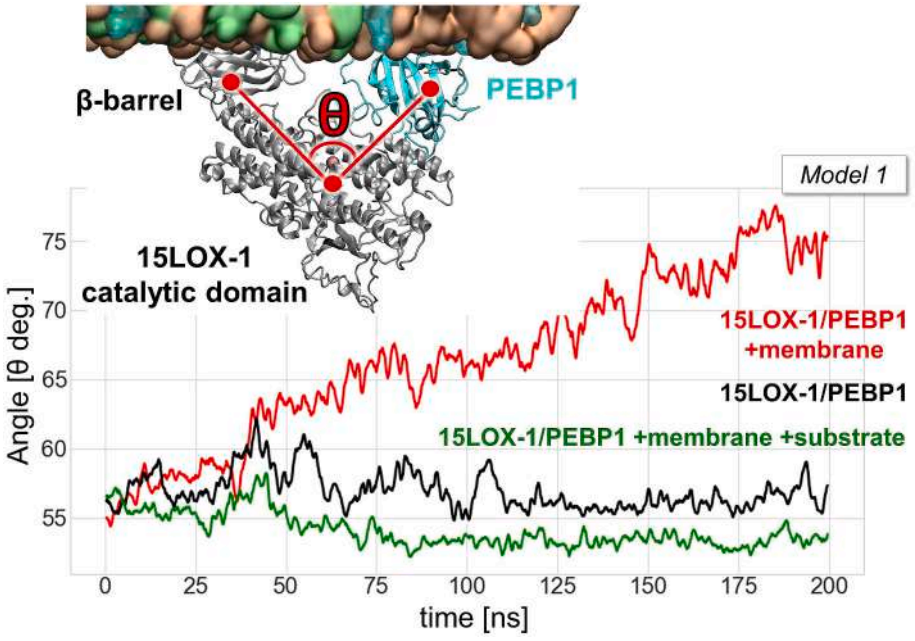

Fig. 2. Time evolution of the angle θ in *Model 1* for the 15LOX-1/PEBP1 complex simulations with/without the membrane and in the presence of bound SAPE at the catalytic site. θ is defined as the angle between center of the mass of β-barrel, catalytic domain and PEBP1 structure as indicated by the inset.

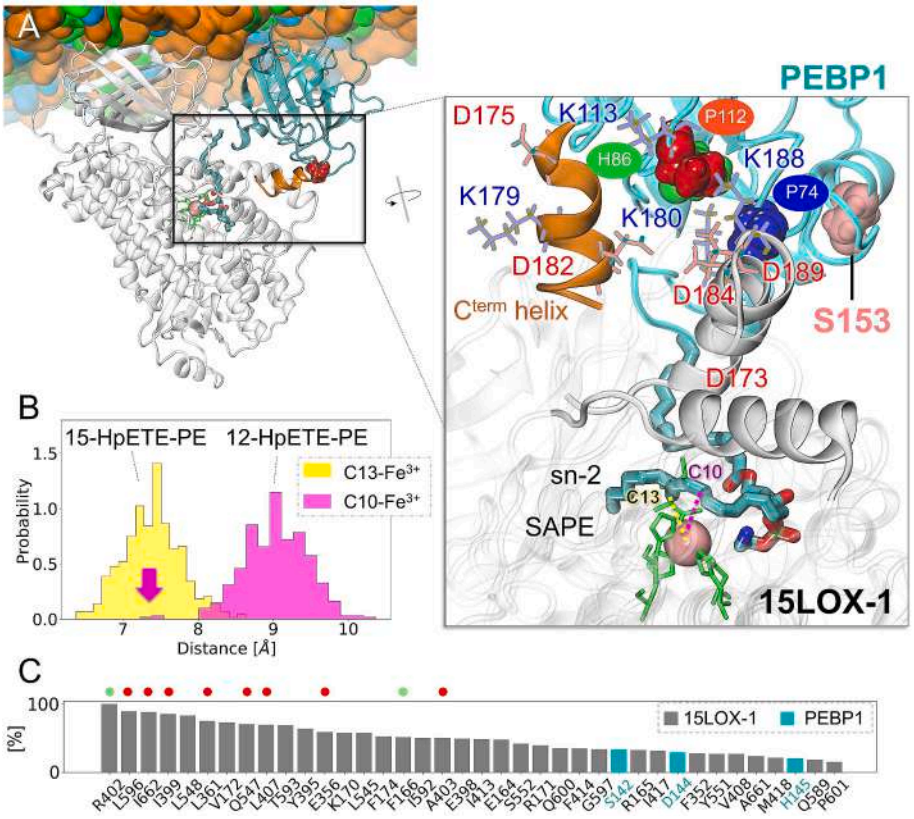

Fig. 3. Interactions between 15LOX-1/PEBP1 and SAPE. (A) 15LOX-1/PEBP1/SAPE complex in *Model 1* after 200 ns MD simulation with the membrane. The *inset* shows a close view of the SAPE-binding interface of 15LOX-1/PEBP1. The C-terminal helix (D175-Y186) is shown in *orange*; *red, blue, green*, and *pink spheres* refer to P112, P74, H86 and S153 of PEBP1, respectively. The catalytic residues H365, H540, H544 and I662 are displayed in *green sticks*. All charged residues within 7 Å from P112 are displayed. **(B)** Probability distribution of the distance between iron and hydrogen donors (C13 (*yellow histogram*) and C10 carbons (*pink histogram*)) of SAPE which correspond to the 15-HpETE-PE and 12-HpETE-PE products. *Pink arrow* refers to the occurrence of C10-iron distance at ~7.2 Å. **(C)** Distribution of the most frequent contacts between SAPE and 15LOX-1/PEBP1. The count numbers are normalized.

binding interactions with 15LOX-1: i) crosslinking by an amine-directed reagent, glutaric dialdehyde and ii) Far Western blotting [65]. Results demonstrated that treatment of the proteins with glutaraldehyde leads to the appearance of additional band detectable by silver staining and anti-PEBP1 antibody. To assess the role of different amino acids in PEBP1/15LOX-1 association, we prepared several mutants of PEBP1, such as P112E, H86A, H86E, Y176X and P74L. Complex formation was strongly suppressed when P112E mutant was used, while the other mutations did not affect the PEBP1/15LOX-1 complex formation (Fig. 4B). In the Far Western blotting protocol, an antibody-positive "bait" protein (15LOX-1) is used to detect the target "prey" protein (PEBP1). The bands corresponding to PEBP1 were also 15LOX-1-positive (Fig. 4C). These experiments also showed that the formation of PEBP1/15LOX-1 complex was strongly suppressed when P112E was used in place of wt PEBP1. In contrast, the interactions of the other PEBP1 mutants with 15LOX-1 were similar to that of the wt protein.

P112E mutation also inhibited the production of both 15-HpETE-PE and 12-HpETE-PE by 15LOX-1/PEBP1 (Fig. 4D). This was particularly obvious for 15-HpETE-PE whose formation was completely abrogated by the P112 mutation (compare Fig. 4A and D).

To computationally examine the validity of the predicted model, we next considered the experimentally analyzed mutations, H86A, H86E, P74L and P112E (Fig. 4) on PEBP1 and their potential effect on the complex formation. Therefore, we prepared four types of 15LOX-1/PEBP1/SAPE systems, each corresponding to a different mutant of PEBP1, and performed 75 ns MD simulations in the presence of the membrane (Fig. 5). The results indicate that the mutations H86A, H86E and P74L were neutral (Fig. 5A, *blue, green,* and *black* insets). The corresponding complexes were stable and angle θ defined above exhibited the same behavior as that observed for the wt PEBP1 in its complex with 15LOX-1/SAPE (Fig. 2 *vs blue, green* and *black* curves in Fig. 5A). In contrast, the P112E mutation caused a significant conformational change in the PEBP1/15LOX-1/SAPE system that triggered the opening of the complex after ~20 ns (Fig. 5A, *red* curve, #2, Movie 1). This reorganization led to a short period of more favorable interactions at a slightly different 15LOX-1 region (30–40 ns), but finally resulted in a wide opening of the complex (>45 ns; *red inset*, #3).

During this period, the electrostatic potential at P112E changed drastically compared to that of the wt PEBP1 (Fig. 5B). Initially, the negatively charged regions, similar for both wt and mutant P112E PEBP1, were centered on D134-E135, S142-D144, E159, and E182-G186 (*dark red*, #1). However, after 20–24 ns, the potential energy increased by over 20% (from −63 to −77 kT/e, #2) and additional residues, such as D69, D72, G108-S109, P112E, D144-H155, contributed to a highly negative potential energy which resulted in the repulsion of the α2 helix of 15LOX-1 (see Movie 1). This effect was coupled to a loss of interactions near a hub residue E175 (on 15LOX-1, *pink sphere* in Movie 1) with PEBP1 K148, Y81 and W84 (*thin blue, green and white sticks*), thus leading to E175-K113 interaction instead, and further reorganization in electrostatic potential in P112E PEBP1 (#3). During the simulations, we observed slight changes in the electrostatic potential of the wt PEBP1 at the interface with 15LOX-1. Originally, the interface was negatively charged, indicated by a *white dashed oval* at 1 ns; then it underwent a transition to a more neutral and positive state upon complexation with 15LOX-1, particularly near R141 and S142. This transition facilitated multiple interactions between E175 and wt PEBP1, as depicted by a *pink sphere* in Movie 2. Furthermore, negatively charged regions formed on both sides of the α2 helix of 15LOX-1 (P112 mutant >100 ns) centered around G108-S109, Y181-G186, and D134-E135. Those changes, however, did not affect PEBP1/15LOX-1 interactions which were constantly maintained for over 100 ns. Additionally, we noticed that the loss of interactions between P112E mutant and 15LOX-1 (Movie 1) not only initiated the opening of the complex, but might also have impacted the catalytic activity of the enzyme by destabilization of the E164-F174 loop that interacts with the catalytic I662 through K170 (Movie 1, *thick blue sticks*). This loop maintained stable interactions in wt PEBP1 system.

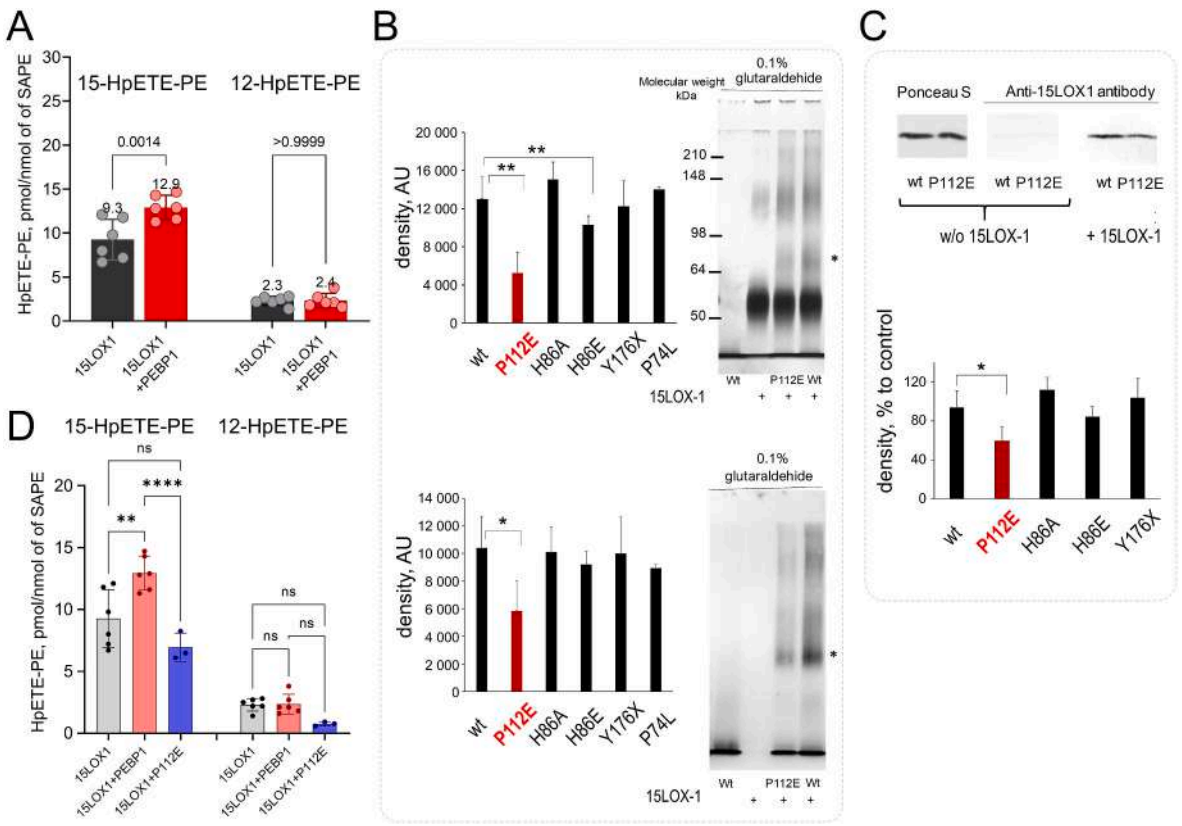

Fig. 4. Mutations in PEBP1 and their effects observed by LC-MS. (A) *Bar plot* comparing 15-HpETE-PE and 12-HpETE-PE formation by 15LOX-1 and by 15LOX-1/PEBP1. Data are mean ± s.d., n = 6 (ANOVA test). SAPE:DOPC liposomes were incubated with 0.04 μM 15LOX-1±PEBP1 (1:1) for 2.5 min. **(B)** Interaction of 15LOX-1 with wild type and mutated forms of PEBP1. Samples containing 15LOX-1 and PEBP1 were treated with 0.1% glutaraldehyde for 20 min at room temperature and reaction was stopped by the addition 200 mM of Tris –HCl (pH 7.5). Samples were run in SDS-PAGE and in some cases, electro-transferred to nitrocellulose membrane. Proteins were revealed by staining with silver (*upper panel*) or by incubation with anti–PEBP1 antibodies (*lower panel*). The density of the band that appeared after incubation of PEBP with 15LOX-1 in the presence of glutaraldehyde (marked by asterisks) was assessed to be significant only in the presence of P112E and H86A mutants.**P < 0.001, *P < 0.05. **(C)** Binding of 15LOX-1 to wt PEBP1 and PEBP1 mutants in the presence of dioleoyl-PE containing liposomes revealed by Far Western blotting. Ponceau S staining of proteins (*left panel*). Immuno-detection of 15LOX-1 bound to PEBP1 using anti-15LOX-1 antibody (*right panel*). Membrane containing electro-transferred PEBP1, but not incubated with 15LOX-1, was used as a control (*central panel*).*P < 0.05. Quantitation of 15LOX-1 bound to wt PEBP1 and mutant forms of PEBP1 with anti-15LOX-1 antibody. **(D)** *Bar plot* comparing 15-HpETE-PE and 12-HpETE-PE formation by 15LOX-1, 15LOX-1/PEBP1, and by 15LOX-1/P112E PEBP1. SAPE:DOPC (1:1, 100 μM) liposomes were incubated with 0.04 μM 15LOX-1 ± PEBP1 (1:1) for 2.5 min or 0.04 μM 15LOX-1 ± PEBP1 mutant P112 (1:1) for 5 min. Data are mean ± s.d., One-way ANOVA.

4. Discussion

Ferroptosis is an iron-dependent cell death driven by the production of PUFA-PE hydroperoxides which serve as ferroptotic death signals [19]. Our recent work revealed that Fe-containing 15-LOX plays a major role in catalyzing the peroxidation of PUFA-PE, and in particular SAPE; and this catalytic activity is endowed upon complexation of 15-LOX with PEBP1 which modulates the substrate specificity of 15-LOX [12,19,31,33]. We demonstrated that the anti-ferroptotic action of the most commonly used ferroptosis inhibitor ferrostatin-1 is not limited to radical scavenging but also includes the suppression of SAPE peroxidation by 15LOX/PEBP1 [30]. Furthermore, we recently proposed two compounds that effectively suppress ferroptosis *in vitro* and *in vivo* upon targeting the interactions with 15LOX-2/PEBP1 [66]. These studies consistently highlight the pivotal role of PEBP1 in ferroptotic events. With this in mind and given the still largely enigmatic nature of enzymatic peroxidation, we conducted here a first computational study of the membrane-bound 15LOX-1/PEBP1/SAPE system dynamics, and showed that the computational predictions are consistent with previous [19] and current experimental data. The study helps advance our understanding of the molecular mechanisms underlying this crucial form of cell death.

Our study shows that the membrane plays a regulatory role in 15LOX/PEBP1 catalytic activity by inducing a conformational change that exposes an entry site conducing to 15LOX catalytic pocket, thus allowing SAPE molecules to access the catalytic site (Fig. 1). Additionally, the binding of SAPE not only stabilizes but also tightly locks the complex (Fig. 2), leading to an optimal pose for the peroxidation reaction (Fig. 3). Membrane interactions are known to trigger the activation of peripheral proteins, including those strictly associated with PL oxidation and the hydrolysis of PL oxidized forms (e.g., cytochromes [35–37] or phospholipases [10,38]). The current study provides another example of the important regulatory role of the lipid bilayer, this time in facilitating the catalytic activity of 15LOX in the 15LOX-1/PEBP1 complex to generate pro-ferroptotic oxidized PEs.

Our computational findings are at many levels consistent with the experimental data (Fig. 4A). The complex can generate two distinct peroxidation products, 15-HpETE-PE and 12-HpETE-PE. Among them, the former is PEBP1-dependent as indicated by LC-MS data and conformed by computations (Fig. 3A and B). We identified key residues involved in stabilizing the 15LOX-1/PEBP1 complex (Supplementary Fig. S9) and in the interactions with SAPE (Fig. 3C). Evaluations of the predicted 15LOX-1/PEBP1 interactions with PEBP1 mutations at residues participating in interfacial interactions with 15LOX-1, both *in silico* and in experiments (Fig. 4B–D and **5**) revealed the key role of P112. Among five such mutations (H86A, H86E, P74L, Y176X and P112E), P112E was distinguished by its effect on both 15LOX-1/PEBP1 complex

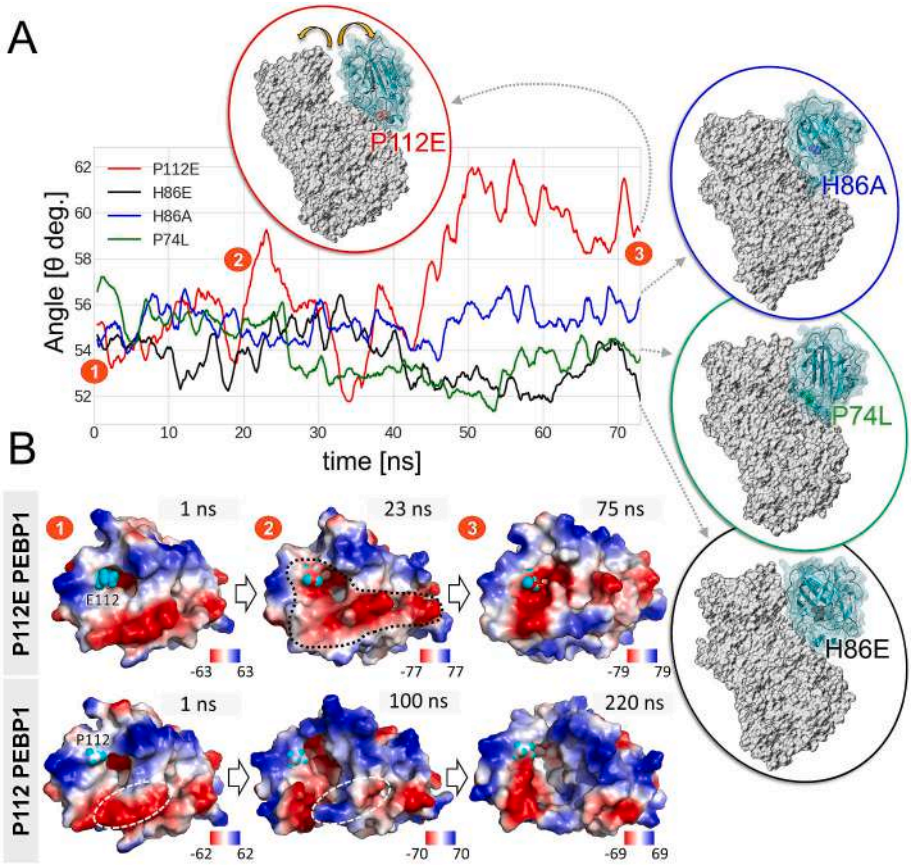

Fig. 5. Mutations at PEBP1 interfacial residues and their effects observed in simulations. (A) Time evolution of the angle θ for the complex of 15LOX-1/SAPE and four types of PEBP1 mutants, P112E, H86A, H86E, and P74L. The definition of the angle θ together with the wt PEBP1 results can be found in Fig. 2. *Yellow arrows* indicate a significant conformational change, which appears in the complex with P112E mutant. Displayed complexes are the final conformations from 75 ns of MD simulations. **(B)** Electrostatic surface potentials obtained from APBS-PDB2PQR software suite for wt PEBP1 and mutant P112E conformations from the simulations (0–220 ns for wt and 0–75 ns for P112E mutant). Positively charged regions are shown in *blue*, and negatively charged regions in *red*. The energy values are in units of kT/e.

formation (Fig. 4B and C, Fig. 5) and peroxidation mechanism (Fig. 4D).

Overall, the present study provides new insights into the molecular basis of the formation of the enzymatic complex 15LOX-1/PEBP1, the modulation of 15LOX catalytic activity by both PEBP1 and membrane lipid molecules themselves, and the access of the substrate, SAPE, into the catalytic pocket of 15LOX. The study highlights the significance of the localization of 15LOX/PEBP1 at the membrane periphery for the occurrence of membrane-induced conformational changes thus predispose 15LOX to catalyze the hydroperoxidation of PUFA-PEs. We further provide a plausible mechanism for PUFA-PE binding and insertion into the catalytic pocket of 15LOX, thus elucidating the way 15LOX-1/PEBP1 complex acquires lipids from the membrane to the catalytic site, a critical step in the production of peroxidized PUFA-PEs, the accumulation of which leads to ferroptosis. These findings, including those validated by experiments, holds significant potential for designing novel therapeutics that selectively target 15LOX-1/PEBP1 complexes for modulating ferroptotic events.

Author contributions

K.M.-R. H.B., I·B., and V.E.K. designed research; T.M., K.M.-R., A. O·K., S·N·S., Y·Y.T, V.A.T. performed research; A.P.V. contributed new reagents/analytic tools; T.M., K.M.-R. A.O.K., S·N·S., Y·Y.T, V.A.T., W·N., H·B., I·B., and V.E.K. analyzed data; and K.M.-R., I·B., H.B. and V. E.K. wrote the paper. All co-authors read the paper.

Declaration of competing interest

The authors declare that they have no known competing financial interests or personal relationships that could have appeared to influence the work reported in this paper.

Acknowledgements

This work was supported by NIH (HL114453, U01AI156924, U01AI156923, CA165065, NS076511, NS061817, P01DK096990 and R01GM139297), by Polish National Science Centre no. 2019/35/D/ST4/02203. We kindly thank Theodore R. Holman for providing the 15LOX-1 structure for experimental studies. K.M.-R. is thankful for the facilities and computer time allocated by the Interdisciplinary Center for Modern Technologies (NCU) for quantum chemistry calculations in Gaussian. K.M-R and W.N. are members of #MEMOBIT and EF "Nanoscale Biophysics" Teams.

Appendix A. Supplementary data

Supplementary data to this article can be found online at https://doi.org/10.1016/j.freeradbiomed.2023.09.001.

References

[1] B.R. Stockwell, J.P. Friedmann Angeli, H. Bayir, A.I. Bush, M. Conrad, S.J. Dixon, S. Fulda, S. Gascon, S.K. Hatzios, V.E. Kagan, K. Noel, X. Jiang, A. Linkermann, M. E. Murphy, M. Overholtzer, A. Oyagi, G.C. Pagnussat, J. Park, Q. Ran, C. S. Rosenfeld, K. Salnikow, D. Tang, F.M. Torti, S.V. Torti, S. Toyokuni, K. A. Woerpel, D.D. Zhang, Ferroptosis: a regulated cell death nexus linking metabolism, Redox Biology, and Disease, Cell 171 (2) (2017) 273–285.
[2] I. Ćepelak, S. Dodig, D.Ć. Dodig, Ferroptosis: regulated cell death, Arh. Hig. Rada. Toksikol. 71 (2) (2020) 99–109.
[3] X. Jiang, B.R. Stockwell, M. Conrad, Ferroptosis: mechanisms, biology and role in disease, Nat. Rev. Mol. Cell Biol. (2021) 1–17.
[4] K. Mikulska-Ruminska, I. Shrivastava, J. Krieger, S. Zhang, H. Li, H. Bayır, S. E. Wenzel, A.P. VanDemark, V.E. Kagan, I. Bahar, Characterization of differential dynamics, specificity, and allostery of lipoxygenase family members, J. Chem. Inf. Model. 59 (2019) 2496–2508.
[5] H.H. Dar, Y.Y. Tyurina, K. Mikulska-Ruminska, I. Shrivastava, H.-C. Ting, V. A. Tyurin, J. Krieger, C.M. St Croix, S. Watkins, E. Bayir, G. Mao, C.R. Armbruster, A. Kapralov, H. Wang, M.R. Parsek, T.S. Anthonymuthu, A.F. Ogunsola, B.

A. Flitter, C.J. Freedman, J.R. Gaston, T.R. Holman, J.M. Pilewski, J. S. Greenberger, R.K. Mallampalli, Y. Doi, J.S. Lee, I. Bahar, J.M. Bomberger, H. Bayır, V.E. Kagan, Pseudomonas aeruginosa utilizes host polyunsaturated phosphatidylethanolamines to trigger theft-ferroptosis in bronchial epithelium, J. Clin. Invest. 128 (10) (2018) 4639–4653.
[6] D. Tang, R. Kang, T.V. Berghe, P. Vandenabeele, G. Kroemer, The molecular machinery of regulated cell death, Cell Res. 29 (5) (2019) 347–364.
[7] W.-D. Bao, P. Pang, X.-T. Zhou, F. Hu, W. Xiong, K. Chen, J. Wang, F. Wang, D. Xie, Y.-Z. Hu, Loss of ferroportin induces memory impairment by promoting ferroptosis in Alzheimer's disease, Cell Death Differ. 28 (5) (2021) 1548–1562.
[8] N. Yan, J. Zhang, Iron metabolism, ferroptosis, and the links with Alzheimer's disease, Front. Neurosci. 13 (2020) 1443.
[9] S.J. Guiney, P.A. Adlard, A.I. Bush, D.I. Finkelstein, S. Ayton, Ferroptosis and cell death mechanisms in Parkinson's disease, Neurochem. Int. 104 (2017) 34–48.
[10] W.-Y. Sun, V.A. Tyurin, K. Mikulska-Ruminska, I.H. Shrivastava, T. S. Anthonymuthu, Y.-J. Zhai, M.-H. Pan, H.-B. Gong, D.-H. Lu, J. Sun, Phospholipase iPLA 2 β averts ferroptosis by eliminating a redox lipid death signal, Nat. Chem. Biol. (2021) 1–12.
[11] G. Miotto, M. Rossetto, M.L. Di Paolo, L. Orian, R. Venerando, A. Roveri, A.-M. Vučković, V.B. Travain, M. Zaccarin, L. Zennaro, Insight into the mechanism of ferroptosis inhibition by ferrostatin-1, Redox Biol. 28 (2020), 101328.
[12] T.S. Anthonymuthu, E.M. Kenny, I. Shrivastava, Y.Y. Tyurina, Z.E. Hier, H.-C. Ting, H.H. Dar, V.A. Tyurin, A. Nesterova, A.A. Amoscato, K. Mikulska-Ruminska, J. C. Rosenbaum, G. Mao, J. Zhao, M. Conrad, J.A. Kellum, S.E. Wenzel, A. P. VanDemark, I. Bahar, V.E. Kagan, H. Bayır, Empowerment of 15-lipoxygenase catalytic competence in selective oxidation of membrane ETE-PE to ferroptotic death signals, HpETE-PE, J. Am. Chem. Soc. 140 (51) (2018) 17835–17839.
[13] M. Yang, C.L. Lai, SARS-CoV-2 infection: can ferroptosis be a potential treatment target for multiple organ involvement? Cell death discovery 6 (1) (2020) 1–6.
[14] A.M. Fratta Pasini, C. Stranieri, D. Girelli, F. Busti, L. Cominacini, Is ferroptosis a key component of the process leading to multiorgan damage in COVID-19? Antioxidants 10 (11) (2021) 1677.
[15] S. Tavakol, A.M. Seifalian, Vitamin E at a High Dose as an Anti-ferroptosis Drug and Not Just a Supplement for COVID-19 Treatment, Biotechnology and Applied Biochemistry, 2021.
[16] Y. Singh, G. Gupta, I. Kazmi, F.A. Al-Abbasi, P. Negi, D.K. Chellappan, K. Dua, SARS CoV-2 aggravates cellular metabolism mediated complications in COVID-19 infection, Dermatol. Ther. 33 (6) (2020), e13871.
[17] B.R. Stockwell, J.P.F. Angeli, H. Bayir, A.I. Bush, M. Conrad, S.J. Dixon, S. Fulda, S. Gascón, S.K. Hatzios, V.E. Kagan, Ferroptosis: a regulated cell death nexus linking metabolism, redox biology, and disease, Cell 171 (2) (2017) 273–285.
[18] M. Conrad, V.E. Kagan, H. Bayir, G.C. Pagnussat, B. Head, M.G. Traber, B. R. Stockwell, Regulation of lipid peroxidation and ferroptosis in diverse species, Genes Dev. 32 (9–10) (2018) 602–619.
[19] S.E. Wenzel, Y.Y. Tyurina, J. Zhao, C.M.S. Croix, H.H. Dar, G. Mao, V.A. Tyurin, T. S. Anthonymuthu, A.A. Kapralov, A.A. Amoscato, PEBP1 wardens ferroptosis by enabling lipoxygenase generation of lipid death signals, Cell 171 (3) (2017) 628, 641. e26.
[20] Z. Shen, J. Song, B.C. Yung, Z. Zhou, A. Wu, X. Chen, Emerging strategies of cancer therapy based on ferroptosis, Adv. Mater. 30 (12) (2018), 1704007.
[21] C. Liang, X. Zhang, M. Yang, X. Dong, Recent progress in ferroptosis inducers for cancer therapy, Adv. Mater. 31 (51) (2019), 1904197.
[22] R. Kim, A. Hashimoto, N. Markosyan, V.A. Tyurin, Y.Y. Tyurina, G. Kar, S. Fu, M. Sehgal, L. Garcia-Gerique, A. Kossenkov, Ferroptosis of tumour neutrophils causes immune suppression in cancer, Nature (2022) 1–9.
[23] D. Stoyanovsky, Y. Tyurina, I. Shrivastava, I. Bahar, V. Tyurin, O. Protchenko, S. Jadhav, S. Bolevich, A. Kozlov, Y. Vladimirov, Iron catalysis of lipid peroxidation in ferroptosis: regulated enzymatic or random free radical reaction? Free Radic. Biol. Med. 133 (2019) 153–161.
[24] J.-Y. Lee, W.K. Kim, K.-H. Bae, S.C. Lee, E.-W. Lee, Lipid metabolism and ferroptosis, Biology 10 (3) (2021) 184.
[25] N.K. Singh, G.N. Rao, Emerging role of 12/15-Lipoxygenase (ALOX15) in human pathologies, Prog. Lipid Res. 73 (2019) 28–45.
[26] C. Schneider, D.A. Pratt, N.A. Porter, A.R. Brash, Control of oxygenation in lipoxygenase and cyclooxygenase catalysis, Chem. Biol. 14 (5) (2007) 473–488.
[27] V.E. Kagan, G. Mao, F. Qu, J.P.F. Angeli, S. Doll, C. St Croix, H.H. Dar, B. Liu, V. A. Tyurin, V.B. Ritov, Oxidized arachidonic and adrenic PEs navigate cells to ferroptosis, Nat. Chem. Biol. 13 (1) (2017) 81–90.
[28] J.P. Friedmann Angeli, M. Schneider, B. Proneth, Y.Y. Tyurina, V.A. Tyurin, V. J. Hammond, N. Herbach, M. Aichler, A. Walch, E. Eggenhofer, Inactivation of the ferroptosis regulator Gpx 4 triggers acute renal failure in mice, Nat. Cell Biol. 16 (12) (2014) 1180–1191.
[29] R.G. Snodgrass, B. Brüne, Regulation and functions of 15-lipoxygenases in human macrophages, Front. Pharmacol. 10 (2019) 719.
[30] T.S. Anthonymuthu, Y.Y. Tyurina, W.-Y. Sun, K. Mikulska-Ruminska, I. H. Shrivastava, V.A. Tyurin, F.B. Cinemre, H.H. Dar, A.P. VanDemark, T. R. Holman, Y. Sadovsky, B.R. Stockwell, R.-R. He, I. Bahar, H. Bayır, V.E. Kagan, Resolving the paradox of ferroptotic cell death: ferrostatin-1 binds to 15LOX/PEBP1 complex, suppresses generation of peroxidized ETE-PE, and protects against ferroptosis, Redox Biol. 38 (2020), 101744.
[31] A.A. Kapralov, Q. Yang, H.H. Dar, Y.Y. Tyurina, T.S. Anthonymuthu, R. Kim, C.M. S. Croix, K. Mikulska-Ruminska, B. Liu, I.H. Shrivastava, V.A. Tyurin, H.-C. Ting, Y. L. Wu, Y. Gao, G.V. Shurin, M.A. Artyukhova, L.A. Ponomareva, P.S. Timashev, R. M. Domingues, D.A. Stoyanovsky, J.S. Greenberger, R.K. Mallampalli, I. Bahar, D. I. Gabrilovich, H. Bayır, V.E. Kagan, Redox lipid reprogramming commands susceptibility of macrophages and microglia to ferroptotic death, Nat. Chem. Biol. 16 (3) (2020) 278–290.
[32] T.S. Anthonymuthu, E.M. Kenny, I. Shrivastava, Y.Y. Tyurina, Z.E. Hier, H.-C. Ting, H.H. Dar, V.A. Tyurin, A. Nesterova, A.A. Amoscato, K. Mikulska-Ruminska, J. C. Rosenbaum, G. Mao, J. Zhao, M. Conrad, J.A. Kellum, S.E. Wenzel, A. P. VanDemark, I. Bahar, V.E. Kagan, H.l. Bayir, Empowerment of 15-lipoxygenase catalytic competence in selective oxidation of membrane ETE-PE to ferroptotic death signals, HpETE-PE, J. Am. Chem. Soc. 140 (2018) 17835–17839.
[33] K. Mikulska-Ruminska, T.S. Anthonymuthu, A. Levkina, I.H. Shrivastava, O. O. Kapralov, H. Bayır, V.E. Kagan, I. Bahar, NO● represses the oxygenation of arachidonoyl PE by 15LOX/PEBP1: mechanism and role in ferroptosis, Int. J. Mol. Sci. 22 (10) (2021) 5253.
[34] P.V. Escribá, J.M. González-Ros, F.M. Goñi, P.K. Kinnunen, L. Vigh, L. Sánchez-Magraner, A.M. Fernández, X. Busquets, I. Horváth, G. Barceló-Coblijn, Membranes: a meeting point for lipids, proteins and therapies, J. Cell Mol. Med. 12 (3) (2008) 829–875.
[35] J.L. Baylon, I.L. Lenov, S.G. Sligar, E. Tajkhorshid, Characterizing the membrane-bound state of cytochrome P450 3A4: structure, depth of insertion, and orientation, J. Am. Chem. Soc. 135 (23) (2013) 8542–8551.
[36] I.L. Nantes, M.R. Zucchi, O.R. Nascimento, A. Faljoni-Alario, Effect of heme iron valence state on the conformation of cytochrome c and its association with membrane interfaces: a CD and EPR investigation, J. Biol. Chem. 276 (1) (2001) 153–158.
[37] V.E. Kagan, V.A. Tyurin, J. Jiang, Y.Y. Tyurina, V.B. Ritov, A.A. Amoscato, A. N. Osipov, N.A. Belikova, A.A. Kapralov, V. Kini, Cytochrome c acts as a cardiolipin oxygenase required for release of proapoptotic factors, Nat. Chem. Biol. 1 (4) (2005) 223–232.
[38] V.D. Mouchlis, D. Hayashi, A.M. Vasquez, J. Cao, J.A. McCammon, E.A. Dennis, Lipoprotein-associated phospholipase A2: a paradigm for allosteric regulation by membranes, Proc. Natl. Acad. Sci. USA 119 (2) (2022), e2102953118.
[39] Y. Yan, H. Tao, J. He, S.Y. Huang, The HDOCK server for integrated protein-protein docking, Nat. Protoc. 15 (5) (2020) 1829–1852.
[40] J. Choi, J.K. Chon, S. Kim, W. Shin, Conformational flexibility in mammalian 15S-lipoxygenase: reinterpretation of the crystallographic data, Proteins: Struct., Funct., Bioinf. 70 (3) (2008) 1023–1032.
[41] A. Waterhouse, M. Bertoni, S. Bienert, G. Studer, G. Tauriello, R. Gumienny, F. T. Heer, T.A.P. de Beer, C. Rempfer, L. Bordoli, R. Lepore, T. Schwede, SWISS-MODEL: homology modelling of protein structures and complexes, Nucleic Acids Res. 46 (W1) (2018) W296–W303.
[42] M.J. Banfield, J.J. Barker, A.C. Perry, R.L. Brady, Function from structure? The crystal structure of human phosphatidylethanolamine-binding protein suggests a role in membrane signal transduction, Structure 6 (10) (1998) 1245–1254.
[43] D.R. Koes, M.P. Baumgartner, C.J. Camacho, Lessons learned in empirical scoring with smina from the CSAR 2011 benchmarking exercise, J. Chem. Inf. Model. 53 (8) (2013) 1893–1904.
[44] J. Phillips, R. Braun, W. Wang, J. Gumbart, E. Tajkhorshid, E. Villa, C. Chipot, R. Skeel, L. Kale, K. Schulten, Scalable molecular dynamics with NAMD, J. Comput. Chem. 26 (16) (2005) 1781–1802.
[45] A. MacKerell Jr., D. Bashford, M. Bellott, R. Dunbrack Jr., J. Evanseck, M. Field, S. Fischer, J. Gao, H. Guo, S. Ha, All-atom empirical potential for molecular modeling and dynamics studies of proteins, J. Phys. Chem. B 102 (18) (1998) 3586–3616.
[46] M. Frisch, G. Trucks, H. Schlegel, G. Scuseria, M. Robb, J. Cheeseman, J. Montgomery Jr., T. Vreven, K. Kudin, J. Burant, Gaussian 03, Revision B. 05, Gaussian, Inc., Pittsburgh, PA, 2003, 12478.
[47] S. Jo, J.B. Lim, J.B. Klauda, W. Im, CHARMM-GUI Membrane Builder for mixed bilayers and its application to yeast membranes, Biophys. J. 97 (1) (2009) 50–58.
[48] M.A. Lomize, I.D. Pogozheva, H. Joo, H.I. Mosberg, A.L. Lomize, OPM database and PPM web server: resources for positioning of proteins in membranes, Nucleic Acids Res. 40 (D1) (2011) D370–D376.
[49] S. Zhang, J.M. Krieger, Y. Zhang, C. Kaya, B. Kaynak, K. Mikulska-Ruminska, P. Doruker, H. Li, I. Bahar, ProDy 2.0: increased scale and scope after 10 Years of protein dynamics modelling with Python, Bioinformatics (2021).
[50] W. Humphrey, A. Dalke, K. Schulten, VMD: visual molecular dynamics, J. Mol. Graph. 14 (1) (1996) 27–28, 33-8.
[51] E. Jurrus, D. Engel, K. Star, K. Monson, J. Brandi, L.E. Felberg, D.H. Brookes, L. Wilson, J. Chen, K. Liles, Improvements to the APBS biomolecular solvation software suite, Protein Sci. 27 (1) (2018) 112–128.
[52] A.J. Lam, F. St-Pierre, Y. Gong, J.D. Marshall, P.J. Cranfill, M.A. Baird, M. R. McKeown, J. Wiedenmann, M.W. Davidson, M.J. Schnitzer, Improving FRET dynamic range with bright green and red fluorescent proteins, Nat. Methods 9 (10) (2012) 1005–1012.
[53] S. Xu, T.C. Mueser, L.J. Marnett, M.O. Funk, Crystal structure of 12-lipoxygenase catalytic-domain-inhibitor complex identifies a substrate-binding channel for catalysis, Structure 20 (9) (2012) 1490–1497.
[54] J. Folch, M. Lees, G.H. Sloane Stanley, A simple method for the isolation and purification of total lipids from animal tissues, J. Biol. Chem. 226 (1) (1957) 497–509.
[55] A.L. Lomize, I.D. Pogozheva, M.A. Lomize, H.I. Mosberg, The role of hydrophobic interactions in positioning of peripheral proteins in membranes, BMC Struct. Biol. 7 (2007) 44.
[56] F. Geng, G. Zhang, Y. Wang, J. Lu, Membrane phosphatidylserine allosterically regulates the cytosolic phospholipase A2 activity via an electrostatic-switch mechanism, Soft Matter 18 (11) (2022) 2203–2210.

[57] N. Bhattarai, B.S. Gerstman, R.V. Stahelin, P.P. Chapagain, Plasma membrane association facilitates conformational changes in the Marburg virus protein VP40 dimer, RSC Adv. 7 (37) (2017) 22741–22748.
[58] D. Tieleman, B. Sejdiu, E. Cino, P. Smith, E. Barreto-Ojeda, H. Khan, V. Corradi, Insights into lipid-protein interactions from computer simulations, Biophysical Reviews (2021) 1–9.
[59] I. Ivanov, D. Heydeck, K. Hofheinz, J. Roffeis, V.B. O'Donnell, H. Kuhn, M. Walther, Molecular enzymology of lipoxygenases, Arch. Biochem. Biophys. 503 (2) (2010) 161–174.
[60] C. Mascayano, G. Núñez, W. Acevedo, M.C. Rezende, Binding of arachidonic acid and two flavonoid inhibitors to human 12-and 15-lipoxygenases: a steered molecular dynamics study, J. Mol. Model. 16 (2010) 1039–1045.
[61] P. Saura, R. Suardíaz, L. Masgrau, A.n. González-Lafont, E. Rosta, J.M. Lluch, Understanding the molecular mechanism of the Ala-versus-Gly concept controlling the product specificity in reactions catalyzed by lipoxygenases: a combined molecular dynamics and QM/MM study of coral 8 R-lipoxygenase, ACS Catal. 7 (7) (2017) 4854–4866.
[62] K. Deiss, C. Kisker, M.J. Lohse, K. Lorenz, Raf kinase inhibitor protein (RKIP) dimer formation controls its target switch from Raf 1 to G protein-coupled receptor kinase (GRK) 2, J. Biol. Chem. 287 (28) (2012) 23407–23417.
[63] K. Lorenz, M.J. Lohse, U. Quitterer, Protein kinase C switches the Raf kinase inhibitor from Raf-1 to GRK-2, Nature 426 (6966) (2003) 574–579.
[64] H.-f. Yan, T. Zou, Q.-z. Tuo, S. Xu, H. Li, A.A. Belaidi, P. Lei, Ferroptosis: mechanisms and links with diseases, Signal Transduct. Targeted Ther. 6 (1) (2021) 1–16.
[65] Y. Wu, Q. Li, X.-Z. Chen, Detecting protein–protein interactions by far western blotting, Nat. Protoc. 2 (12) (2007) 3278–3284.
[66] H.H. Dar, K. Mikulska-Ruminska, T.Y. Y, D.K. Luc, A. Yasgar, S.N. Samovich, A. Kapralov, A.B. Souryavong, V.A. Tyurin, A.A. Amoscato, M.W. Epperly, G. V. Shurin, M. Standley, T.R. Holman, A.P. VanDemark, S. Rana, A.V. Zakharov, A. Simeonov, J. Marugan, R.K. Mallampalli, S.E. Wenzel, J.S. Greenberger, G. Rai, H. Bayir, I. Bahar, V.E. Kagan, Discovering Selective Antiferroptotic Inhibitors of the 15LOX/PEBP1 Complex Noninterfering with Biosynthesis of Ipid Mediators, Proceedings of the National Academy of Sciences of the United States of America, 2023.

6.2 Article B

WatFinder: a ProDy tool for protein–water interactions

Bioinformatics, 2024, **40(8)**, btae516
https://doi.org/10.1093/bioinformatics/btae516
Advance Access Publication Date: 17 August 2024
Applications Note

OXFORD

Structural bioinformatics

WatFinder: a *ProDy* tool for protein–water interactions

James M. Krieger[1,†], Frane Doljanin[2,3,†], Anthony T. Bogetti[4], Feng Zhang[4], Thiliban Manivarma[2], Ivet Bahar[4,5,*], Karolina Mikulska-Ruminska[2,*]

[1]Biocomputing Unit, Department of Macromolecular Structure, National Center for Biotechnology (CNB-CSIC), Calle Darwin 3, Campus UAM Cantoblanco, 28049, Madrid, Spain
[2]Institute of Physics, Faculty of Physics, Astronomy and Informatics, Nicolaus Copernicus University in Torun, 87100, Torun, Poland
[3]Department of Physics, Faculty of Science, University of Split, 21000, Split, Croatia
[4]Laufer Center for Physical and Quantitative Biology, Stony Brook University, Stony Brook, NY 11794, United States
[5]Department of Biochemistry and Cell Biology, Renaissance School of Medicine, Stony Brook University, Stony Brook, NY 11794, United States

*Corresponding authors. Laufer Center for Physical and Quantitative Biology, Stony Brook University, Stony Brook, NY 11794, United States. E-mail: bahar@laufercenter.org (I.B.); Institute of Physics, Faculty of Physics, Astronomy and Informatics, Nicolaus Copernicus University in Torun, Grudziadzka 5 Street, 87100 Torun, Poland. E-mail: karolamik@fizyka.umk.pl (K.M.-R.)

†Equal contribution.

Associate Editor: Arne Elofsson

Abstract

Summary: We introduce *WatFinder*, a tool designed to identify and visualize protein–water interactions (water bridges, water-mediated associations, or water channels, fluxes, and clusters) relevant to protein stability, dynamics, and function. *WatFinder* is integrated into *ProDy*, a Python API broadly used for structure-based prediction of protein dynamics. *WatFinder* provides a suite of functions for generating raw data as well as outputs from statistical analyses. The *ProDy* framework facilitates comprehensive automation and efficient analysis of the ensembles of structures resolved for a given protein or the time-evolved conformations from simulations in explicit water, as illustrated in five case studies presented in the Supplementary Material.

Availability and implementation: *ProDy* is open-source and freely available under MIT License from https://github.com/ProDy/ProDy.

1 Introduction

The significance of accurate evaluation of protein–water interactions in the design of drugs, ligand binding, enzymatic reaction mechanisms, ion and substrate channeling, or proton/electron transfer, has long been recognized (Ladbury 1996, Verdonk *et al.* 2005, Maurer and Oostenbrink 2019). Water molecules are often active participants in the functional interactions of proteins, as they can donate or accept protons to form bridges between pairs of amino acids, form clusters, or perturb structure, thus directly impacting protein stability and function (Mattos 2002). They often facilitate binding, channeling, and transport events.

Understanding the effect of water molecules on protein structure and dynamics requires the examination of ensembles of conformations to capture recurrent patterns or the time evolution of interactions. To enable ensemble analyses, we developed a new tool *WatFinder* that takes advantage of the computing environment of the widely used *ProDy* application programming interface (API) (Bakan *et al.* 2011). *WatFinder* is designed to provide insights into key protein–water interactions that contribute to protein stability, conformational dynamics, and thereby function. Evaluation of these interactions is essential to designing small molecule modulators and assessing the effect of residue substitutions.

While comparable resources for detecting water interactions exist, they are mostly oriented toward water involvement in protein-ligand interactions and/or lack user-friendly interfaces for data processing or visualization. The currently available methods can be divided into two groups: (i) static methods, exemplified by 3D-RISM, SZMAP, or WaterFLAP (Nittinger *et al.* 2019) and (ii) dynamic methods relying on molecular dynamics (MD) simulations, such as WaterMap, GIST, WATsite, ProBiS H2O, WATCLUST (López *et al.* 2015), and AquaMMapS (Cuzzolin *et al.* 2018, Tošović *et al.* 2022). *WatFinder* is equipped with algorithms to analyze both static and dynamic objects. It offers full customization through the utilization of advanced force field parameters. It enables users to fine-tune their search criteria to achieve greater specificity and to extract the requisite level of information. Moreover, its integrated use within *ProDy* allows for advanced data processing and elaborate analyses and interpretation of the outputs in the light of the structural dynamics of protein families. Its use and utility are described in the tutorial page http://www.bahargroup.org/prody/tutorials/watfinder_tutorial/. Five case studies in the Supplementary Material illustrate its application to various systems, from membrane proteins to supramolecular machines.

Received: 14 June 2024; **Revised:** 8 August 2024; **Editorial Decision:** 12 August 2024; **Accepted:** 15 August 2024

2 Description and functionality

2.1 Inputs and outputs

The *WatFinder* tool uses several types of input data on protein and water coordinates: A single biomolecular structure, an ensemble of structures [using the Protein Data Bank (PDB) or mmCIF format], or a series of snapshots from an MD trajectory (DCD format generated by NAMD or CHARMM) (Fig. 1A). The ensemble of structures used as input may be the multiple models deposited for a given protein (e.g. NMR models), the structures resolved for the same protein under different states (bound/unbound, active/inactive, open/closed forms, different stages of an allosteric cycle, outward- or inward-facing states, etc.), or structural homologs that may retrieved using the *SignDy* (Zhang *et al.* 2019) module of *ProDy*. The user can provide the input files or fetch the data directly from the PDB using the PDB IDs, or downstream data from *ProDy*. Other types of MD trajectory file formats, such as TRR [*GROMACS* (Lindahl *et al.* 2001)] or CRD

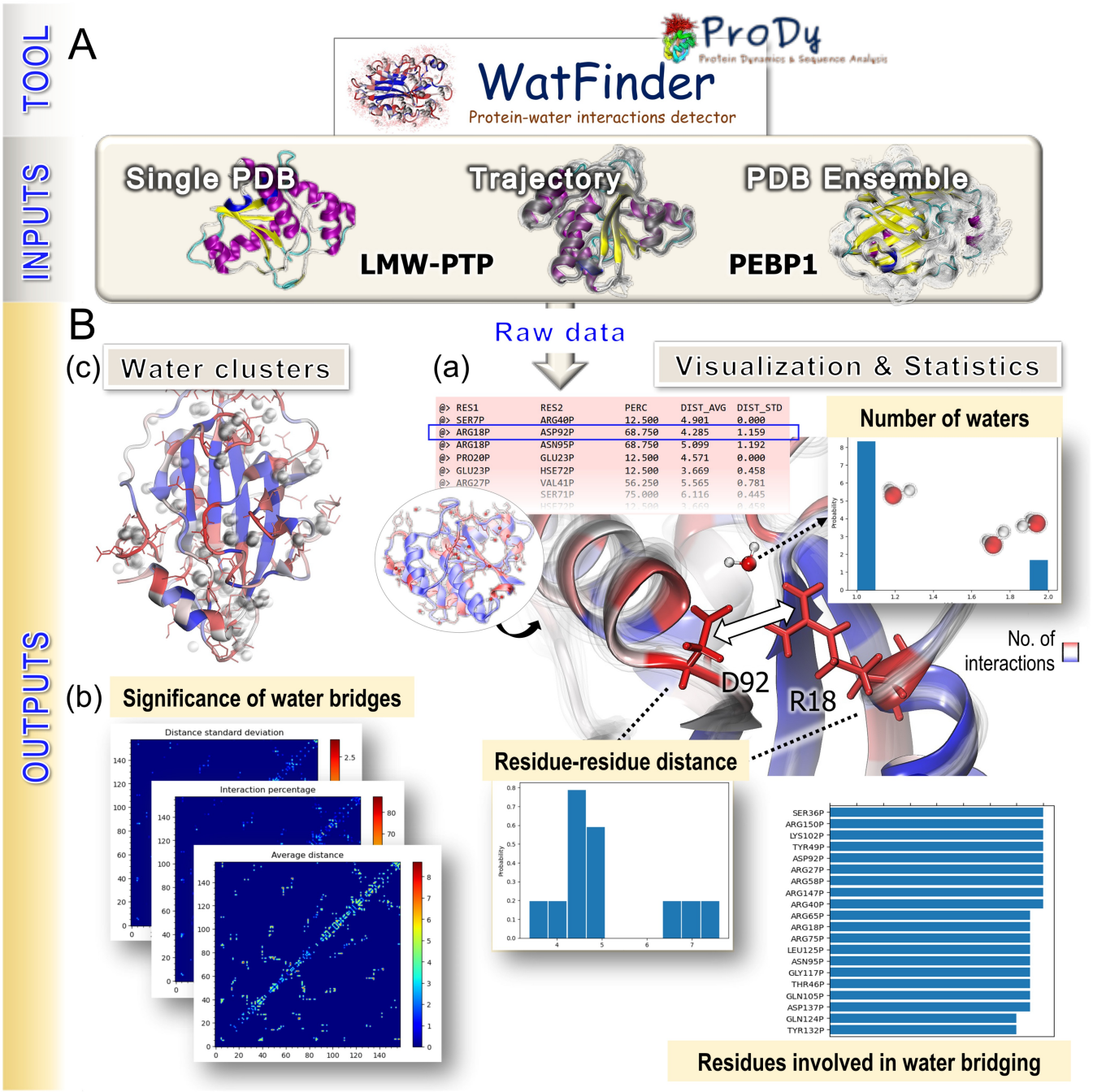

Figure 1. Schematic description of *WatFinder* implemented in *ProDy*. (A) *WatFinder* uses as input: (i) a single protein structure, (ii) an ensemble of structures as multiple structures resolved for the protein of interest, multiple models deposited in the PDB file, or homologous structures from multiple PDB files retrieved by *SignDy*, (iii) MD trajectory files. Here, we use for illustration the results for (i) low molecular weight protein tyrosine phosphatase [LMW-PTP; PDB: 5KQM (He *et al.* 2016)] and a short MD trajectory of the same structure using NAMD, and (ii) a multi-model ensemble of phosphatidyl ethanolamine-binding protein 1 [PEBP1, PDB: 1BEH (Banfield *et al.* 1998)]. Results for (i) are shown in the Supplementary Material. (B) Examples of (a) pairs of amino acids identified to be associated through water bridges, (b) the frequency or probabilistic occurrence of such water bridges between residue pairs, shown as heat maps based on different metrics, and (c) visualization of water clusters.

[*AMBER* (Salomon-Ferrer *et al.* 2013)] can be converted to multi-model PDB or to DCD format using external tools.

WatFinder functionalities are illustrated in Fig. 1. The outputs include: (i) raw data with a list of water bridges and associated residues; (ii) coordinates of protein structure and selected water molecules and/or water centers for visualization, and (iii) various plots and maps reflecting results from statistical analyses (Fig. 1B) using NumPy and Matplotlib.

2.2 Computing protein–water interactions

We have developed new classes for predicting the probabilistic occurrence of protein–water interactions, water bridges, or clusters of water molecules. *WatFinder* is adaptable and versatile, allowing users to change the geometric criteria for water bridge detection, including the threshold donor-acceptor distance (*distDA*) and orientational states (*anglePAWD*, *anglePDWA*, *angleWW*; see Fig. 2 and Supplementary Material), the threshold distance for residue-water interaction, and the number of water molecules away from residues of interest whose interactions are mediated by water bridge(s) (*maxDepth*). Water molecules can donate and accept up to two hydrogen bonds. While most bridges between residue pairs are established through one water molecule, multiple water molecules may also form a network of interactions or a cluster which is itself subject to time-dependent changes (e.g., formation of the water channel in Fig. 2, *bottom right*), thus affecting the protein's structure and dynamics. To address such occurrences, *WatFinder* is equipped with two algorithms: (i) a *Chain method* and (ii) a *Cluster method* (Fig. 2). The *Chain method* allows the user to

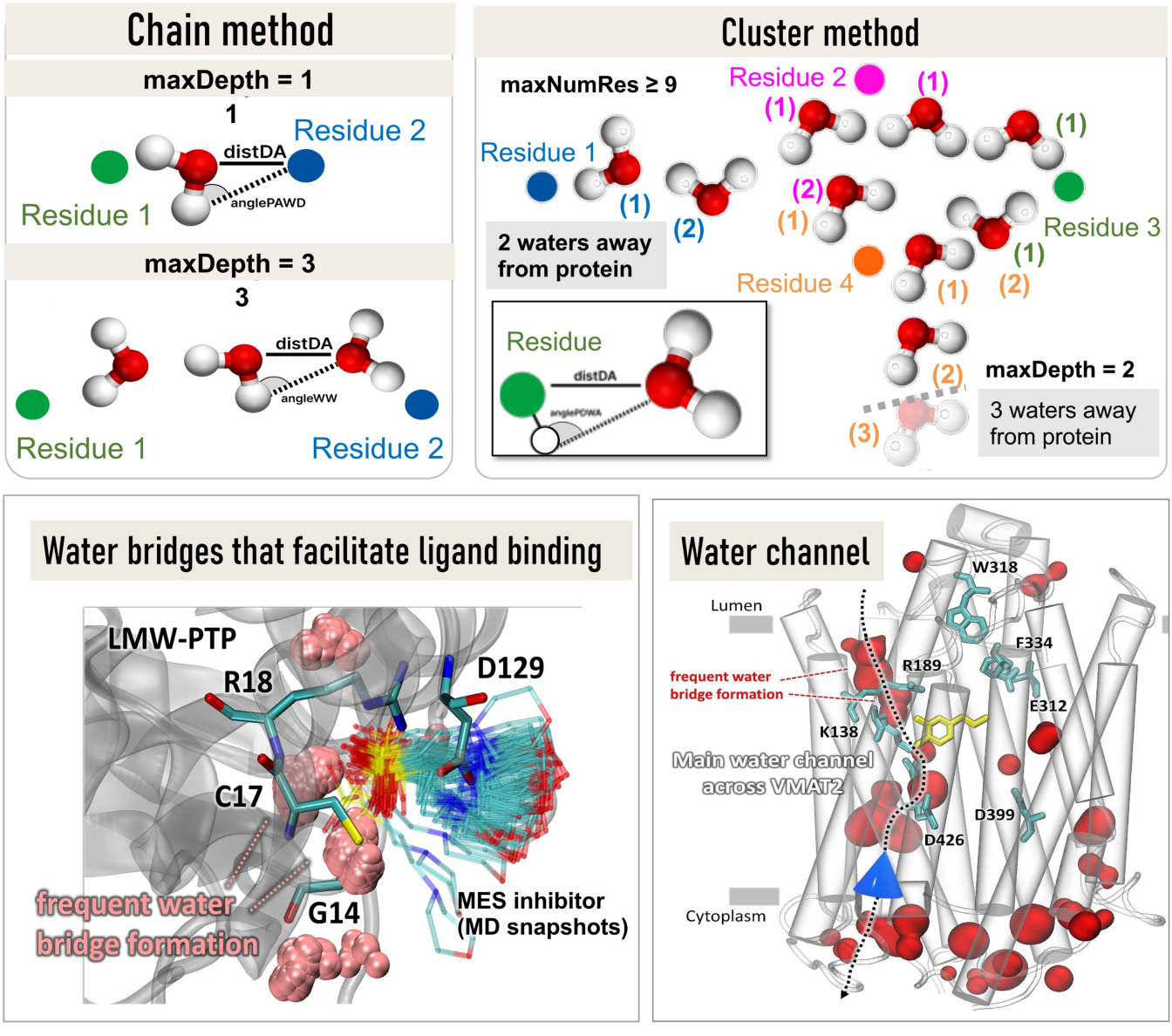

Figure 2. Description of two algorithms implemented in *WatFinder* for detecting protein–water interactions, and illustrative examples. *Top panels* describe the two algorithms: the chain method (*left*) and the cluster method (*right*). *Colored circles* represent hydrophilic residues interacting through water bridges. Water molecules are labeled by color-coded numbers in parentheses (on the *right*) to indicate their separations from the residues whose interactions they mediate. Distance and angle metrics are illustrated on the *left*, and lower bottom inset on the *right*. *Bottom panels*: Application of *WatFinder* to the identification of water bridges that facilitate inhibitor (MES) binding to a protein tyrosine phosphatase (*left*), and to detection of a water channel in the simulations of the vesicular monoamine transporter VMAT2. Details on these examples and others are presented in the Supplementary Material.

identify pairs of residues associated with a water bridge. The *Cluster method* additionally finds clusters involving multiple water molecules and multiple residues. Missing hydrogen atoms in the protein or water structure are added using PDBfixer/OpenMM (Eastman *et al.* 2017) or Open Babel (O'Boyle *et al.* 2011). *WatFinder* can also forecast in the absence of angular criteria for hydrogen atoms, as elaborated in the Supplementary Methods.

The major strength of *WatFinder* is its ability to analyze ensembles of structures. In addition to detecting and visualizing the water bridges occurring in each conformation, the tool identifies the most frequent bridges across the ensemble of structures, with output structures color-coded from 0 (*blue*) to 1 (*red*) (Fig. 1B). Moreover, *WatFinder* provides statistical data on the duration of interactions for each water bridge, on the average distances between hydrophilic residues involved in water bridges and their standard deviation, and on the number of water molecules participating in the interaction (Fig. 1Ba). Those data can be obtained for selected water bridges as well as the whole protein using color-coded maps (Fig. 1Bb). *WatFinder* is equipped with a cluster analyzer and characterizes the most favorable sites for water molecules within the structure [Figs 1Bc and 2 *(bottom left)*].

The power of *WatFinder* as a tool for exploring protein structure and dynamics originates from its integration with the *ProDy* framework. The user can distinguish the most significant protein–water interactions and examine their impact on protein dynamics in relation to (i) the normal modes evaluated by *ProDy* using elastic network models, (ii) the principal motions extracted by principal component analysis of MD trajectories using the *ProDy* ensemble analysis module, and (iii) the signature dynamics of family members accessible via the *SignDy* module of *ProDy*.

3 Conclusion

The *WatFinder* module provides a fast and straightforward way to analyze protein–water interactions to obtain statistically significant outputs with user-friendly graphical and visualization tools. The tool can generate high-quality, publication-ready plots and maps. The new features provided by *WatFinder* extend *ProDy*'s capabilities to identify sites potentially affected by solvation, or prone to protonation, which may be critically important for interpreting observed behavior and designing small molecule modulators of function. From the structural and computational biology points of view, *WatFinder* offers powerful methods for complementing current studies on the impact of mutations on protein structure and dynamics, and for protein–drug/ligand design, by providing robust information on sites susceptible to interactions with water molecules, to water-mediated associations and to protonation upon exposure to water.

Supplementary data

Supplementary data are available at *Bioinformatics* online.

Conflict of interest

None declared.

Funding

This work was supported by the Polish National Science Centre [2022/46/E/ST4/00053 to K.M.-R.]; the National Institutes of Health [R01 GM139297 to I.B.]; the European Union and Spanish Research Council (Consejo Superior de Investigaciones Científicas; CSIC) [H2020-MSCA-IF-2020/101024130 to J.M. K.]; and the Torun Students Summer Program in Exact Science (TSSP ExSci) program [F.D., K.M.-R.].

Data availability

Tutorials are available at http://www.bahargroup.org/prody.

References

Bakan A, Meireles LM, Bahar I. ProDy: protein dynamics inferred from theory and experiments. *Bioinformatics* 2011;**27**:1575–7.

Banfield MJ, Barker JJ, Perry AC *et al.* Function from structure? The crystal structure of human phosphatidylethanolamine-binding protein suggests a role in membrane signal transduction. *Structure* 1998;**6**:1245–54.

Cuzzolin A, Deganutti G, Salmaso V *et al.* AquaMMapS: an alternative tool to monitor the role of water molecules during protein–ligand association. *ChemMedChem* 2018;**13**:522–31.

Eastman P, Swails J, Chodera JD *et al.* OpenMM 7: rapid development of high performance algorithms for molecular dynamics. *PLoS Comput Biol* 2017;**13**:e1005659.

He R, Wang J, Yu Z-H *et al.* Inhibition of low molecular weight protein tyrosine phosphatase by an induced-fit mechanism. *J Med Chem* 2016;**59**:9094–106.

Ladbury JE. Just add water! the effect of water on the specificity of protein-ligand binding sites and its potential application to drug design. *Chem Biol* 1996;**3**:973–80.

Lindahl E, Hess B, Van Der Spoel D. GROMACS 3.0: a package for molecular simulation and trajectory analysis. *J Mol Model* 2001;**7**:306–17.

López ED, Arcon JP, Gauto DF *et al.* WATCLUST: a tool for improving the design of drugs based on protein–water interactions. *Bioinformatics* 2015;**31**:3697–9.

Mattos C. Protein–water interactions in a dynamic world. *Trends Biochem Sci* 2002;**27**:203–8.

Maurer M, Oostenbrink C. Water in protein hydration and ligand recognition. *J Mol Recog* 2019;**32**:e2810.

Nittinger E, Gibbons P, Eigenbrot C *et al.* Water molecules in protein–ligand interfaces. Evaluation of software tools and SAR comparison. *J Comput Aided Mol Des* 2019;**33**:307–30.

O'Boyle NM, Banck M, James CA *et al.* Open Babel: an open chemical toolbox. *J Cheminform* 2011;**3**:33.

Tošović J, Fijan D, Jukič M *et al.* Conserved water networks identification for drug design using density clustering approaches on positional and orientational data. *J Chem Inf Model* 2022;**62**:6105–17.

Verdonk ML, Chessari G, Cole JC *et al.* Modeling water molecules in protein–ligand docking using GOLD. *J Med Chem* 2005;**48**:6504–15.

Zhang S, Li H, Krieger JM *et al.* Shared signature dynamics tempered by local fluctuations enables fold adaptability and specificity. *Mol Biol Evol* 2019;**36**:2053–68.

Bioinformatics, 2024, 40, 1–4
https://doi.org/10.1093/bioinformatics/btae516
Applications Note

6.3 Article C

The presence of substrate warrants oxygen access tunnels toward the catalytic site of lipoxygenases

The presence of substrate warrants oxygen access tunnels toward the catalytic site of lipoxygenases

Thiliban Manivarma[1], Wieslaw Nowak[1], Yulia Y. Tyurina[2], Vladimir A Tyurin[2], Hülya Bayir[2,3,4], Valerian E. Kagan[2,5,6,7], Karolina Mikulska-Ruminska[1*]

[1] Institute of Physics, Faculty of Physics, Astronomy and Informatics, Nicolaus Copernicus University in Torun, PL87100 Torun, Poland.
[2] Department of Environmental and Occupational Health, Center for Free Radical and Antioxidant Health, School of Public Health, University of Pittsburgh, Pittsburgh, PA 15261, USA.
[3] Department of Pediatrics, Division of Critical Care and Hospital Medicine, Redox Health Center, Vagelos College of Physicians and Surgeons, Columbia University Irving Medical Center, New York, NY 10032, USA.
[4] Department of Critical Care Medicine, Safar Center for Resuscitation Research, Children's Neuroscience Institute, Children's Hospital of Pittsburgh, University of Pittsburgh, Pittsburgh, PA 15213, USA.
[5] Department of Radiation Oncology, University of Pittsburgh, Pittsburgh, PA 15213, USA.
[6] Department of Chemistry, University of Pittsburgh, Pittsburgh, PA 15260, USA.
[7] Department of Pharmacology and Chemical Biology, University of Pittsburgh, Pittsburgh, PA 15261, USA.

**corresponding author:* karolamik@fizyka.umk.pl (KMR)

Keywords:

Ferroptosis, 15-lipoxygenase, PEBP1, ligand transport, molecular dynamics, phospholipids

Abstract

Ferroptosis is a regulated form of cell death driven by lipid peroxidation, with 15-lipoxygenase (15LOX) enzyme playing a critical role in catalyzing the oxygenation of polyunsaturated fatty acid-containing phospholipids, such as 1-stearoyl-2-arachidonoyl-sn-glycero-3-phosphoethanolamine (SAPE), to initiate this process. The molecular oxygen required for this catalytic reaction is subject to continuous competition among various oxygen-consuming enzymes, which influences the efficiency of lipid peroxidation. In this study, we utilized structure-based modeling and all-atom molecular dynamics simulations to explore the oxygen diffusion pathways in 15LOX-1 under varying oxygen concentrations and in the presence of key components, including a substrate, binding partner PE-binding protein 1 (PEBP1), and the membrane environment. Extensive computational experiments were performed on various system configurations, examining the role of substrate binding, membrane presence, and PEBP1 association in oxygen acquisition. Our computational results indicate that the substrate binding induces a conformational change in 15LOX-1, facilitating the simultaneous recruitment of one or two O_2 molecules, which drive peroxidation to predominantly singly- or less frequently doubly-oxidized products, respectively. A similar trend was observed by in our redox lipidomics analysis. Moreover, we noticed that the presence of the membrane significantly reduces irrelevant oxygen binding spots, directing oxygen molecules toward a primary tunnel essential for the catalytic activity. We identified two primary oxygen tunnels with sequentially and structurally conserved regions across the lipoxygenase family. These findings provide novel insights into the regulation of oxygen acquisition mechanism for LOX members, shedding light on the molecular basis of ferroptosis signaling.

Introduction

Ferroptosis is a recently conceptualized form of regulated cell death program, which operates by utilizing phospholipid peroxidation as the main mechanism for the destruction of the plasma membrane [1, 2]. The peroxidation of phospholipids that contain a polyunsaturated fatty acid (PUFA) tail at the sn2-position is a mandatory feature of this process [3]. Although different types of PUFAs can be subject to peroxidation, depending on cell types, it is PUFA-phosphatidylethanolamines (PE) that have been identified as the major pro-ferroptotic cell death signal [4-6]. It was established that two fatty acids - arachidonoyl (C20:4, AA) and adrenoyl (C22:4, AdA) esterified into PE after oxidation become a ferroptotic cell death signal [6]. Moreover, a recent study has demonstrated the involvement of yet another type of PUFA PE lipids - 1,2-di-arachidonoyl-PE (di-AA-PE) that also induce ferroptotic cell death [7]. The above studies also show that an enzyme 15-lipoxygenase (15LOX), forming in both isoforms, 15LOX-1 and 15LOX-2, a complex with PE-binding protein 1 (PEBP1), which plays a key role in triggering the peroxidation. An important aspect of 15LOX based catalysis is the iron-driven abstraction of hydrogen from a carbon atom in bis-allylic positions of arachidonoyl-PE (SAPE or ETE-PE) as a substrate, which generates a carbon-centered radical. This step involves a concerted mechanism composed of a proton-coupled electron transfer in which the electron is transferred to the ferric iron (Fe^{3+}-OH^-), which is then reduced to an inactive ferrous form (Fe^{2+}-H_2O), and the proton is acquired simultaneously by the hydroxide ligand [8]. After cis-double bond migration by one carbon atom, the SAPE radical then undergoes an oxidation by the dioxygen molecule (O_2). Thus formed peroxyl-radical SAPE-OO$^\bullet$ (or 15p-ETE-PE$^\bullet$) is then reduced by an electron transfer. The ferrous iron undergoes re-oxidation to a ferric form and the peroxy radical is protonated [8, 9], resulting in the main product, 15-HpETE-PE for both 15LOXs, or an alternative product 12-HpETE-PE for 15LOX-1 [10]. Once the hydroperoxyl product is created, the Fe^{3+}-OH^- cofactor is regenerated, and LOX can start a new catalytic cycle. The accumulated lipid hydroperoxides are denoted as a ferroptotic cell death signal. Molecular oxygen utilized in this process has to reach the active site deeply buried in 15LOX using free space in a protein matrix. The full understanding of where the oxygen transport tunnels are located or where the oxygen molecules are concentrated during the catalytic reaction is still elusive. Although the role of 15LOX and PEBP1 as a critical complex in the onset of ferroptosis is now well-established [6, 11-14], the precise mechanisms behind ferroptosis are still objects of debate. Some propose that ferroptosis can occur entirely non-enzymatically through the Fenton reaction [15, 16], while others imply that it can be driven entirely enzymatically via iron-containing enzymes like lipoxygenases [17, 18], or

being a combination of both mechanisms on different stages and depending on the cell type [19, 20].

As a consequence of ferroptosis-associated processes, the formation of reactive lipid electrophiles is observed. Thus, covalent adducts with cellular components are formed [21], further amplifying the detrimental effects on a cell. Among the most significant byproducts of lipid peroxidation during ferroptosis are reactive aldehydes, such as 4-hydroxynonenal (4-HNE) and malondialdehyde (MDA) [22, 23]. Those aldehydes, being highly electrophilic, readily react with nucleophilic amino acid residues such as lysine, cysteine, and histidine, resulting in the formation of protein adducts [24]. Such modifications can disrupt protein function [25] and also affect other cellular targets, including membrane lipids [26] and DNA [27]. The formation of those protein adducts is directly tied to the iron-catalyzed lipid peroxidation process, a hallmark of ferroptosis. Importantly, these adducts may contribute to the progression and execution of ferroptotic cell death, reinforcing the idea that ferroptosis is not solely a consequence of a membrane disruption but also involves extensive cellular damage mediated by lipid peroxidation products [22].

In aerobic organisms, molecular oxygen is essential for many biochemical pathways. Therefore, the ability to sense and acquire it, especially in hypoxia conditions, is critical for proper metabolism. There is constant competition between O_2-consuming enzymes to recruit O_2, which is limited but at the same time essential in cellular processes [28, 29]. Therefore, some of the enzymes are able to do it more effectively than competitors, and one of the factors that may drive such ability is the incorporation of structural adaptation that enhances O_2 binding. Cytochrome c oxidase in mitochondria is known to have a high affinity for O_2 (Km = 0.5 μM) [30]. This high affinity is beneficial for cellular respiration, especially under low-oxygen conditions. Lipoxygenases (Km ranging from 13 to 26 μM) or cyclooxygenases (Km between 10 and 12 μM) demonstrate lower oxygen affinity; however, they remain effective consumers of O_2 across a broad range of concentrations, which may vary between 0.5 μM (in hypoxia condition) through 200-300 uM (the highest natural levels in tissues), to over 500 μM (in hyperoxic conditions, during oxygen therapy) [30]. This functional capacity may be a result of a high catalytic activity of 15LOXs, which in the presence of PEBP1 oxygenate SAPE at rates K_{cat} of $0.11 \cdot 10^{-2}$ s^{-1} (15LOX-1) and $1.4 \cdot 10^{-2}$ s^{-1} (15LOX-2) [31]. Fast local consumption of oxygen facilitates diffusion of those molecules in the neighbourhood of LOXs. This raises the question whether specific structural elements of oxygen-dependent enzymes facilitate the acquisition or temporary storage of O_2, thereby enhancing their efficiency. Some structural studies on LOXs have suggested that the presence of hydrophobic tunnels within the enzyme that may facilitate the movement of O_2 directly

to the active site [32]. This could allow LOXs to access and potentially store O_2 and acquire this substrate more effectively than other enzymes lacking such tunnels.

In the current work, we employed structure-based modeling and all-atom molecular dynamics (MD) simulations to investigate oxygen diffusion pathways in human 15LOX-1 under varying oxygen concentrations and in the presence of key system components, including the SAPE substrate, PEBP1, and the membrane. Our study builds on previous findings where the 15LOX-1/PEBP1 complex model, generated through molecular docking and MD simulations, successfully explained the role of the P112 residue in 15LOX-1/PEBP1 interaction and its impact on substrate production ratios [6, 10]. Furthermore, our earlier work underscored the importance of a phospholipid membrane in initiating the mechanism of SAPE substrate acquisition to the catalytic site of 15LOX-1, thereby triggering the peroxidation process associated with ferroptosis [10]. In this study, we extend those insights through a series of computational experiments under different system configurations to examine the specific roles of the substrate, PEBP1, and the membrane in oxygen acquisition. Our approach aims to provide a deeper understanding of how these components collectively contribute to the initiation of ferroptotic signaling. By integrating structural modeling with MD simulations and redox lipidomics, we seek to elucidate the mechanisms by which oxygen is captured to the catalytic site and how this process is regulated within the 15LOX-1/PEBP1 complex.

Results and discussion

Identification of the O_2 diffusion pathways in the 15LOX-1/PEBP1 complex. To determine the localization of O_2 diffusion pathways within 15LOX-1 in the presence of different components of the system, we embarked on a series of 160 all-atom MD simulations (in total 20 μs, **Supplementary Tab. 1**). Herein, to delineate the tunnels involved in both, entering and exiting the catalytic site of the enzyme, we applied two initial models: (i) one or two O_2 molecules placed in proximity to the catalytic site of 15LOX-1 and (ii) fifteen O_2 molecules distributed randomly in the water environment. In both cases, we observed two primary tunnels for O_2 molecules, herein referred to as *Entrance A* and *Entrance B* (see **Fig. 1**). *Entrance A* (in red), governed by the structural arrangement of three helices located at V172- L191 (helix α2), Y395-T420, and N582-G597, facilitated O_2 passage (**Fig. 1a**). Along the tunnel several residues, such as I413, L588, L178, G181, S177, Q416, I592, I417, L182, G412, and L185 were exhibiting notable interactions with O_2 molecules (**Fig. 1b**, red asterisks). *Entrance B* (in blue, **Fig. 1a**), characterized by residues

A403, L361, R404, V408, N400, L366, and W144, facilitates O_2 movement along the pathway (**Fig. 1b**, blue asterisks). Despite both entrances offering access to the catalytic site, in our simulations *Entrance A* predominated in facilitating O_2 transit, with approximately 81% utilization compared to 19% for *Entrance B*, of observed events (**Supplementary Tab. 2)**.

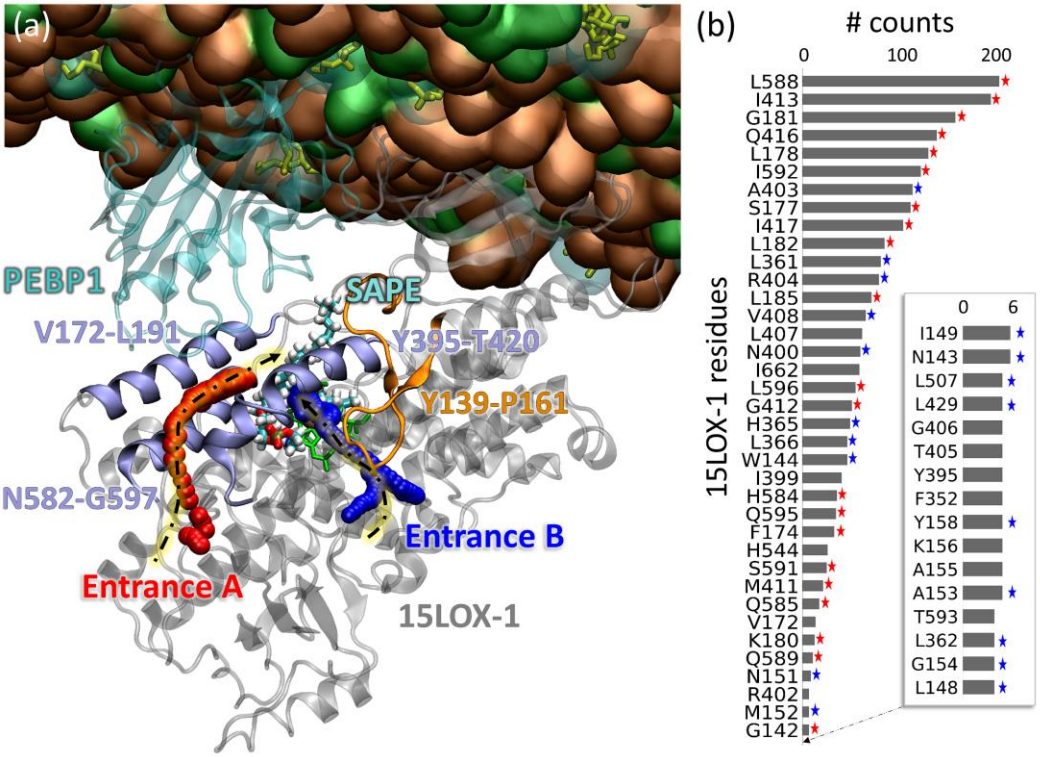

Figure 1. Oxygen pathways to the catalytic site of 15LOX-1 in the presence of PEBP1, substrate, and membrane. (a) The spatial structure of 15LOX-1/PEBP1/SAPE complex in the presence of the phospholipid membrane (upper part) with O_2 access tunnels leading to the catalytic site of LOX (green residues: H360, H365, H540, H544, I662). 15LOX-1 and PEBP1 are displayed in grey and cyan ribbon diagrams, respectively, and SAPE in cyan sticks at the catalytic site. The series of red and blue dots represent the diffusion path for O_2 through *Entrance A* and *Entrance B*, respectively. Three helices shown in ice blue (regions: V172-L191, Y395-T420, and N582-G597) form *Entrance A*. *Entrance B* is localized behind the loop W144-L150 (shown in orange). Membrane components are shown (DOPC in orange, DOPE in green, SAPE in blue). **(b)** The most frequent contacts of O_2 molecules with 15LOX-1 at *Entrance A* (red asterisks) and *Entrance B* (blue asterisks) are shown in histograms. Residues without asterisks are localized at the catalytic site cavity. Results are based on 500 ns of 75 MD trajectories for the 15LOX-1/PEBP1/SAPE system.

Is water assisting catalysis? Subsequently, using our newly developed tool for detecting water bridges and their associations, *WatFinder* [33], we identified recurrent water bridges within the 15LOX-1 structure in MD simulations and compared them with the localization of the crystallographic waters in 140 available PDB structures of LOXs **(Supplementary Tab. 3)**. We used ProDy tools [34] to select structures with spatial similarity to 15LOX-1 using the Dali server [35], and filtered out those shorter than 50% of the total residue length of 15LOX-1 or with an

RMSD value exceeding 1 Å. We further analyzed each structure with the *WatFinder* tool, selecting only water molecules involved in forming water bridges with the protein structure. Next, we assessed how many of these water molecules were located in the same region. Those that appeared at least 17 times within a ±0.9 Å range in the same region are displayed in **Fig. 2a** as green spheres. Water play an important role for proteins, and it is not only limited to the mechanical stability of the protein structure, but it may also participate in ligand binding or in facilitating O_2 transport [36]. Analysis of crystallographic structures provides valuable insights into water associations with LOXs structures. However, those are all rigid structures captured by experiments in a specific conditions. To include the whole spectrum of conformational changes with water interactions, we also analyzed our MD simulations with a similar approach. *WatFinder* analysis of trajectories revealed five major water-rich regions (see **Fig. 2a**, red spheres): (i) *Site 1A* and *Site 1B*, both located at the catalytic site, involving catalytic residues H544 and H360 (*Site 1A*) and residues H540, E657, and S659 (*Site 1B*); (ii) *Site 2*, at the *Entrance B*, encompassing G147-L150 region; and (iii-iv) *Site 3* and *Site 4,* potential allosteric sites for inhibitors, previously identified in rabbit 15LOX-1 (PDB: 2P0M) [37] and in human 5-LOX (PDB: 3O8Y) [38], respectively (**Fig. 2a**, **Supplementary Tab. 4**). Moreover, both sets of data, i.e., for 140 various crystallographic LOX structures (**Fig. 2a**, green spheres) and MD simulations (**Fig. 2a**, red spheres), revealed a similar association of water molecules for three regions: *Site 1B*, *Site 3*, and *Site 4* (see **Fig. 2a** and the inset). The crystallographic waters were also observed near *Site 2* but closer to the L366 hidden behind the loop region G147-L150 (**Fig. 2a**, inset). The exact localization may vary here due to the flexibility of the loop during the MD simulation. *Site 1A* was not populated by the crystallographic water molecules but may have formed due to the additional presence of SAPE in the catalytic site in our model. Water molecules clusters were, however, not detected along *Entrance A*, neither in MD nor in crystallographic structures, most likely due to the larger dimensions of a tunnel between V172-L191, Y395-T410, and N582-G597 helices that facilitate unrestricted water flow. These findings align with other studies that emphasize the role of water in (i) promoting O_2 mobility [39], possibly by lowering energy barriers at the entrance, modulating protein conformation by opening and closing the entrance to the tunnel, or offering transient hydrogen bonds that direct molecules to follow certain pathways, and (ii) contributing functionally at the active site [40, 41]. The conserved positioning of water molecules may also play yet another function. A role in stabilizing the emerging polar hydroperoxyl groups, thereby facilitating their displacement from the catalytic site following enzymatic reaction. As the lipid becomes enriched in hydroperoxyl groups, it loses hydrophobicity, increasing its affinity for the aqueous environment. This, and possibly additional factors, may also contribute to the product

release. One of them might be a substantial conformational change of the ligand after oxidation, as observed in [42], where the membrane-bound product of the 15LOX-1/PEBP1 complex, SAPE-OOH (or 15-HpETE-PE) changed its oxidized sn-2 tail shape due to the migration of double bond and -OOH insertion and orient its toward the aqueous environment. Another could be simply changes in the interactions between the enzyme and the lipid after oxidation. In total, we observed up to three simultaneous water molecules at the catalytic site per one enzyme in the crystallographic structures (see **Fig. 2a**, inset, KDE plots) and up to two in MD simulations.

Two binding sites of oxygen at the catalytic site of 15LOX-1. Next, we compared the localization of water clusters with the most frequent oxygen binding spots at the catalytic site. Two main oxygen clusters were detected using *WatFinder*, and they were district from the conserved waters (**Fig. 2b**, inset, in yellow). Cluster #1 was localized between the sn-2 SAPE and catalytic iron in a position predestined for its insertion at the C15 carbon atom, and Cluster #2 was located in close proximity to SAPE and surrounded by F352, I413, I417, Y551, I592, and T593 (see **Fig. 2b**, the inset). An equivalent binding site for the second cluster was also identified in our 15LOX-2 study [14]. In the simulations, we predominantly observed a single O_2 molecule at the catalytic site. However, in some cases, we also observed simultaneously up to two O_2 molecules (yellow KDE plot, **Fig. 2b**), occupying the exact locations defined as Cluster #1 and Cluster #2 in **Fig. 2b** (the inset). This suggests that while the first O_2 is ready to be inserted into the SAPE sn-2 tail (Cluster #1), the second O_2 molecule may already be positioned nearby, waiting for its turn (Cluster #2). Such a scenario corresponds to the formation of doubly-oxidized products.

The number of O_2 molecules in the catalytic site has a direct impact on the potential product generated by the enzyme. Therefore, to verify the computational prediction, we further performed LC-MS analysis to quantify the ratio of the oxygenated SAPE species formed during the catalytic reactions in both 15LOX isoforms, 15LOX-1 (**Fig. 2c**, left panel) and 15LOX-2 (**Fig. 2c**, right panel). We identified SAPE species containing between one (1[O]) to four (4[O]) oxygen atoms, with a significant predominance of two oxygen atoms for both 15LOXs, regardless of the presence of PEBP1 (**Fig. 2c**, 2[O]). This indicates the presence of a single O_2 molecule at the catalytic site, which aligns well with the MD simulations (**Fig. 2b**, KDE plot) and results in the formation of the SAPE-OOH product. The product requiring two O_2 molecules dispalyed a similar trend in both the experiments and simulations, being approximately 8-10 times less frequent in LC-MS experiments and 2-3 times less frequent in MD simulations. Lipidomics data also suggest that the presence of PEBP1 partially increases the abundance of the most predominant products. However, this trend was not captured by the MD simulations **(Fig. 2b)**.

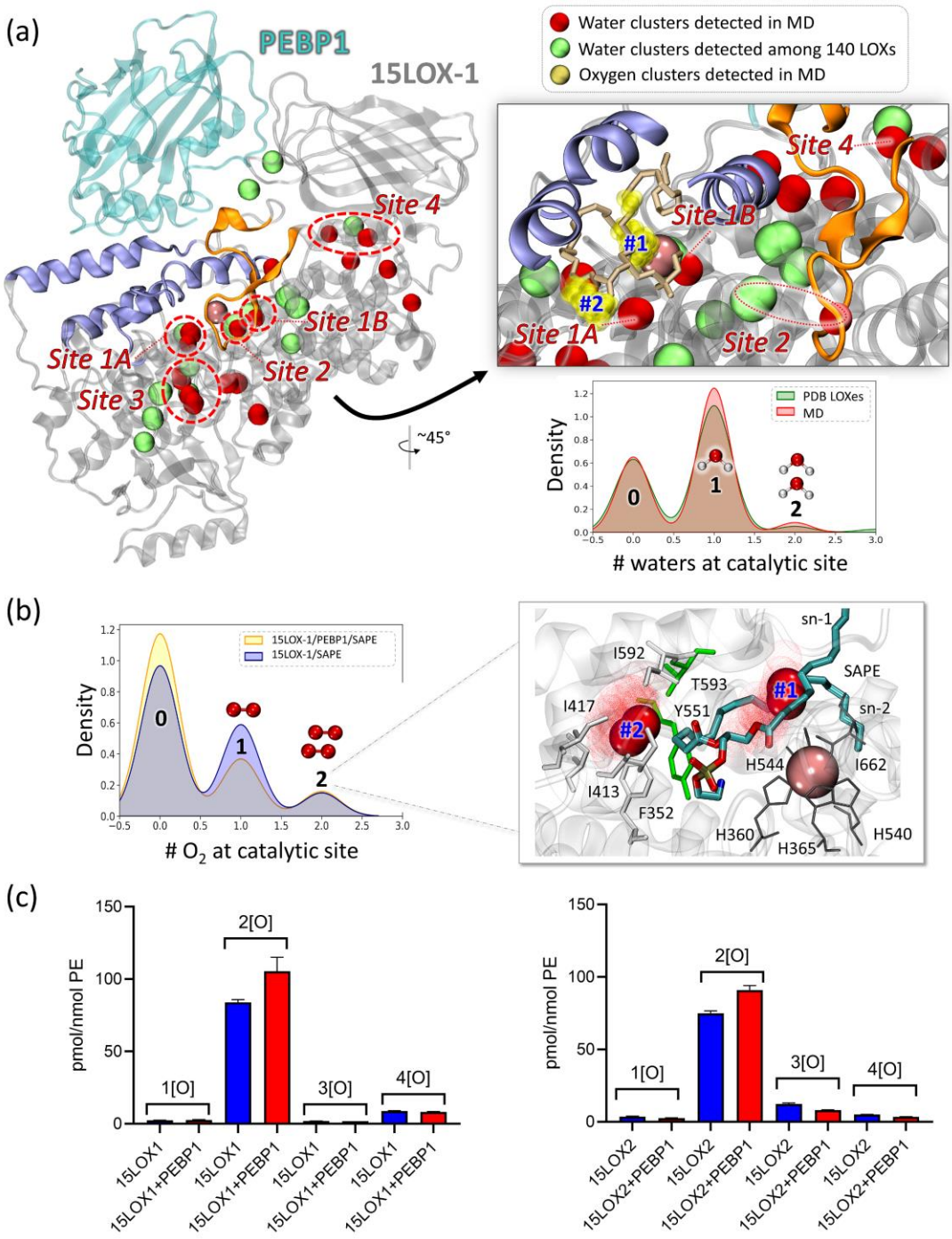

Figure 2. Analysis of water and O_2 clusters in the catalytic site of 15LOX-1 and the oxygenation products generated upon reaction with O_2 molecules. (a) Clusters of water (in green and red) and O_2 molecules (in yellow) which were identified using the *WatFinder* tool [33] from ProDy [34]. **(b)** KDE plots denote the number of waters and O_2 molecules detected in the catalytic site during MD simulation or, in the case of waters, also in 140 crystallographic PDB structures of LOXs. In the inset, the localization of O_2 molecules at the catalytic site of 15LOX-1. Dotted beads corresponds to the multiple oxygen positions (Cluster #1 and #2) when two O_2 molecules are present at the catalytic site. Residues involved in the coordination are displayed. Catalytic residues are displayed as grey sticks and catalytic iron as pink sphere. **(c)** Content of stearoyl-arachidonoyl PE (SAPE) oxygenated species with 1-4 oxygens formed in reaction catalyzed by 15LOX-1 (left panel) and 15LOX-2 (right panel) in the absence and in the presence of PEBP1.

The impact of the different components of the system on oxygen acquisition. Continuing our investigation, we explored the localization of O_2 tunnels in different configurations of the system, i.e., without membrane and with or without substrate to see the effect of each component on the system. Interestingly, the absence of a membrane did not affect the preference of the tunnels or their accessibility, as illustrated in **Fig. 3b** (*bottom panel*) where the most frequent contacts between O_2 and 15LOX-1 structure are displayed. However, the membrane played a crucial role in determining the duration of O_2 interactions with the catalytic site (**Fig. 3b***, upper panel*) and enhanced the presence of O_2 directly in it (**Fig. 3b***, bottom panel*). Moreover, the results imply that without a phospholipid membrane, the O_2 interaction with the enzyme occurs at various random sites more often (interactions outside the red/blue boxes, **Fig. 3b***, bottom panel*) that do not initiate the catalytic reaction. Contrary, in the presence of a membrane, the O_2 molecules due to the particular interactions are more directed toward the entry of the oxygen tunnel leading to the catalytic site (insignificant number of interactions outside the blue/red boxes). Additionally, in the presence of the substrate, we observed a close contacts between O_2 molecules and the catalytic site within 4.5 Å, which does not happen in the absence of substrate as it shown in the **Supplementary Tab. 2**. This imply that the substrate induces changes in the protein complex, enabling a more favorable environment for O_2 interactions. To investigate the cause of this behavior, we calculated the electrostatic potential surface [43, 44], which indicated no significant changes in the charge distribution in all systems studied but rather suggested a structural reorganization of the system in the presence of the substrate (**Fig. 3a**).

Next, we employed perturbation response scanning (PRS) [45] analysis to visualize the distribution of the most potent sensors (receivers of allosteric signals) and effectors (regulators of the global propagation of allosteric signals) within the protein structure. Such analysis helps to understand signaling pathways of the 15LOX-1/PEBP1 complex. We examined how this distribution changes in the presence and absence of the substrate and/or membrane (**Fig. 4**). It enables us to distinguish regions that are linked to the main O_2 and substrate binding sites. The PRS heat maps which provide information about the sensitivity and effectiveness of specific residues in transmitting signals are presented in **Supplementary Fig. 2**. The results indicate that the presence of the membrane reduces the number of potential sensor sites in the protein structure (see **Fig. 4B, D**, yellow ovals), confining them to the regions localized at the predominant tunnel near N192 at *Entrance A* (D189-L194, L290-S292, **Fig. 4A, C**). This fact may explain the observed O_2 propensity to form more stable interactions along the pathway to the catalytic site (**Fig. 3B**). Additionally, the absence of both SAPE and membrane increases PRS sensitivity in the regions closely interacting with substrate and/or membrane binding sites.

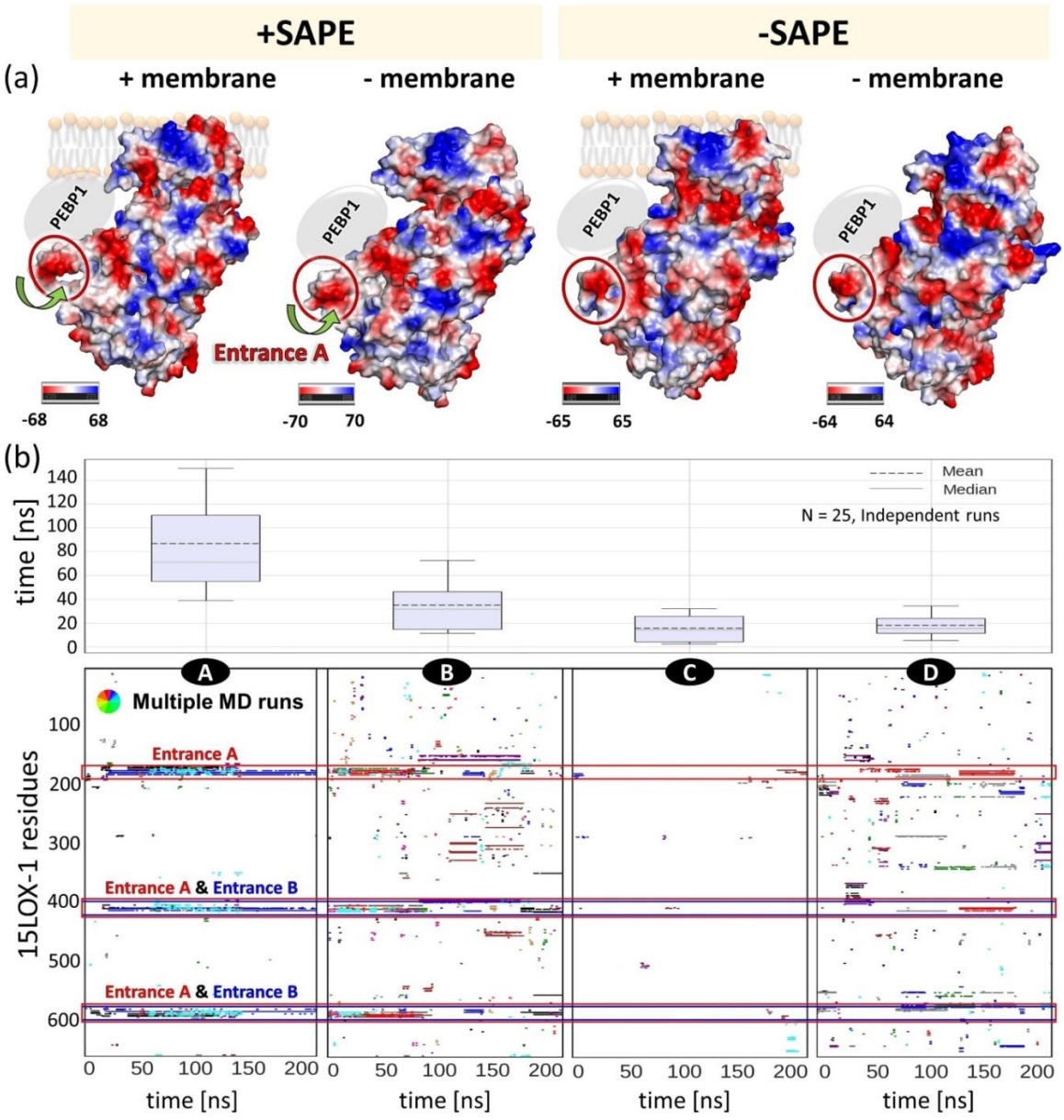

Figure 3. O_2 interactions with 15LOX-1 and entry/exit pathways observed in MD simulations of 15LOX-1/PEBP1 in the presence/absence of SAPE and biological membrane. (a) Global electrostatic potential surface of 15LOX-1 computed using Adaptive Poisson-Boltzmann Solver (ABPS) plugin, used units: kT/e. **(b)** Quantitative analysis of the residence time of O_2 molecules at the catalytic site or along the entrance to the catalytic site. Twenty-five independent MD simulations were considered. The mean value is denoted by a dashed line, and the median is shown in the standard line (*upper panel*). Illustration of the time evolution of contacts between O_2 molecules and 15LOX-1 residues based on 20 MD runs, shown in different colors. In addition to the 15LOX-1/PEBP1 complex, additional components were considered: **(A)** +SAPE +membrane, **(B)** +SAPE -membrane, **(C)** -SAPE +membrane, and **(D)** -SAPE -membrane. Interactions of O_2 with 15LOX-1 with residues located along *Entrance A* are shown in the red box, and for *Entrance B* in the blue box (*bottom panel*).

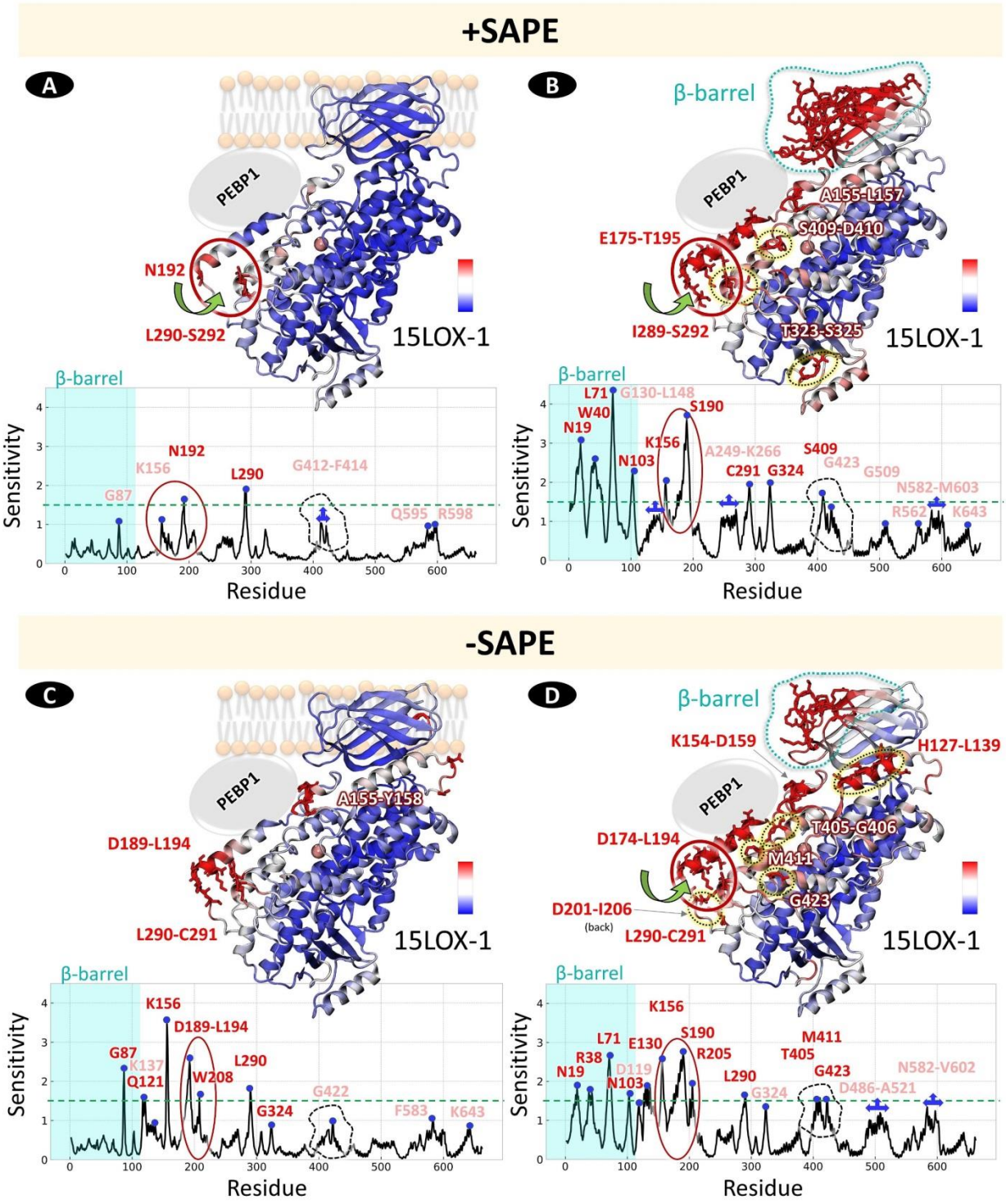

Figure 4. Changes in the role of 15LOX-1 residues as sensors of allosteric signals in the presence of different components of the system. The sensitivity of 15LOX-1 with/without SAPE and/or membrane was obtained from independent MD simulations using the PRS method. The plots display the propensity of residues to serve as sensors. The highest values represent the strongest sensors, shown in dark red on the spatial structures of the enzyme and denoted in the plots. The green dashed lines mark the cutoff for defining the strongest sensors in each system. Residues that reach values above the cutoff line are displayed in the 3D structure. Green arrows denote systems in which O_2 molecules were approaching the catalytic site via *Entrance A*.

Substrate interactions trigger opening the entrance to the catalytic site. Different studies have shown that substrate association may induce conformational changes in proteins, thus triggering acquisition of other substrate, as exemplified by cytochrome c oxidase [46]. When its substrate, cytochrome c, binds to cytochrome c oxidase, it induces a conformational change in the enzyme, exposing the oxygen-binding site and allowing the binding of oxygen as the next substrate. This is essential for the four-electron reduction of oxygen to water and for the proper functioning of the electron transport chain [46-48]. Another example is the cytochrome P450 family, where mechanism of action involves a conformational change upon substrate binding, which leads to a conformational change that exposes the oxygen-binding site. Oxygen binding as the second substrate is required for cytochrome P450 to carry out the monooxygenation reaction, transferring one oxygen atom to the substrate [49]. The opposite effect, wherein substrate binding induces the release of oxygen from the protein structure, is also well-known, as exemplified by the oxygen dissociation from hemoglobin upon 2,3-bisphosphoglycerate (2,3-BPG) binding [50]. Our simulations indicate a similar phenomenon: the interactions of SAPE substrate with 15LOX-1/PEBP1 complex induce a conformation change at *Entrance A* (group of three helices: V172 to L191, Y395 to T420, N582 to G597) and open a passage for O_2 to the catalytic site. More specifically, substrate-induced conformational changes cause one of the helices in the V172 to L191 region to open, creating a passage to the catalytic site of 15LOX-1. To demonstrate such conditional conformational changes, the time evolution of the distance between helix V172-L191 (α2) and helix N582-G597 was selected as a proper measure of the opening of *Entrance A*. Data are shown in **Fig. 5**. Notably, the distance between these helices in *Entrance A* increased by about 2 Å upon association of LOX with the SAPE substrate, as shown in **Fig. 5a, b** that allows to simultaneous aquire up to two O_2 molecules to the catalytic site (yellow KDE plot, **Fig. 2b**).

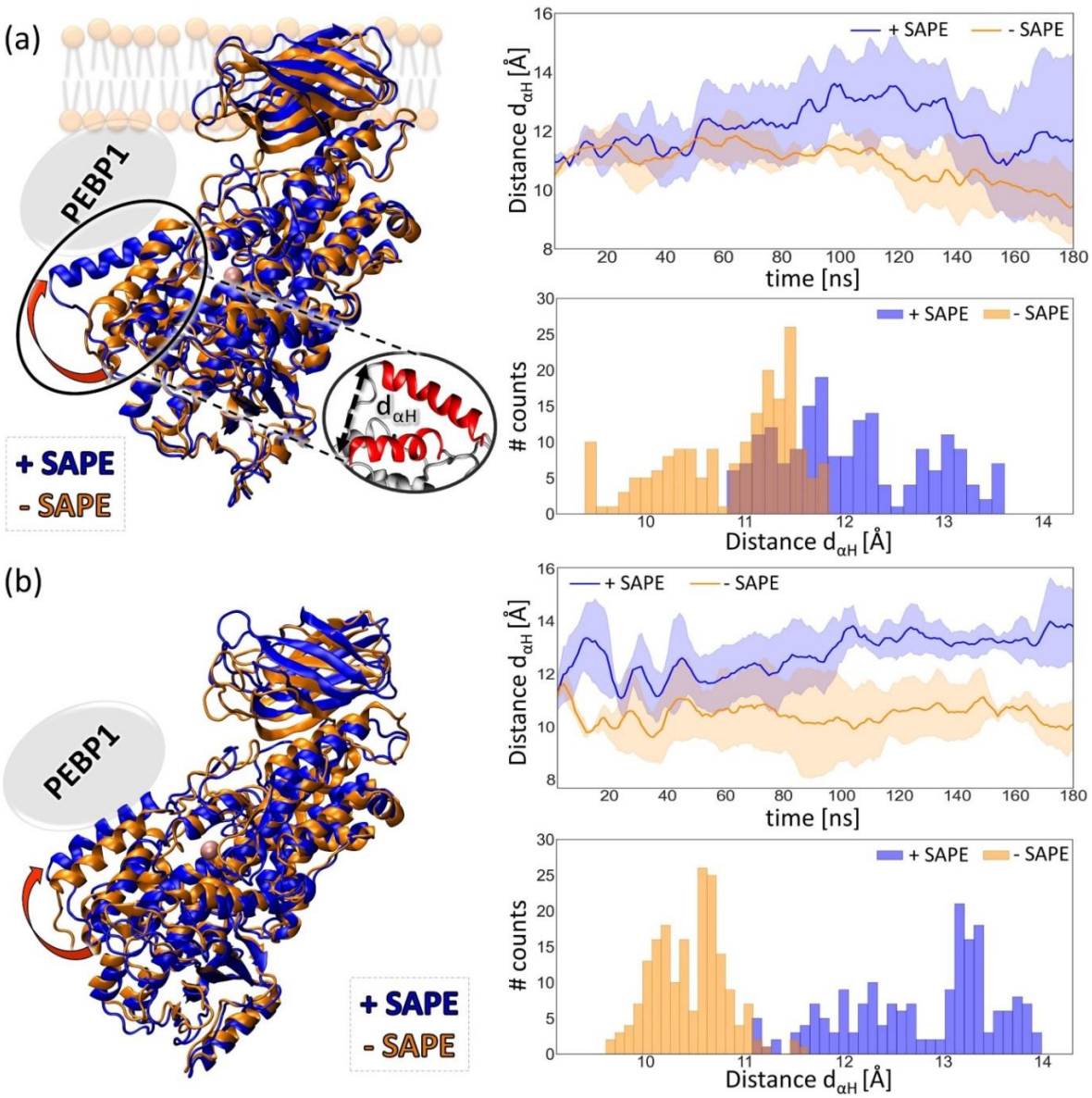

Figure 5. Conformational changes of 15LOX-1/PEBP1 complex upon SAPE interactions revealed by MD simulations. (a) Comparison of the final structures of 15LOX-1/PEBP1 ±SAPE complex in the presence of the membrane. 15LOX-1 with SAPE and 15LOX-1 without SAPE are shown in dark blue and dark orange, respectively. The opening motion of *Entrance A* is denoted by the red arrow. The quantitative analysis (right panels) shows opening of *Entrance A* by time evolution of $d_{\alpha H}$ plot and histogram plots for the 15LOX-1/PEBP1 in the presence and absence of substrate SAPE, with membrane. **(b)** Conformational changes of 15LOX-1/PEBP1 without biological membrane are shown. Dark blue represents 15LOX-1 with substrate SAPE and dark orange represents 15LOX-1 without substrate SAPE, opening of *Entrance A* shown by red arrow and quantitative analysis shows opening of *Entrance A* by time evolution of distance $d_{\alpha H}$ plot and histogram plots for the 15LOX-1/PEBP1 in the presence and absence of substrate SAPE, and without membrane.

Two main oxygen diffusion pathways in LOX family members. Our studies revealed two oxygen channels in the 15LOX-1 structure. To contextualize our findings, we gathered information on other members of the LOX family that have been investigated in previous studies (see **Supplementary Tab. 5**). Those data are illustrated in **Fig. 6a** and **Supplementary Fig. 3**, and demonstrate that similar oxygen pathways have also been observed in various LOX family members. This comparison suggests a conserved mechanism within this family.

To assess the key regions of the oxygen tunnels across various LOX enzymes, we further examined the conservation of the identified regions, both in terms of sequence and structure. Despite the generally low sequence identity among LOX family members - less than 30% [51] - we identified two distinct motifs along the identified oxygen pathways that may have structural or functional significance: I-[ND]-x-x-[AG]-R-x-x-L-[IV] (at *Entrance A*) and [ST]-H-[LW]-[AL]-x-x-H-[LA] (at *Entrance B*), where x is any residue (**Fig. 6a**, **Supplementary Fig. 4**). Further screening of those motifs using MOTIF server feature from GenomeNet [52] pointed to 205 and 96 structures for *Entrance A and B* motifs, respectively, which exhibit similar motifs in their architecture. Among those, we identified LOX family members, kynurenine 3-monooxygenase (*Entrance A* motif) or cytochrome P450 (*Entrance B* motif).

Although the sequence-conserved motifs provided some insight, they did not fully reveal the key regions involved in the mechanisms governing oxygen diffusion pathways present across the LOX family proteins. To gain a deeper understanding, we analyzed structural conservation, which proved to be more informative, indeed. This approach highlighted similarities in the distribution of residues with comparable properties, such as polar (in green, **Fig. 6b**), non-polar (in white), basic (in blue), and acidic (in red) residues, at both *Entrance A* and *Entrance B* (**Fig. 6b**). These residues create a similar environment for O_2 molecules, but their positions in the sequence vary, making them difficult to detect through a standard sequence alignment. This is particularly evident at *Entrance B*, which is formed by a loop which length can vary among LOX enzymes. However, residues with specific properties, such as G147-L148-L149 on 15LOX-1 (see **Fig. 6b**, bottom panel, orange stars) and the neighboring residue L366 (see **Fig. 6b**, bottom panel, thick white sticks), which is a part of the *Entrance B* motif, together form the entrance to the tunnel and are consistently positioned in a similar location across different LOX family members. Furthermore, residues W141 and W144 in 15LOX-1, along with R377, R404, and E501, E369, play a crucial role in stabilizing the loop structure through a combination of π-cation interactions (between W and R residues) and electrostatic interactions (between R and E residues, **Fig. 6b**). Additionally,

a hydrophobic core composed of L397, L160, P161, M152, and Y139 helps to maintain the integrity of the loop.

The second entrance to the LOX catalytic site, *Entrance A*, is characterized by residues that act as sensors for allosteric signals, including N192 and L290-S292 (**Fig. 6b**, upper panel) and additional residues along the N582-G597 helix (marked with red stars). On the opposite side, the Y395-T240 helix contains the *Entrance A* motif. Together, those elements form the entry point to the primary O_2 tunnel (denoted by red arrow in **Fig. 6b**, upper panel).

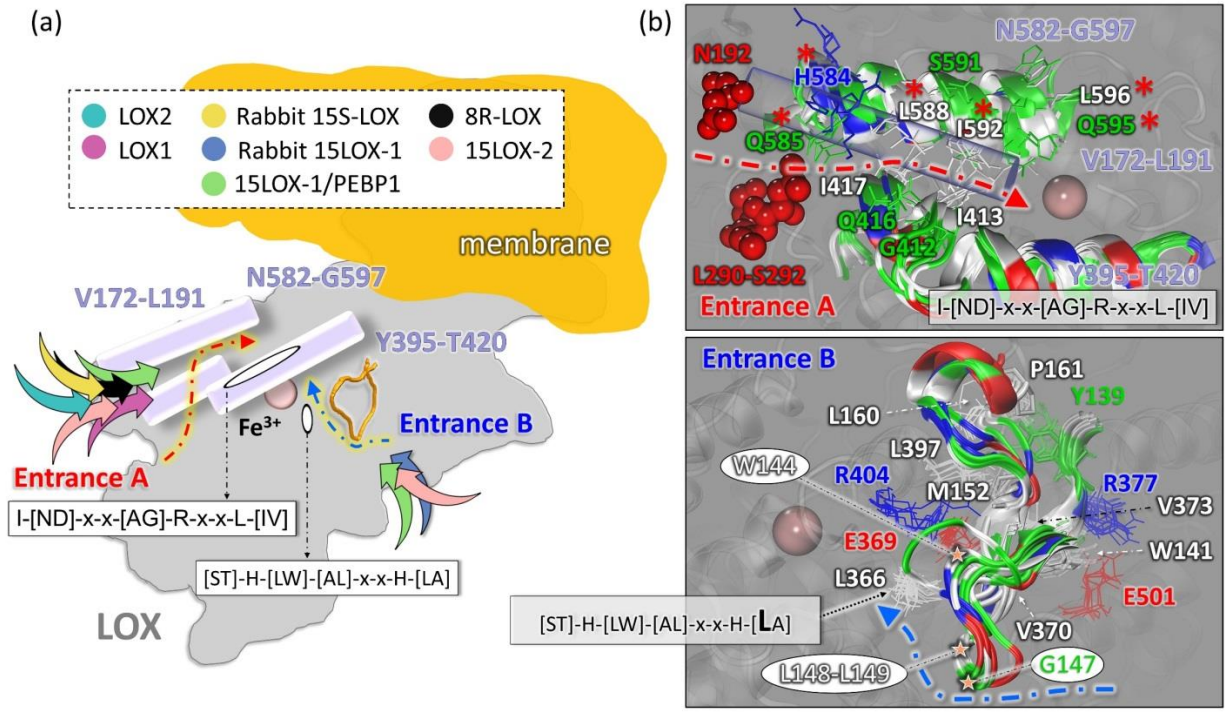

Figure 6. Oxygen pathways in different LOX family members. (a) Schematic representation of oxygen pathways in LOX members including rabbit 15LOX-1 (PDB: 1LOX; in blue), soybean LOX1 (PDB: 1YGE; in pink), rabbit 15S-LOX (PDB: 2P0M; in yellow), 15LOX-2 (PDB: 4NRE; in pink), 8R-LOX (PDB: 4QWT; in black), LOX2 (PDB: 5MED; in cyan), and our model of human 15LOX-1/PEBP1 (in green). Identified tunnels: *Entrance A* maintained by three helices (in purple) and *Entrance B* regulated by the Y395-T420 loop (in orange) are displayed. The directions of the flow of O_2 molecules for both entrances are illustrated with dashed red/blue arrows. Colored arrows show which O_2 entrance was identified for which LOX studies (more details in **Supplementary Tab. 5**). The catalytic iron is represented as a pink sphere. **(b)** A close view of *Entrance A* and *Entrance B* displayed for various structurally aligned LOXs. In addition to the various LOXs from panel a, three additional structures are included in the alignment: 12S-LOX (PDB: 8GHB), 5-LOX (PDB: 3O8Y) and bacterial *P. aeruginosa* PA-LOX (PDB: 5IR4). Sensor residues located at the entry of *Entrance A*, observed for the system with membrane and substrate, are represented as red spheres (N192, L290-S292), whereas sensor residues along the *Entrance A*, identified in the system without the substrate, are marked with red asterisks (H584, L588, I592, L596, Q595). The transparent helix (E175 to L191) is part of *Entrance* A. Helices (Y395 to T420 and N582 to T420) shown in cartoon format are responsible for the opening of *Entrance A*. The residues in *Entrance B* are shown with thin sticks representing neighboring residues (R377, E501, L366, E369, R404) and thick sticks representing conserved residues (P161, Y139, L160, L397, M152, V373, W141, V370). Residues with the same properties in different lipoxygenases are marked with orange stars (W144, G147, L148-L149). Details for other LOXs are presented in **Supplementary Tab. 6**.

Conclusions

Ferroptosis is an iron-dependent cell death driven by the production of PUFA-PE hydroperoxides which serve as ferroptotic death signals. Our recent work revealed that membrane plays a regulatory role in 15LOX-1/PEBP1 catalytic activity by inducing the conformational changes that exposes an entry site conducting to 15LOX-1 catalytic pocket, thus allowing SAPE lipids to access the catalytic site. The binding of SAPE not only stabilizes but also tightly locks the complex, leading to an optimal pose for the peroxidation process [10].

A crucial aspect of the 15LOX-1 catalytic reaction involves iron facilitating the removal of a hydrogen atom from a carbon in a bis-allylic position. This creates a carbon-centered radical, which then reacts with oxygen molecules to form hydroperoxyl product [53, 54]. The precise mechanism by which dioxygen molecules access the catalytic site, as well as the sequence in which the substrate and dioxygen arrive at the catalytic pocket, and the specific elements that facilitate or regulate this process, remained largely unknown. To investigate these processes, we employed computational modeling and lipidomics experiments to analyze the dynamics and association of O_2 molecules in relation to the 15LOX-1 structure in the presence of various components, including the binding partner PEBP1, the substrate SAPE, and the membrane.

Through extensive MD simulations, we identified two distinct tunnels used by O_2 molecules, referred to as *Entrance A* and *Entrance B* (**Fig. 1**), connecting different regions of the protein surface to a region of high oxygen affinity surrounding the catalytic center in 15LOX-1/PEBP1/SAPE, both in the presence and absence of the membrane (**Fig. 3**). *Entrance A* is shaped by the arrangement of three helices, specifically those spanning residues V172-L191, Y395-T420, and N582-G597 on 15LOX-1. *Entrance B* is localized behind the loop, near the W141-M152 region facing toward structurally conserved L366, which appears to function as a lid over the active site. At these sites, we identified sensors of allosteric signals (*Entrance A*, **Fig. 4**) and water clusters which may facilitate oxygen transport (Site 2 at *Entrance B*, **Fig. 2a**). Additionally, we observed frequently formed water interactions at the catalytic site that may be involved in hydroperoxy product release, along with two potential allosteric sites identified in rabbit 15LOX-1 [37] and 5-LOX [38] (**Fig. 2a**). These water molecules were identified in our MD simulations and among crystallographic structures of other LOX members. These highlight the role of water molecules, potentially in enhancing oxygen mobility [39] or contributing to the catalytic activity [40, 41]. Our findings revealed the simultaneous presence of up to two water molecules (in MD simulations) or three water molecules (based on 140 crystallographic structures) at the catalytic site, occupying four distinct cluster positions (**Fig. 2a**).

To validate our findings, we analyzed various lipoxygenases (**Fig. 6a**), considering both sequence and structural aspects. This integrated approach revealed key residues along the oxygen tunnels, some of which are conserved at the sequence level, including two LOX-conserved motifs: I-[ND]-x-x-[AG]-R-x-x-L-[IV] at *Entrance A*, and [ST]-H-[LW]-[AL]-x-x-H-[LA] at *Entrance B*. Additionally, other residues showed structural conservation, further supporting the functional relevance of these regions in oxygen transport across LOX architecture (**Fig. 6b**).

Our studies also examined the roles of various system components in regulating 15LOX-1 activity. Specifically, our data imply that the presence of a membrane reduces insignificant interactions between O_2 and random regions of 15LOX-1 (**Fig. 3-4**), instead promoting the directed movement of oxygen toward the tunnel entry leading to the catalytic site. Upon SAPE interaction, conformational changes at *Entrance A*, specifically the movement of V172-L191 region, facilitate the opening of a passage for oxygen to access the catalytic site (**Fig. 5**). Although the opening permits the simultaneous recruitment of up to two O_2 molecules, that are occupying distinct cluster positions (**Fig. 2a-b**), our analysis indicates that the catalytic site is more frequently occupied by a single O_2 molecule. This preference may reflect the formation of both singly- and doubly-oxidized products by LOXs which is observed in redox lipidomics data (**Fig. 2c**). A single O_2 molecule (**Fig. 2a-b**, Cluster #1) is required to generate a singly oxidized hydroperoxide during the LOX catalytic cycle. As the lipid becomes enriched with hydroperoxyl groups, it probably loses hydrophobicity and gains affinity for the aqueous environment, prompting its release from the catalytic site. It is tempteing to expect that if, at that moment, a second O_2 molecule is present (**Fig. 2a-b**, Cluster #2) and an additional bis-allylic carbon aligns properly with the regenerated Fe^{3+}-OH^- cofactor, a subsequent catalytic reaction may occur, leading to the formation of a doubly-oxidized product. Our studies suggest that F352, I413, I417, Y551, I592, and T593 residues may play the role of an O_2 trap for 15LOX-1 (**Fig. 2b**).

Overall, our study provides new insights into the complex mechanisms governing oxygen transport and ferroptotic lipid peroxidation in LOX members. By identifying specific oxygen tunnels, structurally or sequentially conserved residues, and a potentially regulatory role of water molecules, we have highlighted the intricate coordination between the enzyme structure, membrane environment, and substrate interactions. These findings not only advance our understanding of 15LOXs activity but also open new avenues for exploring targeted interventions that modulate ferroptosis, with potential implications for therapeutic strategies against diseases involving lipid peroxidation.

Acknowledgment

This work was supported by the Polish National Science Centre grant number: 2019/35/D/ST4/02203, by NIH (HL174611, NS076511, NS061817, CA243142). W.N. thanks for facilities of ICNT UMK.

Conflict of interest

The authors declare no conflict of interest.

Methods

Molecular Dynamics simulations. Full-atomic MD simulations were performed for 15LOX-1/PEBP1 with biological membrane model using NAMD [55] package, the CHARMM force field, and 2 fs time steps. The proteins were solvated with explicit water (TIP3P) at physiological salt concentrations. CHARMM force field parameters for bonded iron were obtained using Gaussian [10], a variant of DFT method (B3LYP/6-31(d,p) method). We performed multiple sets of simulations for each system 15LOX-1/PEBP1. Prior to productive runs without membrane, the following protocol was adopted: 0.2 ns of water equilibration, 10,000 steps of minimization, 0.35 ns of heating from 0 to 300 K, and 0.15 ns equilibration of the whole system. A cutoff of 12 Å for non-bonded interactions was applied. Langevin dynamics and the Langevin piston algorithm were used to maintain the temperature at 300 K and the pressure at 1 atm. For each system we performed >200 ns (20+ MD runs, each >200 ns). Simulations with the membrane composed of 1,2-dioleoy-sn-glycero-3-phosphocholine (DOPC, 50%), 1,2-dioleoy-sn-glycero-3-phosphoethanolamine (DOPE, 30%), and 1-stearoyl-2-arachidonyl-phosphoethanolamine (SAPE, 20%) were prepared in CHARMM GUI [56] server (**Supplementary Fig. 1)**. We used the PPM/OPM [57] server to predict the orientation of the protein complex in the membrane. We have following set of simulations, included the complex 15LOX-1/PEBP1 and 15LOX-1, encompassing both substrate-bound and substrate-free states, in the presence and absence of a membrane under different O_2 concentrations: 1 O_2, 2 O_2, 15 O_2 (in total: 20 µs, see **Supplementary Tab. 1**). To investigate the oxygen pathways in 15LOX-1, we positioned one O_2 and two O_2 molecules near the active site to study the exit pathways, and randomly placed 15 O_2 molecules around the protein to study the entry pathways from the outer surface to the active site. The incorporation of an oxygen from atmospheric dioxygen into an organic substrate as occurs during oxidation process in the active site of 15LOX-1. Throughout the simulation with 15 randomly distributed O_2

molecules, the membrane was constrained, and we employed the *keep_water_out.tcl* (http://www.ks.uiuc.edu/Research/namd/; NAMD website) script to prevent oxygen molecules from entering the hydrophobic regions of the membrane, such as DOPC, SAPE, and DOPE, at a frequency of every 100 fs.

Multiple sequence alignment. Multiple Sequence Alignment (MSA) of different lipoxygenase protein species was performed using ClustalX2 [58] and is available in FASTA format. MSA visualization was done via Jalview [59]. Following UniProt IDs were used P16050 (Human 15-lipoxygenase-1), P12530 (Rabbit reticulocyte 15-lipoxygenase-1), P08170 (Lipoxygenase-1 (soybean)), O15296 (15-Lipoxygenase 2), O16025 (8R-Lipoxygenase), B7JX99 (Lipoxygenase 2).

Protein-water interactions. The analysis of meaningful protein-water interactions were performed using *WatFinder* tool [33] from ProDy package [34]. Water clusters of MD trajectories were identified using the *findClusterCenters()* function with *cluster* methods and maximum distances between water molecules set to 0.6 Å (*dictC*) and minimum number of identified waters set to 15 (*numC*). The total number of analyzed frames was 170 (saved every 1 ns, which gives in total 170 ns).

The analysis of 140 LOX structures was performed using ProDy [34] tools and *WatFinder* [33]. First, we used a Dali search that provided 1731 PDB structures. Among those, we selected 140 structures with higher than 50% of the total residue length and with an RMSD value lower than 1 Å. Hydrogen atoms were filled using the *Openbabel* method of *WatFinder,* and structures were aligned using the *matchChain* method in ProDy with seqid equal to 5 and overlap of sequence higher than 50%. We used default parameters to predict water bridges. Next, we assessed how many water bridges across 140 crystallographic structures of LOX are located in the same region using findClusterCerters() function of *WatFinder* with *distC* = 0.9 Å and *numC* = 17. Similar approach was used to cluster O_2 molecules in MD simulations with *distC* = 1.0 Å and *numC* = 10.

Perturbation Response Scanning. Perturbation Response Scanning (PRS) approach is based on the linear response theory and allows evaluating residue displacements in response to external forces [45]. In the map provided by PRS, each element maps the response value of one residue (corresponding to the disturbance residue on the horizontal axis) perturbed by another residue

(the sensitive residue on the vertical axis). The average effect of all disturbance residues in each column is called validity, which indicates the ability of one residue to affect the dynamic changes of all other residues, and the strongest effectors can be interpreted as an element that applies global control to the propagation of allosteric signals. Conversely, the mean value of the sensitive residues of each column corresponds to the perturbed level of the residues. The strongest sensors can be interpreted as an effective receiver of allosteric signals. An integration tool, ProDy [34], is used for PRS analysis [60].

Liposome preparation and LC-MS analysis. Liposomes consisting of dioleoyl-phosphatidylcholine (100 µM) and stearoyl-arachidonoyl-PE (100 µM) were incubated with human 15LOX-2 (0.4 µM) or human 15LOX-1 (0.4 µM) in the absence or in the presence of PEBP1 (0.4 µM) in 25 mM HEPES buffer (pH 7.4) containing DTPA (100 µM) and 0.5 µM 9-HpODE at 37 °C for 5 min. At the end of incubation, lipids were extracted by Folch procedure [61] and analyzed by LC–MS using on a Dionex HPLC system coupled to a hybrid quadrupole-orbitrap mass spectrometer, Q-Exactive (ThermoFisher, Inc., San Jose, CA) with the Xcalibur operating system in the negative ion mode (at a voltage differential of –3.5-5.0 kV, source temperature was maintained at 150^{o}C). The scan range for MS analysis was 150-1800 m/z with a maximum injection time of 128 ms using 1 microscan and a resolution of 140,000. An isolation window of 1.0 Da was set for the MS and MS^2 scans. The S-lens Rf level was set to 70. Oxygenated PE molecular species were separated on a C30 reverse phase column (Accucore 2.6 µm, 2.1 mm × 25 cm, Thermo Scientific). Solvent A: acetonitrile/water (50/50); Solvent B: 2-propanol/acetonitrile/water (85/10/5). Both A and B solvents contained 5 mM ammonium formate and 0.1% formic acid as modifiers. Gradient method was as follows: 0–40 min, 15%–50% B (linear, 5); 40–130 min, 50–100% B (linear, 5); 130–135 min, hold at 100% B; 135–140 min, 15% B (linear, 5); 140–150 min, 15% B for equilibration. The flow was maintained at 100 µl/min. Column temperature was set at 35 ˚C. Commercially available 1-stearoyl-2-15(S)-HpETE-sn-glycero-3-phosphoethanolamine, 1-stearoyl-2-15(S)-HETE-sn-glycero-3-phospho-ethanolamine, 1-stearoyl-2-15(S)-HpETE-sn-glycero-3-phosphocholine, 1-stearoyl-2-15(S)-HETE-sn-glycero-3-phosphocholine (Cayman Chemicals) and 1-stearoyl-2-oleoyl-sn-glycero-3-phosphoethanolamine (Avanti Polar Lipids) were used as reference standards. 1-hexadecanoyl(d31)-2-(9Z-octadecenoyl)-sn-glycero-3-phospho-ethanolamine (PE(16:0D31/18:1)) (Avanti Polar Lipids) was used as internal standard.

References:

[1] M. Conrad, V.E. Kagan, H. Bayir, G.C. Pagnussat, B. Head, M.G. Traber, B.R. Stockwell, Regulation of lipid peroxidation and ferroptosis in diverse species, Genes Dev 32(9-10) (2018) 602-619.

[2] A.R. Bogdan, M. Miyazawa, K. Hashimoto, Y. Tsuji, Regulators of Iron Homeostasis: New Players in Metabolism, Cell Death, and Disease, Trends Biochem Sci 41(3) (2016) 274-286.

[3] B.R. Stockwell, J.P. Friedmann Angeli, H. Bayir, A.I. Bush, M. Conrad, S.J. Dixon, S. Fulda, S. Gascon, S.K. Hatzios, V.E. Kagan, K. Noel, X. Jiang, A. Linkermann, M.E. Murphy, M. Overholtzer, A. Oyagi, G.C. Pagnussat, J. Park, Q. Ran, C.S. Rosenfeld, K. Salnikow, D. Tang, F.M. Torti, S.V. Torti, S. Toyokuni, K.A. Woerpel, D.D. Zhang, Ferroptosis: A Regulated Cell Death Nexus Linking Metabolism, Redox Biology, and Disease, Cell 171(2) (2017) 273-285.

[4] V.E. Kagan, G. Mao, F. Qu, J.P.F. Angeli, S. Doll, C. St Croix, H.H. Dar, B. Liu, V.A. Tyurin, V.B. Ritov, Oxidized arachidonic and adrenic PEs navigate cells to ferroptosis, Nature Chem. Biol. 13(1) (2017) 81-90.

[5] J.P. Friedmann Angeli, M. Schneider, B. Proneth, Y.Y. Tyurina, V.A. Tyurin, V.J. Hammond, N. Herbach, M. Aichler, A. Walch, E. Eggenhofer, Inactivation of the ferroptosis regulator Gpx4 triggers acute renal failure in mice, Nat Cell Biol 16(12) (2014) 1180-1191.

[6] S.E. Wenzel, Y.Y. Tyurina, J. Zhao, C.M. St Croix, H.H. Dar, G. Mao, V.A. Tyurin, T.S. Anthonymuthu, A.A. Kapralov, A.A. Amoscato, K. Mikulska-Ruminska, I.H. Shrivastava, E.M. Kenny, Q. Yang, J.C. Rosenbaum, L.J. Sparvero, D.R. Emlet, X. Wen, Y. Minami, F. Qu, S.C. Watkins, T.R. Holman, A.P. VanDemark, J.A. Kellum, I. Bahar, H. Bayir, V.E. Kagan, PEBP1 Wardens Ferroptosis by Enabling Lipoxygenase Generation of Lipid Death Signals, Cell 171(3) (2017) 628-641 e26.

[7] S.N. Samovich, K. Mikulska-Ruminska, H.H. Dar, Y.Y. Tyurina, V.A. Tyurin, A.B. Souryavong, A.A. Kapralov, A.A. Amoscato, O. Beharier, S.A. Karumanchi, C.M. St Croix, X. Yang, T.R. Holman, A.P. VanDemark, Y. Sadovsky, R.K. Mallampalli, S.E. Wenzel, W. Gu, Y.L. Bunimovich, I. Bahar, V.E. Kagan, H. Bayir, Strikingly High Activity of 15-Lipoxygenase Towards Di-Polyunsaturated Arachidonoyl/Adrenoyl-Phosphatidylethanolamines Generates Peroxidation Signals of Ferroptotic Cell Death, Angew Chem Int Ed Engl 63(9) (2024) e202314710.

[8] Y. Benatzy, M.A. Palmer, B. Brüne, Arachidonate 15-lipoxygenase type B: Regulation, function, and its role in pathophysiology, Front Pharmacol 13 (2022) 1042420.

[9] R. Chrisnasari, T.A. Ewing, R. Hilgers, W.J. van Berkel, J.-P. Vincken, M. Hennebelle, Versatile ferrous oxidation–xylenol orange assay for high-throughput screening of lipoxygenase activity, Appl Microbiol Biotechnol 108(1) (2024) 266.

[10] T. Manivarma, A.A. Kapralov, S.N. Samovich, Y.Y. Tyurina, V.A. Tyurin, A.P. VanDemark, W. Nowak, H. Bayir, I. Bahar, V.E. Kagan, K. Mikulska-Ruminska, Membrane regulation of 15LOX-1/PEBP1 complex prompts the generation of ferroptotic signals, oxygenated PEs, Free Radic Biol Med 208 (2023) 458-467.

[11] T.S. Anthonymuthu, Y.Y. Tyurina, W.-Y. Sun, K. Mikulska-Ruminska, I.H. Shrivastava, V.A. Tyurin, F.B. Cinemre, H.H. Dar, A.P. VanDemark, T.R. Holman, Y. Sadovsky, B.R. Stockwell, R.-R. He, I. Bahar, H. Bayır, V.E. Kagan, Resolving the paradox of ferroptotic cell death: ferrostatin-1 binds to 15LOX/PEBP1 complex, suppresses generation of peroxidized ETE-PE, and protects against ferroptosis, Redox Biol. 38 (2020) 101744.

[12] A.A. Kapralov, Q. Yang, H.H. Dar, Y.Y. Tyurina, T.S. Anthonymuthu, R. Kim, C.M.S. Croix, K. Mikulska-Ruminska, B. Liu, I.H. Shrivastava, V.A. Tyurin, H.-C. Ting, Y.L. Wu, Y. Gao, G.V. Shurin, M.A. Artyukhova, L.A. Ponomareva, P.S. Timashev, R.M. Domingues, D.A. Stoyanovsky, J.S. Greenberger, R.K. Mallampalli, I. Bahar, D.I. Gabrilovich, H. Bayır, V.E. Kagan, Redox lipid reprogramming commands susceptibility of macrophages and microglia to ferroptotic death, Nature Chem. Biol. 16(3) (2020) 278-290.

[13] T.S. Anthonymuthu, E.M. Kenny, I. Shrivastava, Y.Y. Tyurina, Z.E. Hier, H.-C. Ting, H.H. Dar, V.A. Tyurin, A. Nesterova, A.A. Amoscato, K. Mikulska-Ruminska, J.C. Rosenbaum, G. Mao, J. Zhao, M. Conrad, J.A. Kellum, S.E. Wenzel, A.P. VanDemark, I. Bahar, V.E. Kagan, H. Bayır, Empowerment of 15-Lipoxygenase Catalytic Competence in Selective Oxidation of Membrane ETE-PE to Ferroptotic Death Signals, HpETE-PE, J Am Chem Soc 140(51) (2018) 17835-17839.
[14] K. Mikulska-Ruminska, T.S. Anthonymuthu, A. Levkina, I.H. Shrivastava, O.O. Kapralov, H. Bayır, V.E. Kagan, I. Bahar, NO● Represses the Oxygenation of Arachidonoyl PE by 15LOX/PEBP1: Mechanism and Role in Ferroptosis, Inter. J. Mol. Sci. 22(10) (2021) 5253.
[15] S.J. Dixon, K.M. Lemberg, M.R. Lamprecht, R. Skouta, E.M. Zaitsev, C.E. Gleason, D.N. Patel, A.J. Bauer, A.M. Cantley, W.S. Yang, B. Morrison, 3rd, B.R. Stockwell, Ferroptosis: an iron-dependent form of nonapoptotic cell death, Cell 149(5) (2012) 1060-72.
[16] S. Toyokuni, F. Ito, K. Yamashita, Y. Okazaki, S. Akatsuka, Iron and thiol redox signaling in cancer: An exquisite balance to escape ferroptosis, Free Radic Biol Med 108 (2017) 610-626.
[17] J.O. Onukwufor, R.T. Dirksen, A.P. Wojtovich, Iron Dysregulation in Mitochondrial Dysfunction and Alzheimer's Disease, Antioxidants (Basel) 11(4) (2022).
[18] H. Mao, Y. Zhao, H. Li, L. Lei, Ferroptosis as an emerging target in inflammatory diseases, Prog Biophys Mol Biol 155 (2020) 20-28.
[19] R. Shah, M.S. Shchepinov, D.A. Pratt, Resolving the Role of Lipoxygenases in the Initiation and Execution of Ferroptosis, ACS Cent Sci 4(3) (2018) 387-396.
[20] O. Zilka, R. Shah, B. Li, J.P. Friedmann Angeli, M. Griesser, M. Conrad, D.A. Pratt, On the Mechanism of Cytoprotection by Ferrostatin-1 and Liproxstatin-1 and the Role of Lipid Peroxidation in Ferroptotic Cell Death, ACS Cent Sci 3(3) (2017) 232-243.
[21] J.C. Ullery, L.J. Marnett, Protein modification by oxidized phospholipids and hydrolytically released lipid electrophiles: Investigating cellular responses, Biochim Biophys Acta 1818(10) (2012) 2424-35.
[22] H.T. Endale, W. Tesfaye, T.A. Mengstie, ROS induced lipid peroxidation and their role in ferroptosis, Front. Cell Dev. Biol. 11 (2023).
[23] E. Dai, L. Meng, R. Kang, X. Wang, D. Tang, ESCRT-III-dependent membrane repair blocks ferroptosis, Biochem Biophys Res Commun 522(2) (2020) 415-421.
[24] M. Jove, N. Mota-Martorell, I. Pradas, M. Martin-Gari, V. Ayala, R. Pamplona, The Advanced Lipoxidation End-Product Malondialdehyde-Lysine in Aging and Longevity, Antioxidants (Basel) 9(11) (2020).
[25] D.C. Liebler, Protein damage by reactive electrophiles: targets and consequences, Chem Res Toxicol 21(1) (2008) 117-28.
[26] S.J. Kwack, B. Mu Lee, Correlation between DNA or protein adducts and benzo[a]pyrene diol epoxide I–triglyceride adduct detected in vitro and in vivo, Carcinogenesis 21(4) (2000) 629-632.
[27] W. Luczaj, E. Skrzydlewska, DNA damage caused by lipid peroxidation products, Cell Mol Biol Lett 8(2) (2003) 391-413.
[28] J.A. Stuart, J. Fonseca, F. Moradi, C. Cunningham, B. Seliman, C.R. Worsfold, S. Dolan, J. Abando, L.A. Maddalena, How supraphysiological oxygen levels in standard cell culture affect oxygen-consuming reactions, Oxid. Med. Cell. Longev. 2018 (2018).
[29] I. Juránek, H. Suzuki, S. Yamamoto, Affinities of various mammalian arachidonate lipoxygenases and cyclooxygenases for molecular oxygen as substrate, Biochimica et Biophysica Acta (BBA)-Molecular and Cell Biology of Lipids 1436(3) (1999) 509-518.
[30] L. Li, S. Shen, P. Bickler, M.P. Jacobson, L.F. Wu, S.J. Altschuler, Searching for molecular hypoxia sensors among oxygen-dependent enzymes, Elife 12 (2023) e87705.
[31] S.E. Wenzel, Y.Y. Tyurina, J. Zhao, C.M.S. Croix, H.H. Dar, G. Mao, V.A. Tyurin, T.S. Anthonymuthu, A.A. Kapralov, A.A. Amoscato, K. Mikulska-Ruminska, I.H. Shrivastava, E.M. Kenny, Q. Yang, J.C. Rosenbaum, L.J. Sparvero, D.R. Emlet, X. Wen, Y. Minami, F. Qu, S.C. Watkins, T.R. Holman, A.P. VanDemark, J.A.

Kellum, I. Bahar, H. Bayır, V.E. Kagan, PEBP1 Wardens Ferroptosis by Enabling Lipoxygenase Generation of Lipid Death Signals, Cell 171(3) (2017) 628-641. e26.
[32] J. Saam, I. Ivanov, M. Walther, H.-G. Holzhütter, H. Kuhn, Molecular dioxygen enters the active site of 12/15-lipoxygenase via dynamic oxygen access channels, Proc. Nat. Acad. Sci. 104(33) (2007) 13319-13324.
[33] J.M. Krieger, F. Doljanin, A.T. Bogetti, F. Zhang, T. Manivarma, I. Bahar, K. Mikulska-Ruminska, WatFinder: A ProDy tool for protein-water interactions, Bioinformatics (2024) btae516.
[34] S. Zhang, J.M. Krieger, Y. Zhang, C. Kaya, B. Kaynak, K. Mikulska-Ruminska, P. Doruker, H. Li, I. Bahar, ProDy 2.0: Increased Scale and Scope after 10 Years of Protein Dynamics Modelling with Python, Bioinformatics (2021).
[35] L. Holm, L.M. Laakso, Dali server update, Nucleic Acids Res 44(W1) (2016) W351-5.
[36] M. Maurer, C. Oostenbrink, Water in protein hydration and ligand recognition, J Mol Recognit 32(12) (2019) e2810.
[37] H. Meng, Z. Dai, W. Zhang, Y. Liu, L. Lai, Molecular mechanism of 15-lipoxygenase allosteric activation and inhibition, Phys Chem Chem Phys 20(21) (2018) 14785-14795.
[38] N.C. Gilbert, J. Gerstmeier, E.E. Schexnaydre, F. Börner, U. Garscha, D.B. Neau, O. Werz, M.E. Newcomer, Structural and mechanistic insights into 5-lipoxygenase inhibition by natural products, Nat Chem Biol 16(7) (2020) 783-790.
[39] H. Yuan, Y. Zhang, X. Huang, X. Zhang, J. Li, Y. Huang, K. Li, H. Weng, Y. Xu, Y. Zhang, Exploration of the Existence Forms and Patterns of Dissolved Oxygen Molecules in Water, Nanomicro Lett 16(1) (2024) 208.
[40] G. Pujadas, J. Palau, Molecular mimicry of substrate oxygen atoms by water molecules in the beta-amylase active site, Protein Sci 10(8) (2001) 1645-57.
[41] T.I. Oprea, G. Hummer, A.E. Garcia, Identification of a functional water channel in cytochrome P450 enzymes, Proc Natl Acad Sci U S A 94(6) (1997) 2133-8.
[42] W.-Y. Sun, V.A. Tyurin, K. Mikulska-Ruminska, I.H. Shrivastava, T.S. Anthonymuthu, Y.-J. Zhai, M.-H. Pan, H.-B. Gong, D.-H. Lu, J. Sun, Phospholipase iPLA 2 β averts ferroptosis by eliminating a redox lipid death signal, Nature Chem. Biol. (2021) 1-12.
[43] N.A. Baker, D. Sept, S. Joseph, M.J. Holst, J.A. McCammon, Electrostatics of nanosystems: application to microtubules and the ribosome, Proc Natl Acad Sci U S A 98(18) (2001) 10037-41.
[44] C.I. Bayly, P. Cieplak, W. Cornell, P.A. Kollman, A well-behaved electrostatic potential based method using charge restraints for deriving atomic charges: the RESP model, J. Phys. Chem. 97(40) (1993) 10269-10280.
[45] C. Atilgan, Z.N. Gerek, S.B. Ozkan, A.R. Atilgan, Manipulation of conformational change in proteins by single-residue perturbations, Biophys J 99(3) (2010) 933-43.
[46] L. Hannibal, F. Tomasina, D.A. Capdevila, V. Demicheli, V. Tortora, D. Alvarez-Paggi, R. Jemmerson, D.H. Murgida, R. Radi, Alternative Conformations of Cytochrome c: Structure, Function, and Detection, Biochemistry 55(3) (2016) 407-28.
[47] R. Bisson, G. Schiavo, C. Montecucco, ATP induces conformational changes in mitochondrial cytochrome c oxidase. Effect on the cytochrome c binding site, J Biol Chem 262(13) (1987) 5992-8.
[48] B. Michel, A.E. Proudfoot, C.J. Wallace, H.R. Bosshard, The cytochrome c oxidase-cytochrome c complex: spectroscopic analysis of conformational changes in the protein-protein interaction domain, Biochemistry 28(2) (1989) 456-62.
[49] D. Hamdane, H. Zhang, P. Hollenberg, Oxygen activation by cytochrome P450 monooxygenase, Photosynth Res 98(1-3) (2008) 657-66.
[50] M.F. Perutz, Stereochemistry of cooperative effects in haemoglobin: haem–haem interaction and the problem of allostery, Nature 228(5273) (1970) 726-734.

[51] K. Mikulska-Ruminska, I. Shrivastava, J. Krieger, S. Zhang, H. Li, H. Bayır, S.E. Wenzel, A.P. VanDemark, V.E. Kagan, I. Bahar, Characterization of Differential Dynamics, Specificity, and Allostery of Lipoxygenase Family Members, J. Chem. Inform. Model. 59 (2019) 2496-2508.
[52] M. Kanehisa, S. Goto, S. Kawashima, A. Nakaya, The KEGG databases at GenomeNet, Nucleic Acids Res 30(1) (2002) 42-6.
[53] J. Li, F. Cao, H.L. Yin, Z.J. Huang, Z.T. Lin, N. Mao, B. Sun, G. Wang, Ferroptosis: past, present and future, Cell Death Dis 11(2) (2020) 88.
[54] T. Hirschhorn, B.R. Stockwell, The development of the concept of ferroptosis, Free Radic Biol Med 133 (2019) 130-143.
[55] J. Phillips, R. Braun, W. Wang, J. Gumbart, E. Tajkhorshid, E. Villa, C. Chipot, R. Skeel, L. Kale, K. Schulten, Scalable molecular dynamics with NAMD, J. Comput. Chem. 26(16) (2005) 1781-1802.
[56] J. Lee, X. Cheng, J.M. Swails, M.S. Yeom, P.K. Eastman, J.A. Lemkul, S. Wei, J. Buckner, J.C. Jeong, Y. Qi, CHARMM-GUI input generator for NAMD, GROMACS, AMBER, OpenMM, and CHARMM/OpenMM simulations using the CHARMM36 additive force field, J. Chem. Theo. Comput. 12(1) (2015) 405-413.
[57] M.A. Lomize, I.D. Pogozheva, H. Joo, H.I. Mosberg, A.L. Lomize, OPM database and PPM web server: resources for positioning of proteins in membranes, Nucl. Aci. Res. 40(D1) (2011) D370-D376.
[58] M.A. Larkin, G. Blackshields, N.P. Brown, R. Chenna, P.A. McGettigan, H. McWilliam, F. Valentin, I.M. Wallace, A. Wilm, R. Lopez, J.D. Thompson, T.J. Gibson, D.G. Higgins, Clustal W and Clustal X version 2.0, Bioinformatics 23(21) (2007) 2947-8.
[59] A.M. Waterhouse, J.B. Procter, D.M. Martin, M. Clamp, G.J. Barton, Jalview Version 2--a multiple sequence alignment editor and analysis workbench, Bioinformatics 25(9) (2009) 1189-91.
[60] A. Bakan, L.M. Meireles, I. Bahar, ProDy: protein dynamics inferred from theory and experiments, Bioinformatics 27(11) (2011) 1575-7.
[61] J. Folch, M. Lees, G.S. Stanley, A simple method for the isolation and purification of total lipides from animal tissues, Journal of biological chemistry 226(1) (1957) 497-509.

7. Co-author contribution statements

University of Pittsburgh

Graduate School of Public Health
Department of Environmental
And Occupational Health

130 De Soto St, Pittsburgh, PA 15261

e-mail olk6@pitt.eduu

Alexandr A. Kapralov, PhD, DSc
Research Associate Professor

Declaration of Contribution

Hereby, I declare that my contributions to the paper Manivarma, T., Kapralov, A. A., Samovich, S. N., Tyurina, Y. Y., Tyurin, V. A., VanDemark, A. P., Nowak, W., Bayir, H., Bahar, I., Kagan, V. E., & Mikulska-Ruminska, K. (2023). Membrane regulation of 15LOX-1/PEBP1 complex prompts the generation of ferroptotic signals, oxygenated PEs. Free Radic Biol Med, 208, 458-467. are as follows:

I was responsible for performing experiments to study interaction of 15LOX-1 with wild type and mutated forms of PEBP1 using crosslinking and far- western blotting and analysed:obtained data.

COLUMBIA | COLUMBIA UNIVERSITY IRVING MEDICAL CENTER

Declaration of Contribution

Hereby, I declare that my contributions to the paper are as follows:

> Manivarma, T., Kapralov, A. A., Samovich, S. N., Tyurina, Y. Y., Tyurin, V. A., VanDemark, A. P., Nowak, W., Bayir, H., Bahar, I., Kagan, V. E., & Mikulska-Ruminska, K. (2023). Membrane regulation of 15LOX-1/PEBP1 complex prompts the generation of ferroptotic signals, oxygenated PEs. Free Radic Biol Med, 208, 458-467.

I was responsible for performing research and analyzing data.

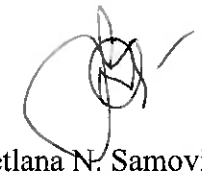

Svetlana N. Samovich, PhD

Assistant Professor of Pediatric Lipid Sciences (in Pediatrics)

Department of Pediatrics at the Columbia University Irving Medical Center

Vagelos College of Physicians and Surgeons of Columbia University

650West 168th Street

New York, NY 10032, United States

+1-412-889-9146, ss7039@cumc.columbia.edu

University of Pittsburgh

Kenneth P. Dietrich School of Arts and Sciences
Department of Biological Sciences

A360 Langley Hall
4249 Fifth Avenue
Pittsburgh, PA 15260
412-648-0110
Fax: 412-624-4759
andyv@pitt.edu
www.biology.pitt.edu

Andrew P. VanDemark
Associate Professor of Biological Sciences

December 11th, 2024

Declaration of Contribution

Hereby, I declare that my contributions to the paper are as follows:

Manivarma, T., Kapralov, A. A., Samovich, S. N., Tyurina, Y. Y., Tyurin, V. A., VanDemark, A. P., Nowak, W., Bayir, H., Bahar, I., Kagan, V. E., & Mikulska-Ruminska, K. (2023). Membrane regulation of 15LOX-1/PEBP1 complex prompts the generation of ferroptotic signals, oxygenated PEs. Free Radic Biol Med, 208, 458-467.

I was responsible for contributing new reagents for experimental analysis.

Sincerely,

Andrew VanDemark
Associate Professor
Department of Biological Sciences
University of Pittsburgh
360A Langley Hall
412-648-0110
andyv@pitt.edu

Author Contribution statement

Hereby, I declare that my contributions to the paper are as follows:

> Manivarma, T., Kapralov, A. A., Samovich, S. N., Tyurina, Y. Y., Tyurin, V. A., VanDemark, A. P., Nowak, W., Bayir, H., Bahar, I., Kagan, V. E., & Mikulska-Ruminska, K. (2023). Membrane regulation of 15LOX-1/PEBP1 complex prompts the generation of ferroptotic signals, oxygenated PEs. Free Radic Biol Med, 208, 458-467.

I designed the research, analyzed the data, wrote the paper ~**Ivet Bahar**

Hereby, I declare that my contributions to the paper are as follows:

> Krieger, J. M., Doljanin, F., Bogetti, A. T., Zhang, F., Manivarma, T., Bahar, I., & Mikulska-Ruminska, K. (2024). WatFinder: A ProDy tool for protein-water interactions. Bioinformatics.

I was responsible for manuscript preparation, and writing the paper, ~**Ivet Bahar**

December 18, 2024

~**Ivet Bahar**

MINISTERIO
DE CIENCIA, INNOVACIÓN
Y UNIVERSIDADES

CSIC
CONSEJO SUPERIOR DE INVESTIGACIONES CIENTÍFICAS

CNB
CENTRO NACIONAL DE BIOTECNOLOGIA

To whom it may concern

Hereby, I declare that my contributions to the paper are as follows:

> Krieger, J. M., Doljanin, F., Bogetti, A. T., Zhang, F., Manivarma, T., Bahar, I., & Mikulska-Ruminska, K. (2024). WatFinder: A ProDy tool for protein-water interactions. Bioinformatics.

As an equal contributor with Frane Doljanin, I was responsible for coding, software development, testing and application to biological systems, manuscript preparation, and writing the paper.

Yours Sincerely

James Krieger

Research Fellow, Biocomputing Unit,

Department of Macromolecular Structure,

National Centre for Biotechnology (CNB-CSIC),

Campus UAM Cantoblanco, 28049, Madrid, Spain

To whom it may concern

Hereby, I declare that my contributions to the paper are as follows:

> Krieger, J. M., Doljanin, F., Bogetti, A. T., Zhang, F., Manivarma, T., Bahar, I., & Mikulska-Ruminska, K. (2024). WatFinder: A ProDy tool for protein-water interactions. Bioinformatics.

As an equal contributor with James M. Krieger, I was responsible for coding, software development, and writing the paper.

Frane Doljanin

fdoljanin@pmfst.hr

Faculty of Science, University of Split

To whom it may concern

Hereby, I declare that my contributions to the paper are as follows:

> Krieger, J. M., Doljanin, F., Bogetti, A. T., Zhang, F., Manivarma, T., Bahar, I., & Mikulska-Ruminska, K. (2024). WatFinder: A ProDy tool for protein-water interactions. Bioinformatics.

As a co-author, I was responsible for running the simulations for one application and, analyzing data for that particular application and help analysis on some of the other applications.

Affiliation: Laufer Center for Physical and Quantitative Biology, Stony Brook University, Stony Brook, NY 11794, United States

University logo: 

Contact email: anthony.bogetti@stonybrook.edu

Signature: *Anthony Bogetti*

To whom it may concern

Hereby, I declare that my contributions to the paper are as follows:

> Krieger, J. M., Doljanin, F., Bogetti, A. T., Zhang, F., Manivarma, T., Bahar, I., & Mikulska-Ruminska, K. (2024). WatFinder: A ProDy tool for protein-water interactions. Bioinformatics.

As an co-author, I was responsible for programming the codes, compile and build the website.

May contact info:

Laufer Center for Physical and Quantitative Biology, Stony Brook University

Stony Brook, NY 11794, USA

University of Pittsburgh

School of Public Health
Department of Environmental and Occupational Health

130 DeSoto Street
Room 4120 Parran Hall
Pittsburgh, PA 15261
412-624-9479
Fax: 412-624-9361

December 30, 2024

Author Contribution statement

Hereby, I declare that my contributions to the paper are as follows:

> Manivarma, T., Kapralov, A. A., Samovich, S. N., Tyurina, Y. Y., Tyurin, V. A., VanDemark, A. P., Nowak, W., Bayir, H., Bahar, I., Kagan, V. E., & Mikulska-Ruminska, K. (2023). Membrane regulation of 15LOX-1/PEBP1 complex prompts the generation of ferroptotic signals, oxygenated PEs. Free Radic Biol Med, 208, 458-467.

I performed the research, analyzed the data.

Hereby, I declare that my contributions to the paper, published as a preprint on SSRN, are as follows:

> Manivarma T, Nowak W, Tyurina YY, Tyurin VA, Bayir H, Kagan VE, Mikulska-Ruminska K. (2024). The presence of substrate warrants oxygen access tunnels toward the catalytic site of lipoxygenases. *SSRN*.

I performed the research, analyzed the data.

Sincerely,

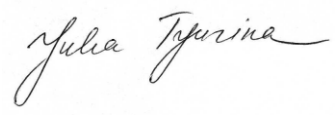

Yulia Tyurina
Research Professor
Department of Environmental and Occupational Health
University of Pittsburgh

University of Pittsburgh

School of Public Health
Department of Environmental and Occupational Health

130 DeSoto Street
Room 4120 Parran Hall
Pittsburgh, PA 15261
412-624-9479
Fax: 412-624-9361

December 30, 2024

Author Contribution statement

Hereby, I declare that my contributions to the paper are as follows:

> Manivarma, T., Kapralov, A. A., Samovich, S. N., Tyurina, Y. Y., Tyurin, V. A., VanDemark, A. P., Nowak, W., Bayir, H., Bahar, I., Kagan, V. E., & Mikulska-Ruminska, K. (2023). Membrane regulation of 15LOX-1/PEBP1 complex prompts the generation of ferroptotic signals, oxygenated PEs. Free Radic Biol Med, 208, 458-467.

I performed the research, analyzed the data

Hereby, I declare that my contributions to the paper, published as a preprint on SSRN, are as follows:

> Manivarma T, Nowak W, Tyurina YY, Tyurin VA, Bayir H, Kagan VE, Mikulska-Ruminska K. (2024). The presence of substrate warrants oxygen access tunnels toward the catalytic site of lipoxygenases. *SSRN*.

I performed the research, analyzed the data

Sincerely,

Vladimir Tyurin
Research Assistant Professor
Department of Environmental and Occupational Health
University of Pittsburgh

COLUMBIA

Hülya Bayir, MD
Division Chief, Pediatric Critical Care and Hospital Medicine

Miriam Diaz
Division Administrator

Department of Pediatrics
Division of Critical Care, Palliative Care and Hospital Medicine
Columbia University Vagelos College of Physicians & Surgeons

December 17, 2024

Computational Biophysics Department
Nicolaus Copernicus University in Torun, Poland

RE: Author Contribution Statement for Thiliban Manivarma's PhD thesis

Dear Thesis Committee members, I declare that I contributed to the research design, data analysis and writing of manuscript for the following published in a in submission work:

Manivarma, T., Kapralov, A. A., Samovich, S. N., Tyurina, Y. Y., Tyurin, V. A., VanDemark, A. P., Nowak, W., Bayir, H., Bahar, I., Kagan, V. E., & Mikulska-Ruminska, K. (2023). Membrane regulation of 15LOX-1/PEBP1 complex prompts the generation of ferroptotic signals, oxygenated PEs. Free Radic Biol Med, 208, 458-467.

Manivarma T, Nowak W, Tyurina YY, Tyurin VA, Bayir H, Kagan VE, Mikulska-Ruminska K. (2024). The presence of substrate warrants oxygen access tunnels toward the catalytic site of lipoxygenases. SSRN.

Please do not hesitate to contact me if I can provide any additional information

Sincerely,

Hülya Bayır, MD
Professor of Pediatrics
Chief, Division of Pediatric Critical Care and Hospital Medicine
Morgan Stanley Children's Hospital of New York
Director of Redox Health Center
Columbia University Vagelos College of Physicians and Surgeons

University of Pittsburgh

School of Public Health
Department of Environmental and Occupational Health
Center for Free Radical and Antioxidant Health

Valerian E. Kagan, PhD, DSc
Professor and Director

Pitt Public Health
130 DeSoto Street, Room 4126
Pittsburgh, PA 15261
Tel: 412-624-9479
Fax: 412-624-9361

December 21, 2024

To whom it may concern:

Author Contribution Statement

Hereby, I cetrtify that Mr. T. M. Manivarma's contributions to the following paper: ". "Membrane regulation of 15LOX-1/PEBP1 complex prompts the generation of ferroptotic signals, oxygenated PEs." by Manivarma, T.M., Kapralov, A. A., Samovich, S. N., Tyurina, Y. Y., Tyurin, V. A., VanDemark, A. P., Nowak, W., Bayir, H., Bahar, I., Kagan, V. E., & Mikulska-Ruminska, K. publisshed in (2023) Free Radic Biol Med, 208, 458-467 is as follows:

> He has been a leading contributor to the design, research, analysis of the data, and writing the maniuscript. This is reflected in him being the first authors on the manuscript.

Furthermore, Mr. T.M. Manivarma, role and contribution to yet another paper: "The presence of substrate warrants oxygen access tunnels toward the catalytic site of lipoxygenases" by Manivarma T, Nowak W, Tyurina YY, Tyurin VA, Bayir H, Kagan VE, Mikulska-Ruminska K. (2024), published in *SSRN (*as a preprint) is as follows:

He designed the research, analyzed the data, wrote the manuscript. This has resulted in him being the first authors on the manuscript.

Sincerely,

Prof. Valerian E. Kagan, PhD, DSc
Director, Center for Free Radical and Antioxidant Health
Professor, Department of Environmental and Occupational Health
Professor of Pharmacology & Chemical Biology, Radiation Oncology, Chemistry
University of Pittsburgh
Visiting Professor, Department of Pediatrics and Consulting Director of the Children's Redox Health Center for the Division of Critical Care and Hospital Medicine in the Department of Pediatrics, Irving Medical Center in the Vagelos College of Physician and Surgeons
Columbia University, New York City

UNIWERSYTET
MIKOŁAJA KOPERNIKA
W TORUNIU

Katedra Biofizyki
Instytut Fizyki
Prof. dr hab. Wiesław Nowak

Toruń, 23/12/2024

Author Contribution statement

Hereby, I declare that my contributions to the paper are as follows:

> Manivarma, T., Kapralov, A. A., Samovich, S. N., Tyurina, Y. Y., Tyurin, V. A., VanDemark, A. P., Nowak, W., Bayir, H., Bahar, I., Kagan, V. E., & Mikulska-Ruminska, K. (2023). Membrane regulation of 15LOX-1/PEBP1 complex prompts the generation of ferroptotic signals, oxygenated PEs. Free Radic Biol Med, 208, 458-467.

I analyzed the data, suggested new computer experiments, reviewed the manuscript

Hereby, I declare that my contributions to the paper, published as a preprint on SSRN, are as follows:

> Manivarma T, Nowak W, Tyurina YY, Tyurin VA, Bayir H, Kagan VE, Mikulska-Ruminska K. (2024). The presence of substrate warrants oxygen access tunnels toward the catalytic site of lipoxygenases. *SSRN*.

I analyzed the data, discussed results, added small comments to the manuscript.

W. Nowak

Wiesław Nowak, prof. (zw.)
Dept. of Biophysics Chair

KATEDRA BIOFIZYKI, Department of Biophysics
Wydział Fizyki, Astronomii i Informatyki Stosowanej
Instytut Fizyki
UNIWERSYTET **MIKOŁAJA KOPERNIKA W TORUNIU**
ul. Grudziądzka 5, 87-100 Toruń, Polska
tel. +48 56 611 32 04, NIP: 879-017-72-91, REGON: 000001324
e-mail: wiesiek@umk.pl, strona internetowa: https://www.ifiz.umk.pl/instytut/struktura/kb/

UNIWERSYTET
MIKOŁAJA KOPERNIKA
W TORUNIU

Toruń, 30/12/2024

Dr hab. Karolina Mikulska-Rumińska, Prof. NCU
Department of Biophysics, Institute of Physics
Nicolaus Copernicus University in Torun
ul. Grudziądzka 5, Toruń, Poland

Author Contribution statement

Hereby, I declare that my contributions to the paper are as follows:

> Manivarma, T., Kapralov, A. A., Samovich, S. N., Tyurina, Y. Y., Tyurin, V. A., VanDemark, A. P., Nowak, W., Bayir, H., Bahar, I., Kagan, V. E., & Mikulska-Ruminska, K. (2023). Membrane regulation of 15LOX-1/PEBP1 complex prompts the generation of ferroptotic signals, oxygenated PEs. Free Radic Biol Med, 208, 458-467.

I designed the research, provided financial support, wrote the paper, and managed correspondence with the journal. Additionally, I collaborated with Thiliban Manivarma on conducting research, analyzing data, and creating figure visualizations.

Hereby, I declare that my contributions to the paper are as follows:

> Krieger, J. M., Doljanin, F., Bogetti, A. T., Zhang, F., Manivarma, T., Bahar, I., & Mikulska-Ruminska, K. (2024). WatFinder: A ProDy tool for protein-water interactions. Bioinformatics.

I was responsible for designing the research, analyzing data, conducting research developing code, visualizing figures, writing the paper, providing financial support, and serving as the corresponding author.

Hereby, I declare that my contributions to the paper, published as a preprint on SSRN, are as follows:

> Manivarma T, Nowak W, Tyurina YY, Tyurin VA, Bayir H, Kagan VE, Mikulska-Ruminska K. (2024). The presence of substrate warrants oxygen access tunnels toward the catalytic site of lipoxygenases. *SSRN*.

I designed the research, provided financial support, and managed correspondence with the journal. Additionally, I collaborated with Thiliban Manivarma on conducting research, analyzing data, writing the paper, and creating figure visualizations.

UNIWERSYTET MIKOŁAJA KOPERNIKA W TORUNIU
ul. Grudziądzka 5, 87-100 Toruń, Polska
tel. +48 56 611 2490, e-mail: karolamik@fizyka.umk.pl,

8. Summary and future prospects

The presented doctoral dissertation aimed to investigate the molecular mechanisms underlying ferroptosis and its regulation induced by the 15LOX-1/PEBP1 protein-protein complex. The findings from these studies allowed for the achievement of several key objectives:

- This research proposes a plausible mechanism for the binding and insertion of PUFA-PE into the catalytic pocket of 15LOX-1. It highlights the process by which the 15LOX-1/PEBP1 complex extracts lipids from the membrane and delivers them to the catalytic site, an essential step in the formation of peroxidized PUFA-PEs. The accumulation of these peroxidized lipids ultimately triggers ferroptosis. Our computational findings are at many levels consistent with the LC-MS data. The complex can generate two distinct peroxidation products, 15-HpETE-PE and 12-HpETE-PE (see figure below).

- Through our analyses, we discovered that P112 is a critical residue in the interactions between 15LOX-1 and PEBP1, focusing on mutations at residues of PEBP1 involved in interfacial interactions. Computational studies and mutagenesis experiments, supported by LC-MS data, revealed that among the five mutations tested (H86A, H86E, P74L, Y176X, and P112E), P112E had the most pronounced effect on both the formation of the 15LOX-1/PEBP1 complex and the peroxidation mechanism.

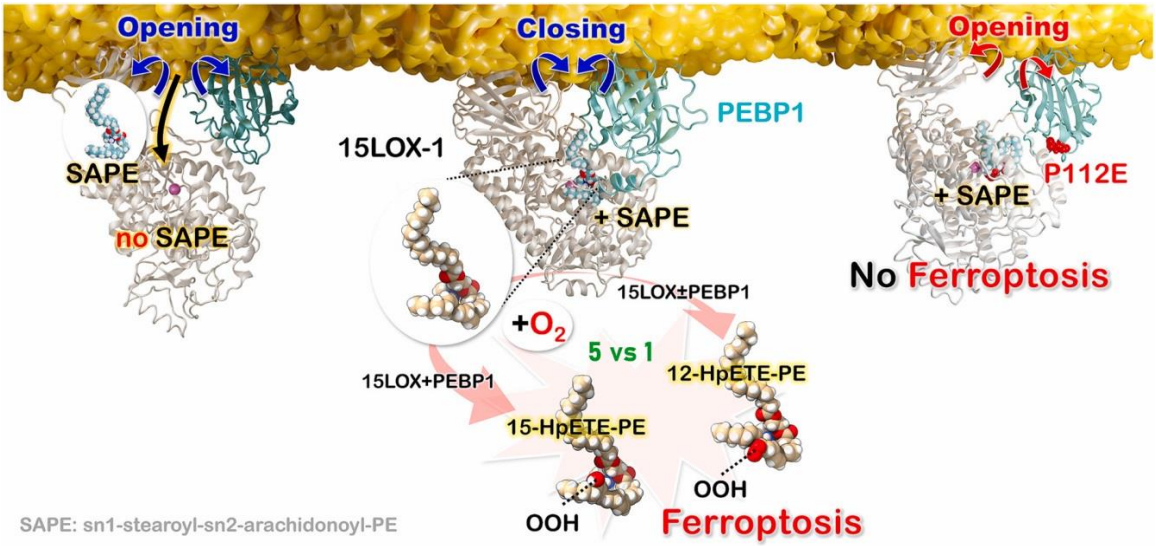

Schematic illustration of the membrane regulation of 15LOX-1/PEBP1 complex that prompts the generation of ferroptotic signals, 15-HpETE-PE or 12-HpETE-PE, and effect of the mutation on residue P112 on the complex formation. Figure published as the graphical abstract of Article A.

We confirmed that membrane association and substrate SAPE binding trigger conformational changes in the 15LOX-1/PEBP1 complex, forming pathways for O_2 access to the catalytic site. Two distinct oxygen channels, termed *Entrance A* and *Entrance B*, were identified, with an 8:2 ratio favoring one oxygen entry route. Additionally, two O_2-binding sites were identified at the 15LOX-1 catalytic site: one facilitates single oxidation, while the other may support double oxidation of the substrate. Additionally, lipidomics experiments prove the possibility of single and double-oxidized products formation.

- Our findings revealed water clusters within the 15LOX-1, which may facilitate the release of hydroperoxy products. These water molecules, identified through MD simulations and observed in crystallographic structures of other 140 LOX family members, may suggest their potential role in enhancing O_2 mobility and contribution to catalytic efficiency.

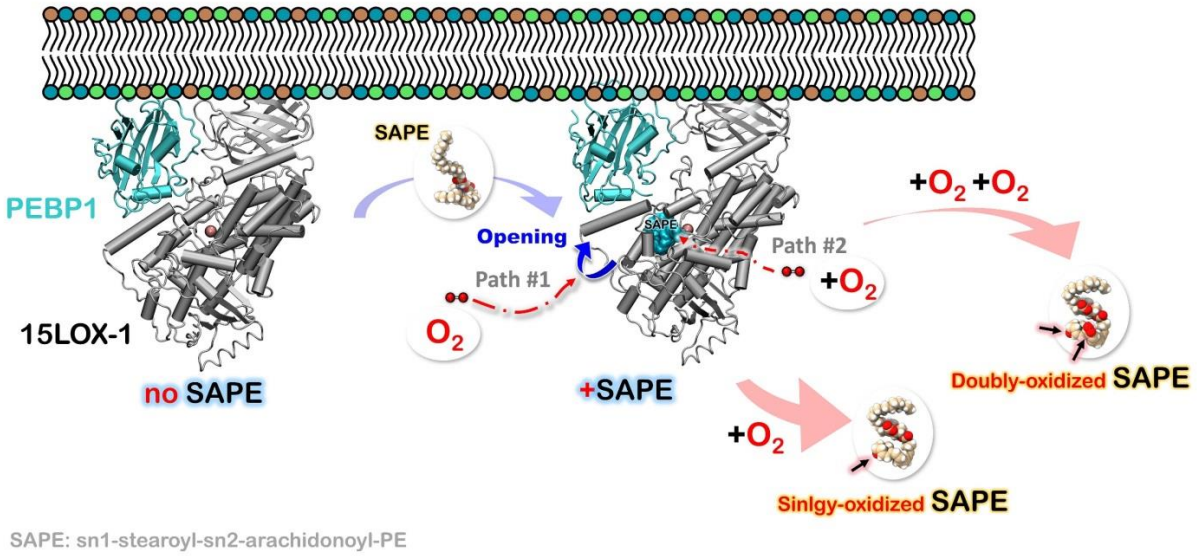

The presence of substrate SAPE warrants O_2 access tunnels toward the catalytic site of 15LOX-1. Figure submitted as the graphical abstract of Article C.

Furthermore, I applied deep learning techniques, such as deep neural networks, to identify hotspot residues in the 15LOX-1/PEBP1 complex. Due to the limited dataset size for training, I explored various machine learning models under the IDUB grant, supervised by Prof. Irina Moreira (University of Coimbra), to pinpoint hotspot residues.

Future work includes investigating the formation of the product 15-HpETE-PE and its release following the peroxidation process. I have started running simulations of singly and doubly oxidized products using all-atom MD simulations. Moreover, based on my MD simulations from *Article C*, in collaboration with Dr. James Mattock, a postdoc working under the supervision of Dr. hab. Karolina Mikulska-Rumińska, Prof. NCU, quantum mechanics/molecular mechanics (QM/MM) simulations will be conducted to gain insights into product formation in the 15LOX-1/PEBP1 complex.

9. Appendix

9.1 WatFinder

Water bridges

Water bridges, formed by water molecules, are essential interactions that significantly impact various biochemical processes, especially in enzyme and protein functions [136]. These bridges operate primarily through transient hydrogen bonding with polar or charged residues, linking different protein regions or connecting proteins with ligands. This dynamic bonding allows for the flexibility and rearrangements needed for biological functions. Water molecules also mediate ionic interactions between charged residues, providing structural stability and flexibility to proteins, which is crucial for maintaining protein conformations and supporting biomolecular recognition processes [136, 137]. These interactions play important roles in various binding processes.

In ligand binding, water bridges facilitate ligand binding by creating a dynamic environment around the binding site [138]. When a ligand approaches, water molecules may be displaced, affecting binding affinity [139]. Displacement of water from a hydrophobic region can enhance binding affinity by reducing unfavorable hydrophilic interactions, while removing stabilizing water can decrease affinity due to an energetic penalty.

In substrate binding, water bridges stabilize enzyme-substrate complexes in enzyme catalysis by mediating interactions between active site residues and substrates [140]. This stabilization improves specificity and facilitates conformational changes necessary for catalysis. In oxygen transport, the role of water promotes O_2 mobility [141] by lowering energy barriers at the entrance,

modulating protein conformation by opening and closing the entrance to the tunnel, or providing transient hydrogen bonds that direct molecules along specific pathways.

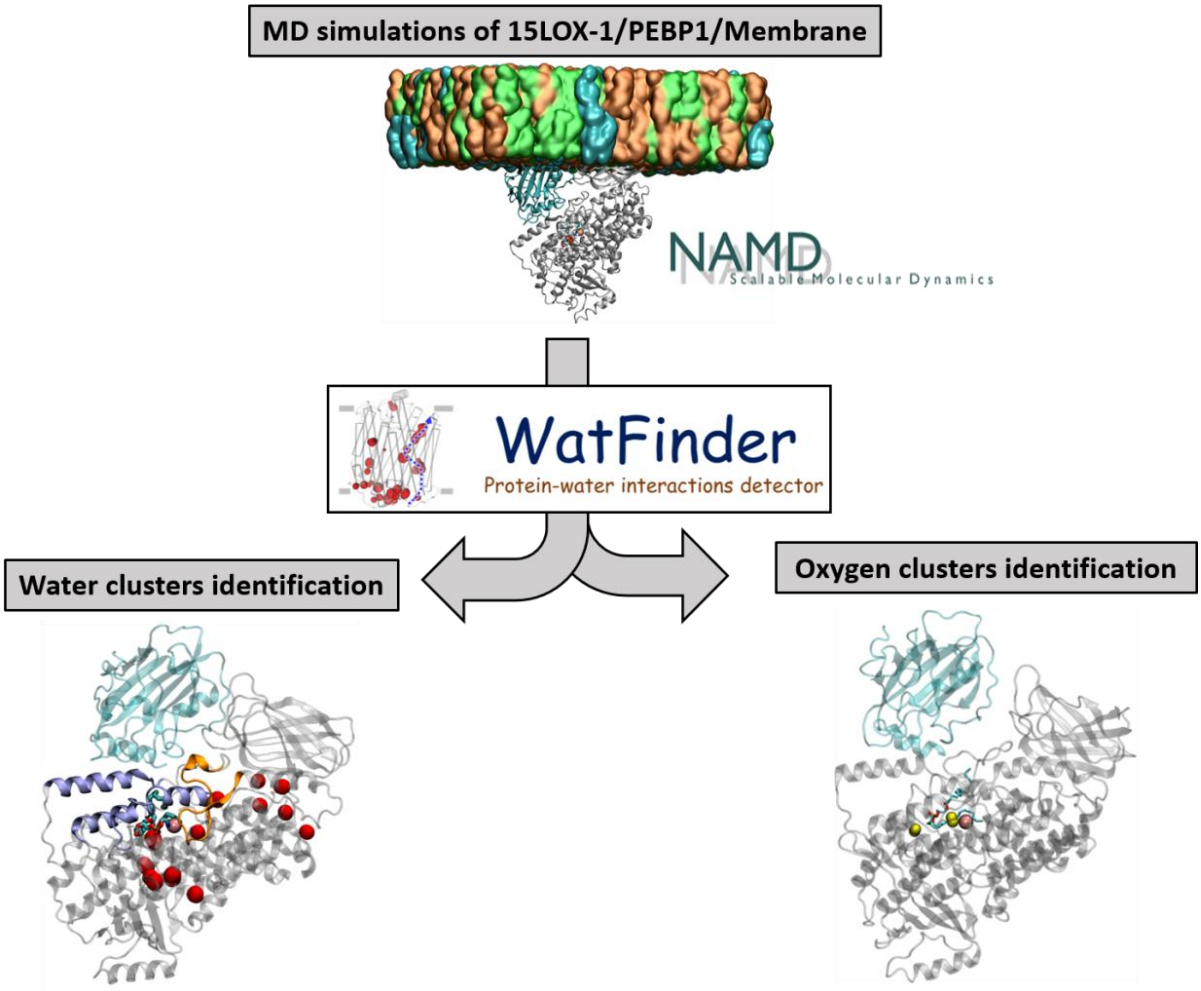

Figure 8. Schematic description of the protocol adopted to find water and oxygen clusters in all-atom MD simulations of the 15LOX-1/PEBP1 complex.

Water clusters in 15LOX-1/PEBP1

We utilized our tool, *WatFinder*, to detect water bridges and their associations using MD trajectories of the 15LOX-1/PEBP1 complex with the SAPE substrate and a biological membrane, as illustrated in the pipeline in Fig. 8. To investigate water bridge formation within the 15LOX-1 structure, we first applied the *calcWaterBridgesTrajectory()* function with *method="cluster"*. This clustering algorithm provides information on water clusters that form between multiple residues of the protein. Next, the *savePDBWaterBridgesTrajectory()* function was used to save the conformations (in PDB format) that contain the detected water bridges. These conformations were

further analyzed using the *findClusterCenters()* function. Additionally, parameters such as *dictC* (maximum distance between independent water molecules in a cluster, measured between oxygen atoms in Å) and *numC* (minimum number of water molecules in a cluster) were adjusted to find optimal settings for the system. Initially, default values were tested, with the distance between water molecules (*distC*) set to 0.5 Å and the minimum number of water molecules in a cluster (*numC*) set to 4. The analysis was repeated with stricter parameters to identify only the most significant water interactions with the protein. Adjusting parameters, such as distC = 0.6 Å and numC = 15, revealed potential water clusters.

The analysis of 140 LOX structures was performed using ProDy [142] tools and WatFinder [143]. First, we used a Dali search that provided 1731 PDB structures. Among those, we selected 140 structures with higher than 50% of the total residue length and with an RMSD value lower than 1 Å. Hydrogen atoms were filled using the Openbabel method of WatFinder, and structures were aligned using the matchChain method in ProDy with seqid equal to 5 and overlap of sequence higher than 50%. We used default parameters to predict water bridges. Next, we assessed how many water bridges across 140 crystallographic structures of LOX are located in the same region using findClusterCerters() function of WatFinder with distC = 0.9 Å and numC = 17. Similar approach was used to cluster O_2 molecules in MD simulations with distC = 1.0 Å and numC = 10.

9.2 Machine learning to predict hotspots in 15LOX-1/PEBP1

Hotspots

A primary objective of molecular biology is to identify all protein–protein interactions (PPIs) within an organism, along with their biochemical and biological roles. PPIs play a crucial role in nearly all biological processes, and pinpointing the specific amino acid residues that affect the specificity and strength of these interactions is a highly significant challenge [144]. Aberrant regulation of these PPI networks is linked to various diseases, such as cancer, neurodegenerative disorders, and infections, among others [145]. PPIs are critically regulated through a few "hot spot" residues at the interface. A generally agreed definition for hotspot residues are those which, upon alanine mutation, generate a binding free energy difference ($\Delta\Delta G_{binding}$) $\geq$2.0 kcal/mol whereas null-spots correspond to residues with $\Delta\Delta G_{binding}$ <2.0 kcal/mol when mutated to alanine [146, 147].

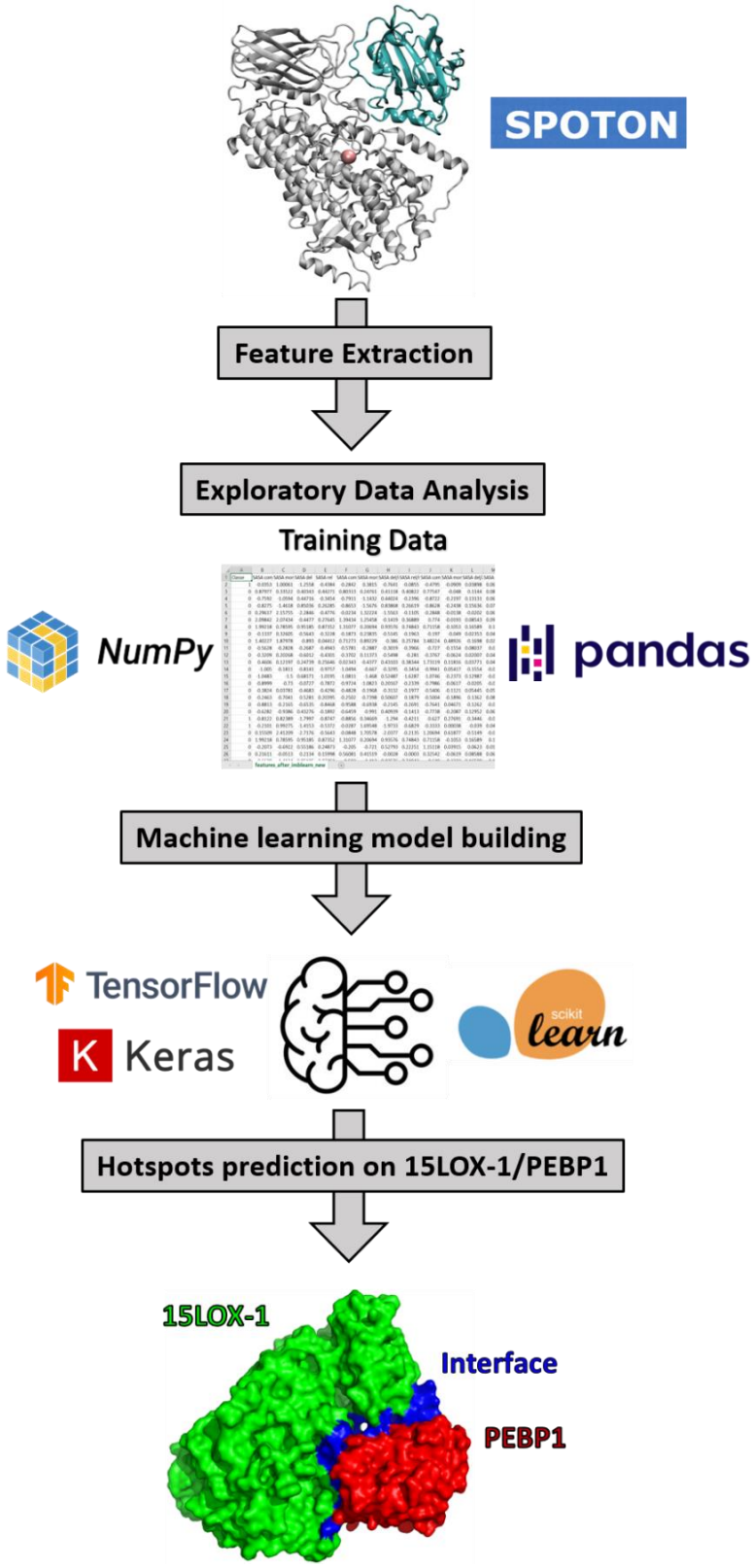

Figure 9. Schematic description of the protocol adopted to find hotspots in 15LOX-1/PEBP1.

Based on our previous experimental data [47] suggesting that residue P112 and the C-terminal helix (D175-Y186) of PEBP1 might be essential for its productive association with 15LOX-1, we began by using a hypothetical structural PDB model of 15LOX-1/PEBP1 to collect the dataset from the SpotOn web server [146]. The SpotOn database already includes information on amino acid composition, solvent-accessible surface area (SASA), position-specific scoring matrices, amino acids within 2.5 and 4.0 Å, nearby hydrophobic residues, total change in SASA, number of interfacial residues, pseudo-amino acid composition, and more.

To enhance this dataset for model prediction, we used the protr R package to add features related to amino acid composition and dipeptide composition. This expanded the dataset to 702 features and 520 amino acid residues, with 122 labeled as hotspots and 398 as non-hotspots. To further reduce bias, we preprocessed the dataset again by removing PDB models with a similarity score above 0.5 (using the TM-align score where we used our model structure as reference). This resulted in a reduction of data points from 520 to 476, with 114 labeled as hotspots and 362 as non-hotspots. To address data class imbalance, we applied the SMOTE (Synthetic Minority Oversampling Technique) to generate additional minority positive samples, achieving a balanced dataset with 362 positive and 362 negative samples. Additional preprocessing steps included data cleaning, handling missing values, and normalizing features to ensure high-quality inputs for model training, as described in Fig. 9.

Training set metrics

Models	Accuracy	Precision	Recall	Sensitivity	Specificity	F1	AUROC	Precision – Recall
RF	0.93	0.91	0.95	0.95	0.91	0.93	0.93	0.89
XGB	0.99	1.00	0.99	0.99	1.00	0.99	0.99	0.99

Validation set metrics

Models	Accuracy	Precision	Recall	Sensitivity	Specificity	F1	AUROC	Precision – Recall
RF	0.85	0.82	0.88	0.88	0.82	0.85	0.85	0.78
XGB	0.88	0.85	0.92	0.92	0.85	0.88	0.88	0.82

Test set metrics

Models	Accuracy	Precision	Recall	Sensitivity	Specificity	F1	AUROC	Precision – Recall
RF	0.85	0.85	0.85	0.85	0.85	0.85	0.85	0.80
XGB	0.86	0.87	0.85	0.85	0.87	0.86	0.86	0.81

We then built and evaluated multiple machine learning models, including Logistic Regression, SVM, KNN, Random Forest, Naive Bayes, Gradient Boosting, and XGBoost, to predict hotspot residues. Each model was fine-tuned and optimized for better performance using GridSearchCV, a function in the scikit-learn Python package. The models' performances were assessed through cross-validation and metrics such as accuracy, precision, recall, F1-score, and other relevant metrics, allowing us to identify the most effective model for hotspot prediction. Among the models tested, tree-based models like Random Forest (RF) and XGBoost (XGB) delivered the most promising results.